



Norwegian University  
of Life Sciences

**Master's Thesis 2023 60 ECTS**

Faculty of Chemistry, Biotechnology and Food Science

# **Deciphering the Mechanistic Nuance of LPMOs: The Critical Role of Second Sphere Glutamine/Glutamate Residue and Electron Donors**

Henriette Nohr

Master of Chemistry



## ACKNOWLEDGEMENT

This thesis, encompassing years of diligent study from August 2019 to August 2023, was conducted with the support of Morten Sørli's Bioorganic research group and the Protein Engineering and Proteomics (PEP) group at the Faculty of Chemistry, Biotechnology and Food Science at the Norwegian University of Life Sciences (NMBU). It served as a cog within a broader research machinery aimed at unraveling the mysteries of LPMO activity. In the foreground of my heartfelt gratitude stands Professor Morten Sørli, my mentor, whose research group helped support my academic and intellectual pursuits. His generous impartation of knowledge, tireless support, and unwavering encouragement sustained me from my initial plunge into the captivating domain of LPMOs to the submission of this master thesis. My sincere appreciation also extends to Dr. Lucas Raider, my co-supervisor, for his pragmatic guidance in the laboratory. His patience and the invaluable slices of time he shared with me are deeply cherished. I also owe a debt of gratitude to Student Adviser Janne Beate Utåker, whose counsel was instrumental in navigating the choppy waters of COVID-19 pandemic and my own health challenges, providing the motivation that propelled me to complete this thesis.

A special mention to associate professor Hilde Vinje who despite me not being one of her direct students, graciously lent me her expertise. Furthermore, the roles played by my general practitioner, Mohammad Fazi, and my neurologist, Maria Kase-Berg, were integral in ensuring my health did not derail the completion of this thesis. I extend my thanks to my peers - Derya Aricigil, Olga Rasten, Nanticha Suyoteetanarat, Christine Copeland, Zarifa Barkatullah, Xiaodi Guo, and Boshra Mohammed. Our camaraderie and uplifting lunch breaks formed a significant portion of my support system during my study years. Also, a shout-out to the incredible residents of the 8th floor at Palisaden, your companionship turned the daunting Corona lockdown into a bearable experience.

Lastly, but certainly not the least, my deepest gratitude to my family, who instilled in me the value of education and nurtured my resolve to pursue my objectives. To my parents, Kristin Nohr and Magnus Nohr, and my sister Vilde Nohr, your faith in me and your unwavering support have been my guiding lights throughout this journey. And to Flora Malmberg Nohr, my beautiful niece, your birth pushed me to finish my studies, so I could be part of your life.

Henriette Nohr Ås, august 2023

## SUMMARY

Lytic polysaccharide monooxygenases (LPMOs) are crucial copper-dependent redox enzymes renowned for ability to oxidize recalcitrant polysaccharides, such as cellulose and chitin. Although they possess significant biotechnological potential, the intricate mechanistic aspects of LPMOs are yet to be fully understood.

This thesis emphasizes the universally conserved second sphere glutamate/glutamine residue within the LPMO active site. Employing site-directed mutagenesis, we fashioned various mutants of two LPMOs, *SmAA10A* and *NcAA9C*, to ascertain the function of this pivotal residue. Specifically, Glu60 in *SmAA10A* was altered to glutamine (E60Q), aspartate (E60D), or asparagine (E60N). Concurrently, for *NcAA9C*-Q164, mutations included changing glutamine to glutamate (Q164E), aspartate (Q164D), and asparagine (Q164N). The data unveiled that these mutations significantly altered enzyme activity.

Notably, all mutants demonstrated diminished activity relative to their wild type counterparts, a pattern consistent with observations by Bissarro *et al.*, 2020. Moreover, turnover for the *SmAA10A* variants in the presence of the hydrogen peroxide quenching horse radish peroxidase (HRP) showed that the wild type was inhibited the least. This aligns well with the proposed hydrogen bonding role of Glu60 in catalysis.

Beyond the structure-function relationship, we explored the enzyme's reliance on electron donors during catalysis. *NcAA9C* experiments suggest that varied electron donors can engage LPMOs, although with differential efficacies. Interestingly, the reductants (gallic acid and cysteine) that resulted in low catalytic rates experienced less degree of inactivation compared to when ascorbic acid was used as the reductant for the mutants of *NcAA9C*. Combined, this study underscores the indispensable roles of specific residues in LPMO efficacy and the impact of reductant selection on their performance.

## SAMMENDRAG

Lytiske polysakkarid monooksygenaser (LPMOer) er viktige kobberavhengige redokszymer kjent for evnen til å oksidere krystallinske regioner i polysakkarider, som cellulose og kitin. Selv om de har betydelig bioteknologisk potensial, er de detaljerte mekaniske aspektene ved LPMOen ennå ikke fullt forstått.

Denne master avhandlingen vektlegger den universelt bevarte andre sfære glutamat/glutamin aminosyren innenfor LPMOens aktive sete. Ved å bruke stedsrettet mutagenese laget vi forskjellige mutanter av to LPMOer, SmAA10A og NcAA9C, for å fastslå funksjonen til denne konserverte aminosyren. Spesielt ble Glu60 i SmAA10A endret til glutamin (E60Q), aspartat (E60D) eller asparagin (E60N). Samtidig, for NcAA9C-Q164, inkluderte mutasjoner endring av glutamin til glutamat (Q164E), aspartat (Q164D) og asparagin (Q164N).

Dataene avslørte at disse mutasjonene betydelig endret enzymaktiviteten. Bemerkelsesverdig, viste alle mutanter redusert aktivitet i forhold til deres ville type motparter, et mønster som stemmer overens med observasjoner av Bisarro et al., 2020. Videre viser reaksjoner for SmAA10A-variantene i nærvær av hydrogenperoksyd-nøytraliserende hesteradik peroksidase at ville type enzymet ble hemmet minst. Dette passer godt med den foreslåtte hydrogenbindingsrollen til Glu60 i katalyse.

Utover struktur-funksjonsforholdet utforsket vi enzymets avhengighet av elektrondonorer under katalyse. Experimentert med NcAA9C antyder at forskjellige elektrondonorer kan redusere LPMOer, selv om det er med varierende effektivitet. Interessant er det at reduktantene (gallisk syre og cystein) som resulterte i lave katalytiske hastigheter, opplevde en mindre grad av inaktivering sammenlignet med når askorbinsyre ble brukt som reduktant for NcAA9C-mutantene. Samlet sett understreker denne studien de uunnværlige rollene til spesifikke konserverte aminosyrer i LPMO-effektivitet og påvirkningen av reduktantvalg på deres ytelse.

# Table of content

ACKNOWLEDGEMENT.....	2
SUMMARY.....	3
SAMMENDRAG.....	4
TABLE OF CONTENT.....	5
ABRIVATIONS.....	8
1 Introduction.....	10
1.1 Polysaccharides.....	11
1.2 The Carbohydrate-Active enZYmes (CAZy) Database.....	12
1.3 Lytic Polysaccharide Monooxygenases.....	13
1.3.1 The history of Lytic polysaccharide monooxygenases.....	13
1.3.2 The structure of Lytic polysaccharide monooxygenases.....	14
1.3.3 Lytic polysaccharide monooxygenases catalysis.....	17
1.3.4 Electron donor.....	18
1.3.5 Oxygen co-substrate.....	20
1.3.6 Lytic polysaccharide monooxygenases Mechanism.....	21
1.3.7 Lytic polysaccharide monooxygenase inactivation.....	23
1.3.8 Purpose of this thesis.....	24
2 Materials.....	26
3 Methods.....	32
3.1 Transforming competent cells with plasmid carrying <i>smaa10a</i> variants.....	32
3.2 Expression and purification of <i>SmAA10A</i> variants.....	33
3.3 Periplasmic extraction.....	34
3.4 Chitin bead affinity chromatography.....	35
3.5 Sodium Dodecyl Sulfate-Polyacrylamide Gel Electrophoresis (SDS-PAGE).....	36
3.6 Determining Protein Concentration - $A_{280}$ .....	37
3.7 Copper-Saturating <i>SmAA10A</i> variants.....	38

3.8	Pre-culture culture of transformed <i>E. coli</i> BL21 (DE3) with plasmid carrying <i>SmAA20</i> gene .....	39
3.9	Cultivation of <i>e.coli</i> in shaker flask and expression of <i>SmGH20</i> .....	39
3.10	Harvest of <i>SmGH20</i> .....	40
3.11	Confirming activity in the <i>SmAA10A</i> wild type and gatekeeper mutants.....	41
3.12	Determining the optimal substrate concentration for <i>SmAA10A</i> variants .....	43
3.13	Determining <i>SmAA10A</i> variant activity without electron donor .....	44
3.14	Determining the activity of <i>SmAA10A</i> variants under <i>in-situ</i> peroxidase conditions .....	45
3.15	Determining activity for <i>SmAA10A</i> wild type and gatekeeper mutants with added H <sub>2</sub> O <sub>2</sub> – First setup.....	46
3.16	Determining activity for <i>SmAA10A</i> wild type and gatekeeper mutants with added H <sub>2</sub> O <sub>2</sub> -second setup.....	47
3.17	<i>SmAA10A</i> wild type and gatekeeper mutants activity in the presence of HRP under in-situ peroxygenase conditions. ....	48
3.18	<i>NcAA9C</i> wild type and gatekeeper mutants activity in the presence of different electron donors under in-situ peroxygenase conditions. ....	49
3.19	Product analysis by ion chromatographic system (ICS) .....	50
4	Results .....	52
4.1	PURIFICATION OF <i>SmAA10A</i> .....	52
4.1.1	Overall results of purification. ....	54
4.1.2	Concentration of isolated <i>SmAA10A</i> variants- A <sub>280</sub> .....	58
4.2	Purification of <i>SmGH20</i> .....	58
4.3	Time course activity assays with the <i>SmAA10A</i> wild type and gatekeeper mutants	59
4.3.1	Evaluating the Functional Activity of <i>SmAA10A</i> variants .....	59
4.3.2	Substrate Saturation Analysis: <i>SmAA10A</i> wild type Response to $\beta$ -Chitin .....	61
4.3.3	Investigating Electron Donor Independence in <i>SmAA10A</i> variant Reactions ..	62
4.3.4	Activity Analysis of <i>SmAA10A</i> Variants under <i>in-situ</i> peroxygenase conditions. ....	63

4.3.5	Activity Analysis of <i>SmAA10A</i> Variants with added hydrogen peroxide.....	64
4.3.6	Activity Analysis of <i>SmAA10A</i> Variants in the presence of HRP under <i>in-situ</i> peroxygenase conditions. ....	66
4.4	Redirected focus from <i>SmAA10A</i> to <i>NcAA9C</i> .....	69
4.5	Time course activity assays with the <i>NcAA9C</i> wildtype and gatekeeper mutants ...	69
4.5.1	Determining the initial rates of <i>NcAA9C</i> activity .....	74
4.5.2	Determining maximum product formation for <i>NcAA9C</i> .....	75
5	Discussion.....	76
6	References .....	80

## ABBREVATIONS

A2 <sup>ox</sup>	Chitobionic acid
AA	Auxiliary activity
Asp (D)	Aspartic acid / aspartate
Asn (N)	Asparagine
CAZy	Carbohydrate-active enzymes
CBM	Carbohydrate-binding module
CBP	Chitin-binding protein
CE	Carbohydrate Esterases
DP2 <sup>ox</sup>	Oxidized cello-oligosaccharide with a degree of polymerization of 2
DP3 <sup>ox</sup>	Oxidized cello-oligosaccharide with a degree of polymerization of 3
EPR	Electron Paramagnetic Resonance
GH	Glycoside hydrolase
GT	They are implicated in the formation of glycosidic bonds
Glu (E)	Glutamic acid / glutamate
Gln (Q)	Glutamine
His (H)	Histidine
HPAEC	High Performance Anion Exchange Chromatography
ICS	Ion Chromatography System
IEC	Ion Exchange Chromatography
LPMO	Lytic Polysaccharide Monooxygenase
MWCO	Molecular Weight CutOff
Nc	<i>Neurospora crassa</i>
Phe (F)	Phenylalanine

PL	Polysaccharide lyases
Rpm	Revolutions per minute
SDS-PAGE	Sodium dodecyl-sulfate polyacrylamide gel electrophoresis
Sm	<i>Serratia marcescens</i>
SOC	Super Optimal Broth
SOD	Superoxide Dismutase
Tyr (Y)	Tyrosine
WT	Wild type

# 1 INTRODUCTION

Imagine a hidden world of microscopic architects, tirelessly working to sculpt and transform the complex landscapes of plant cell walls, fungal networks, and even the battlegrounds of host-pathogen interactions. Among these are lytic polysaccharide monoxygenases (LPMOs), a unique class of copper-dependent enzymes, emerging as a potent and versatile player in diverse biological processes. The uniqueness of LPMOs lies in their novel catalytic mechanism enabling the oxidation of sturdy polysaccharides such as cellulose and chitin, components usually embedded within nature's robust fortresses. The process not only intrigues from a fundamental scientific perspective but also harbors considerable practical potential, offering a fresh perspective on nature's intricate strategies for recycling plant biomass.

The inherent ability of LPMOs to break down complex biopolymers has opened new possibilities in various industrial sectors. A key area of interest lies in the production of biofuels, where the recalcitrant nature of plant biomass has always been a formidable challenge. By leveraging the unique oxidative capabilities of LPMOs, the conversion of biomass into fermentable sugars can be optimized, revolutionizing the biofuel industry. Further, their potential utility extends beyond biofuels, including the production of valuable biochemicals, thus rendering LPMOs a versatile tool in the world of biotechnology.

Despite their remarkable abilities, the exact catalytic workings of LPMOs remain a captivating enigma. One of these mysteries, are a universally conserved glutamate/glutamine residue situated within the enzyme's active site. Suspected to play a crucial role in the enzyme's catalytic activity, these residues potentially influence the way LPMOs harness the reducing potential of co-substrates to perform their oxidative transformations. Another under studied mystery is the electron donor, that provide necessary electrons to the active site of the LPMO, priming it for the catalytic action. Understanding the nature and dynamics of these electron donors can significantly influence the efficiency of LPMO-mediated reactions and holds profound implications for industrial processes, such as biofuel production, where optimized enzyme activity is paramount. This thesis aims to dive into these enigmas, exploring the roles of these Glu/Gln residues in LPMO catalysis and the electron donor. It is through this exploration that we hope to gain a deeper understanding of LPMO function, providing keys to unlock and harness the full potential of these remarkable enzymes.

## 1.1 POLYSACCHARIDES

To grasp the concept of lytic polysaccharide monooxygenases, it's important to first understand polysaccharides, the substrate LPMOs work on. Polysaccharides are sugar-based polymers made up of long chains that include numerous sugar units called monosaccharides. The chains of monomers can range from simple linear structures to more complex branched forms. The sugar units are connected by a specific covalent bond called a glycosidic bond. This bond forms between the hemiacetal or hemiketal group of one sugar unit and a hydroxyl group of another sugar unit. As it so happens, polysaccharides come in many different forms. Some, like starch and glycogen, act as energy storage, while others like cellulose (found in plants) and chitin (found in arthropods) serve as structural components. In certain cases, both in nature and industry, the individual sugar components are more valuable than the original polysaccharide. As a result, the process of breaking down polysaccharides into their simpler components is of great interest.

The process for breaking down polysaccharides into their components is known as saccharification, which can be facilitated by different enzymes. For a long time, people thought that polysaccharide breakdown was mainly helped by two groups of carbohydrate-active enzymes: glycoside hydrolases (GHs) and polysaccharide lyases (PLs) (Cantarel et al., 2009). GHs are widespread enzymes that promote the hydrolysis of glycosidic bonds in complex sugars (CAZy, 2020). On the other hand, PLs are less common and comprise enzymes that cleave polysaccharide chains containing uronic acid through a  $\beta$ -elimination mechanism (Cantarel et al., 2009). However, these enzyme groups struggle to effectively cleave glycosidic bonds in the crystalline regions of polysaccharides.

The issue with crystallized substrates is addressed through a symbiotic relationship with another enzyme group, which introduces breaks in the crystalline regions (Vaaje-Kolstad et al., 2010). This enzyme family, known as lytic polysaccharide monooxygenases or LPMOs, is the focus of this thesis. Therefore, the depolymerization of polysaccharides can be considered to be supported by three enzyme groups: glycoside hydrolases, polysaccharide lyases, and lytic polysaccharide monooxygenases.

## 1.2 THE CARBOHYDRATE-ACTIVE ENZYMES (CAZY) DATABASE

The Carbohydrate-Active enZymes Database or CAZy is an online database for Carbohydrate active enzymes (CAZymes). The Database, was launched in 1998 with a mission to organize, present, and analyze genomic, structural, and biochemical data on CAZymes (Cantarel et al., 2009). With a structure that allows for efficient data exploration, the CAZy database provides two distinct methods to access its content. Users can either navigate through the sequence-based families or delve into the exploration of genomes based on carbohydrate-active enzymes. The credibility and relevance of the CAZy database are preserved through the consistent integration of the latest published genomes. Within the database, these genomes are chiefly organized by the classification of the host organism—whether they belong to Archaea, Bacteria, Eukaryota, or Viruses—and subsequently alphabetized based on their scientific names (Drula et al., 2022).

Within the realm of CAZymes, enzymes can be classified into one of five recognized classes or their associated modules. These classes encompass enzymes that orchestrate the degradation, biosynthesis, or modification of carbohydrates and glycoconjugates. The five classes are constituted as follows:

**Glycoside Hydrolases (GHs):** These enzymes carry out the hydrolysis and/or rearrangement of glycosidic bonds.

**Glycosyl Transferases (GTs):** They are implicated in the formation of glycosidic bonds.

**Polysaccharide Lyases (PLs):** They mediate the non-hydrolytic cleavage of glycosidic bonds.

**Carbohydrate Esterases (CEs):** They perform the hydrolysis of carbohydrate esters.

**Auxiliary Activities (AAs):** This class is made up of redox enzymes that operate alongside CAZymes.

To offer a more nuanced categorization, each of these enzyme classes is further subdivided into various families based on sequence similarity. The inclusion of a new family within an enzyme class requires validated published evidence that confirms the activity of at least one member of the proposed family. Both the content and descriptions of the families within the CAZy database are updated regularly (Drula et al., 2022). It is noteworthy that LPMOs are classified under the enzyme class of Auxiliary Activities. However, it is crucial to highlight that not all members of the AA families are classified as LPMOs. In this thesis we work with enzymes from the AA9 and AA10 LPMO families.

## 1.3 LYTIC POLYSACCHARIDE MONOOXYGENASES

Lytic polysaccharide monooxygenases or LPMOs are copper-dependent redox enzymes that catalyze the oxidative cleavage of glycosidic bonds in polysaccharides, using a reductant and an oxygen co-substrate (Vaaje-Kolstad et al., 2010). They are complex, compact proteins recognized for their distinct, catalytic domain architecture which is fundamental to their enzymatic function. LPMOs typically have a round shape with a relatively flat binding face that features a surface-exposed active site. The three-dimensional structure of the protein is determined by the arrangement of amino acids that make up the protein. Interestingly, LPMOs tend to exhibit similar folds, even with minimal sequence identity both within and between LPMO families (Vaaje-Kolstad et al., 2017). The catalytic domain most of the time have a Carbohydrate Binding Module (CBM) attached. While this provides a general overview, the following sections will delve deeper into the unique features found across various LPMO families, with specific focus on LPMO families AA9 and AA10.

### 1.3.1 THE HISTORY OF LYTIC POLYSACCHARIDE MONOOXYGENASES.

The discovery and systematic classification of lytic polysaccharide monooxygenases form a richly woven narrative of biochemical discoveries and theoretical developments in the scientific literature. Reese *et al.*, in 1950 revolutionized the understanding of polysaccharide degradation by asserting that it wasn't an isolated enzymatic process but a collaborative effort, laying the foundation for the concept of enzymatic priming in polysaccharide solubilization (Reese et al., 1950). Notably, Eriksson *et al.*, linked oxidative mechanisms to polysaccharide breakdown (Eriksson et al., 1974). Yet, for years, oxidative activities remained overshadowed by the focus on carbohydrate-binding proteins (CBP) with minimal depolymerizing activity, such as CBM33s (Sunna et al., 2000).

A major breakthrough came in the 1990s when the GH61 family of enzymes, essential for cellulose degradation, was identified (Saloheimo et al., 1997). Vaaje-Kolstad *et al.*, later found that CBP21 from the CBM33 family enhanced chitin degradation (Vaaje-Kolstad et al., 2005a). In their subsequent work Vaaje-Kolstad *et al.*, revealed that CBP21 as an oxidative enzyme,

necessitating a reductant, oxygen, and a divalent metal ion, further complexifying polysaccharide breakdown (Vaaje-Kolstad et al., 2010).

Proteins from GH61 and CBM33 families displaying similar oxidative, catalytic activities led to their collective recategorization of these families as LPMOs (Horn et al., 2012). They were subsequently classified as Auxiliary Activities (AA) enzymes - AA9 and AA10 in the Carbohydrate-Active enZymes (CAZy) database (Levasseur et al., 2013). Since then, six additional LPMO families, namely AA11, AA13, AA14, AA15, AA16, and AA17, have been discovered and characterized (Couturier et al., 2018; Filiatrault-Chastel et al., 2019; Hemsworth et al., 2014; Sabbadin et al., 2018; Sabbadin et al., 2021; Vu et al., 2014). In 2017 Bissaro *et al.*, published an influential paper that challenged the identity of the co-substrate in LPMOs, proposing H<sub>2</sub>O<sub>2</sub> as a potential alternative to O<sub>2</sub> (Bissaro et al., 2017), spurring further exploration into LPMO mechanisms. Furthermore, Recent studies suggest roles for LPMOs beyond polysaccharide oxidation, such as copper homeostasis (Garcia-Santamarina et al., 2020) and cell wall remodeling (Labourel et al., 2020). The diverse range of LPMOs across microbial genomes suggests untapped biological functions, signaling a future teeming with fresh discoveries in the LPMO landscape with significant industrial implications.

### 1.3.2 THE STRUCTURE OF LYTIC POLYSACCHARIDE MONOOXYGENASES.

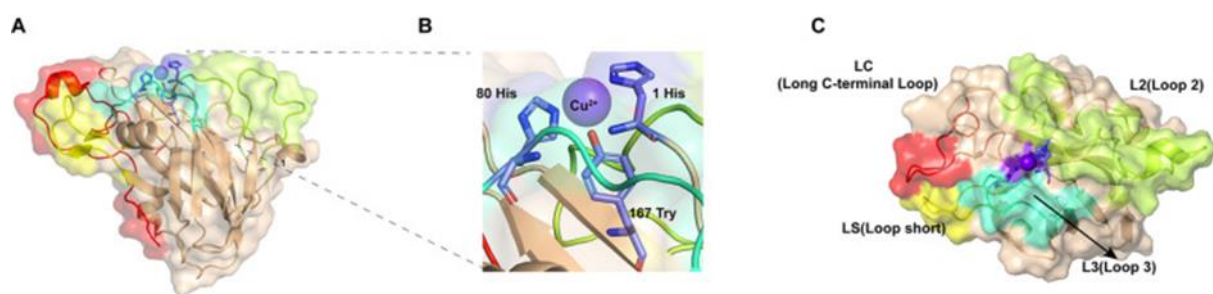


Figure 1-1 **Topology and functional differences of the loops from AA9 LPMOs** (A) Overall structure of LPMO (B) Active center of LPMO. (C) Loops with different functional zones on the substrate-binding surface of LPMO. Figure and text taken from (Yu et al., 2023).

The catalytic domain of the LPMOs is commonly seen as a relatively inflexible molecule consisting of approximately 200 to 250 amino acids, containing disulfide bonds which enhance its structural stability (Beeson et al., 2015). LPMOs comprise a complex structure, with various

regions contributing to their overall function and substrate specificity. These regions can be broadly classified into three main categories: the  $\beta$ -sandwich core, the substrate-binding surface, and the active site.

The core structure of an LPMOs is characterized by a slightly distorted  $\beta$ -sandwich fold, reminiscent of fibronectin-like or immunoglobulin-like structures. The  $\beta$ -sandwich is composed of two  $\beta$ -sheets, each of which consists of three to four  $\beta$ -strands. This results in a total of seven or eight  $\beta$ -strands in the entire core structure (Vaaje-Kolstad et al., 2017). Diversity in LPMO structures arises from the unique configuration of helices and loops interconnecting the core  $\beta$ -strands. These variances in structural composition culminate in the differing dimensions and topologies of the substrate-binding surface. While generally perceived as ‘flat’, the substrate-binding surfaces of LPMOs are not uniform; they exhibit topological variability. Such diversity in topography could potentially underscore the unique substrate specificity observed across different LPMOs. The flat binding face allows LPMOs to work on crystalline substrates, while the variation of amino acid residues contributes to substrate specificity (Vaaje-Kolstad et al., 2017).

The active site of LPMO plays a central role in their enzymatic function and is characterized by a mono-nuclear copper center. The defining feature of the active site is the “histidine brace” motif, a distinctive structural configuration involving a copper ion coordinated by an N-terminal histidine residue (His/H) and an additional histidine side chain (Quinlan et al., 2011). This N-terminal histidine forms a covalent bond with the copper ion through its N $\epsilon$ 2 atom, and it also simultaneously establishes a hydrogen bond with a proximal amino acid. The other histidine residue coordinates with the copper ion through its N $\epsilon$ 2 and N $\delta$ 1 atoms, giving rise to a three-coordinate or T-shaped geometry that is conserved across various LPMO families (Ciano et al., 2018).

Besides the histidine brace, there is several other conserved residues lining the active site of LPMOs, potentially contribute to substrate binding and positioning, as well as influencing the enzyme’s regioselectivity. Fig. 1.2, displays the active site of five enzyme, highlighting conserved residues.

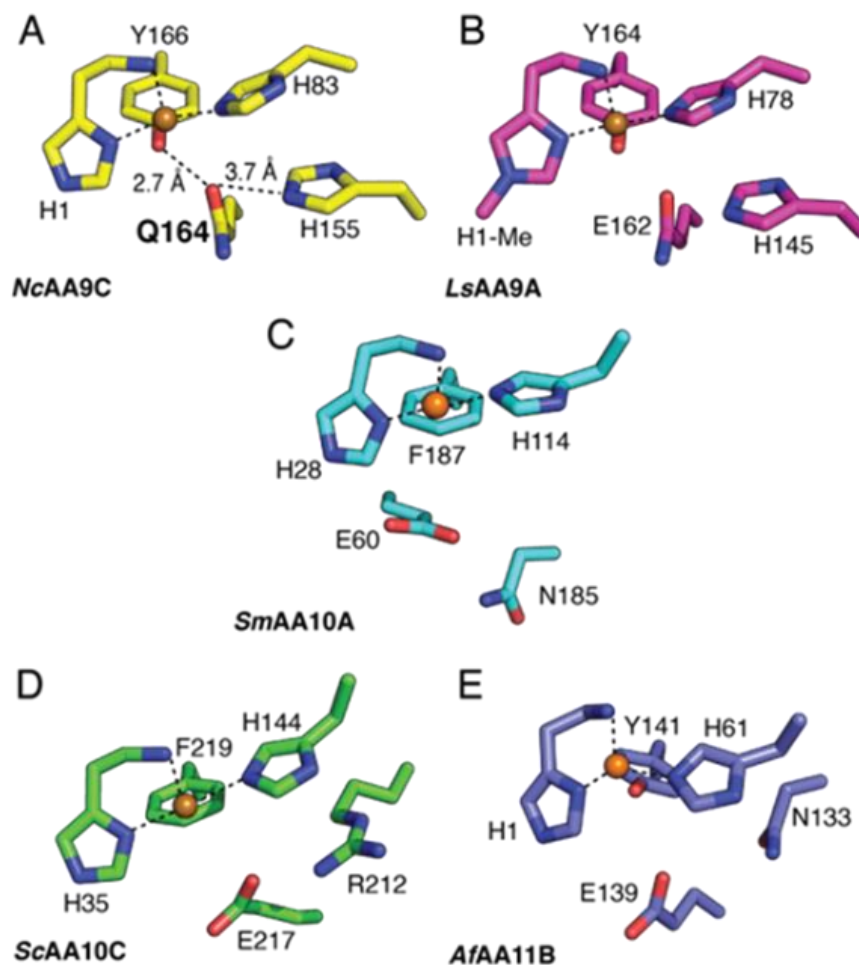


Figure 1-2 **Structural comparison of the catalytic centers in various LPMOs.** The histidine brace, key second sphere residues and the copper center are shown. Examples from three LPMO families, AA9, AA10 and AA11. (A) *NcAA9C*, (B) *LsAA9A*, (C) *SmAA10A*, (D) *ScAA10C* and (E) *AfAA11B* for which a homology model is shown based on the crystal structure of *AoAA11*. Figure made by Dr. Kelsi Hall.

Most LPMOs typically display a conserved tyrosine (Tyr/Y) residue below the copper in the active site (Fig. 12). The exception being most AA10s as they appear to have a conserved phenylalanine (Phe/F) instead causing steric hindrance along with the axial-positioned alanine (Ala/A), resulting in a compressed trigonal-bipyramidal geometry (Sun et al., 2023). An alanine is also present in AA15 at a similar orientation as AA10s (Sabbadin et al., 2018). Another residue that is conserved through LPMO superfamily is a second sphere glutamine(Glu/E)/glutamate(Gln/Q) residue, that is postulated to “gate” the entry to the confined active site and “caging” hydrogen peroxide during catalysis (Bissaro et al., 2020), therefore being referred to as a gatekeeper residue. In fungal AA9, an internally conserved histidine helps the Glu/Gln residue as a second gatekeeper. Fig. 1.2, displays the active site of five enzyme, highlighting conserved residues. Table 1.1 that gives examples of Glu/Gln residues for the different LPMO families.

Table 1-1 Conserved glutamate/glutamine residues in LPMO families. Included *SmAA10A* and *NcAA9C*, and one example from AA9-AA11 and AA13-AA17.

LPMO family	Enzyme	Gatekeeper	C1 or C4	Substrate specificity
AA9	<i>NcAA9C</i>	Q164	C4	Cellulose
AA10	<i>SmAA10A</i>	E60	C1	Chitin
AA9	<i>LsAA9C</i>	E162	C1	Cellulose
AA10	<i>ScAA10C</i>	E217	C1	Cellulose
AA11	<i>AoAA11</i>	E138	C1 /C4	Chitin, cellulose
AA13	<i>AoAA13</i>	Q222	unknown	Starch
AA14	<i>PcAA14B</i>	E97	C1 <sup>a</sup>	Xylen <sup>a</sup>
AA15	<i>TdAA15A.</i>	E182	C1	cellulose and chitin
AA16	<i>MtAA16A</i>	Q153	Unknown	
AA17	<i>PiAA17C</i>	Q153and Q162		Pectin

a: This has been challenged and may no longer be excepted knowledge.

### 1.3.3 LYTIC POLYSACCHARIDE MONOOXYGENASES CATALYSIS

LPMOs catalyze the hydroxylation of one of the carbons (C1 or C4) in the scissile glycosidic bond in way, which ultimately leads to bond breakage by an elimination reaction (Forsberg et al., 2019). However, even though considerable progress has been made throughout the last decade, the mode of action of these monocopper redox enzymes has yet to be fully mechanistically characterized (Bissaro et al., 2020), as LPMOs catalyzes a powerful oxidation reaction that involves multiple factors that may be hard to control (Forsberg et al., 2019). For instance, LPMO catalysis is completely reliant on the availability of; an externally supplied copper Cu (II)-ion, an electron donor, an oxygen co-substrate, and substrate (Vaaje-Kolstad et al., 2010).

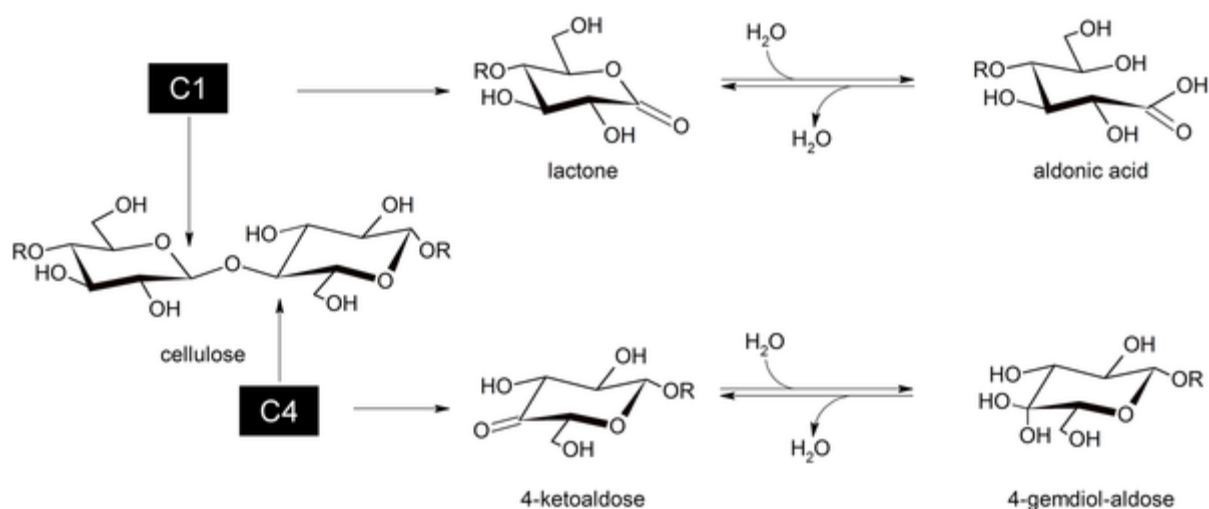


Figure 1-3 **LPMO regioselectivity**. Oxidation of the C1 position generates a lactone, which is hydrated to a reducing-end aldonic acid. C4-oxidation leads to non-reducing-end 4-ketoaldose formation, which will spontaneously hydrate to gemdiols in aqueous conditions. Retrieved from (Danneels et al., 2017).

LPMOs can carry out oxidation on either side of the glycosidic bond. Furthermore, as visualized in Fig. 1.3, different oxidized products are formed depending on which of the carbons (C1 or C4) in the glycosidic bond that is oxidized. Firstly, oxidation of the C1 carbon generates a lactone which, is then hydrated to an aldonic acid. In contrast, oxidation of the C4 carbon leads to the formation of a non-reducing-end 4-ketoaldose, that in aqueous conditions will spontaneously hydrate to a gemdiols (Danneels et al., 2017).

### 1.3.4 ELECTRON DONOR

An electron donor, in essence, is a molecule or substance that donates an electron to another entity within a chemical reaction. This type of reaction is typically characterized as a redox (reduction-oxidation) reaction. The electron donor, also known as a reducing agent, facilitates the reduction of another substance by supplying it with electrons. Parallel to the concept of an electron donor is a reductant, which is a synonym for a reducing agent. In a chemical reaction, a reductant donates its electrons to another species, leading to the reduction of the latter. Simultaneously, the reductant undergoes oxidation, by removing its own electrons. In simpler terms, the reductant causes reduction in another substance by virtue of its own oxidation. While all reductants serve as electron donors, not all electron donors qualify as reductants. This distinction becomes particularly evident in photocatalytic systems where light energy—usually

in the form of visible or ultraviolet light—is employed to excite the electrons within a photocatalyst. This excitation propels the electrons to a higher energy state, priming them for transfer to other molecules or entities, thus enabling their reduction. In this scenario, the photocatalyst itself is the electron donor, yielding its excited electrons. However, this process diverges from conventional chemical reactions involving reductants because it necessitates light energy to facilitate electron donation. Nevertheless, in practical terms, these are simply different names for the same function that a substance can fulfill in these reactions.

Within the context of LPMOs, the electron donor's role is to reduce the copper ion at the active site from its Cu(II) state to the catalytically active Cu(I) state. This transformation is crucial for activating the oxygen-substrate, which subsequently cleaves the polysaccharide chains (Bissaro et al., 2020). An effective electron donor for LPMOs generally embodies a few key traits. The first is reducing power, signifying a substance's inclination to relinquish its electrons, which is correlated with its standard reduction potential. The second trait is stability; the electron donor should be robust under the reaction conditions to prevent degradation or undesirable interactions with other system components. The third trait pertains to solubility; electron donors should be soluble in the medium where the reaction transpires to facilitate their interaction with LPMOs. Fourth, they should be non-inhibitory; the electron donor should not obstruct the enzyme's activity. Some compounds, despite their ability to donate electrons, may interfere with enzyme functioning. Next, is the H<sub>2</sub>O<sub>2</sub> production; the electron donor should oxidize over time concomitantly producing H<sub>2</sub>O<sub>2</sub> by means of the reduction of O<sub>2</sub> (Hemsworth, 2023). Lastly, from a practical standpoint, ideal electron donors should be readily available and economically feasible, especially for industrial or large-scale applications.

Within the purview of LPMOs, various reductants have demonstrated effective performance (Stepnov et al., 2021). Reports have also surfaced of light-driven systems employing a photosensitizer (photocatalyst) as an electron donor, enabling LPMOs to function under remarkably mild conditions (Bissaro et al., 2016; Cannella et al., 2016). It's also important to note that the optimal electron donor can fluctuate depending on the specific LPMO type, the reaction conditions, and the substrate that the LPMO is targeting. Therefore, empirical testing is frequently necessary to pinpoint the most suitable electron donor for a specific application.

### 1.3.5 OXYGEN CO-SUBSTRATE

LPMO catalysis is dependent on the availability of an oxygen co-substrate, to supply a oxygen atom that can be radicalized and then attack the C1 or C4 position in the glycosidic bond, resulting in bond cleavage (Vaaje-Kolstad et al., 2010). Although the purpose of the oxygen co-substrate is generally agreed upon, its nature and identity remain subjects of debate within the scientific community (Kuusk et al., 2019).

In their seminal 2010 paper, Vaaje-Kolstad *et al.*, claimed that O<sub>2</sub> was the natural co-substrate for LPMOs, supported by the observation that a single oxygen atom derived from O<sub>2</sub> was incorporated into the final product when acting on a carbohydrate substrate (R-H) in the presence of excess reductant (Vaaje-Kolstad et al., 2010). This is also why LPMOs are generally recognized as monooxygenases (Bissaro et al., 2020; Aachmann et al., 2012). However, the monooxygenase reaction;  $\text{R-H} + \text{O}_2 + 2\text{e}^- + 2\text{H}^+ \rightarrow \text{R-OH} + \text{H}_2\text{O}$  requires a second electron (the first being stored in Cu(I)) and two protons during catalysis. This posed a conundrum considering LPMOs monocopper, organic co-factor-free nature, and the highly restricted access to the active site when bound to a substrate (Bissaro et al., 2020).

Addressing these questions, Bissaro *et al.* published a paper in 2017 suggesting H<sub>2</sub>O<sub>2</sub> as a viable oxygen co-substrate for LPMOs. They demonstrated that LPMOs could efficiently use H<sub>2</sub>O<sub>2</sub> as a source of oxygen atoms in the hydroxylation reaction, thereby classifying LPMOs as a new type of copper-dependent peroxygenases  $\text{R-H} + \text{H}_2\text{O}_2 \rightarrow \text{R-OH} + \text{H}_2\text{O}$  (Bissaro et al., 2017). This finding resolves the "second electron conundrum," as H<sub>2</sub>O<sub>2</sub> supplies both the oxygen, electron, and proton equivalents necessary for a complete catalytic cycle.

It is important to note that O<sub>2</sub>-driven reactions require the delivery of two electrons per catalytic cycle, whereas H<sub>2</sub>O<sub>2</sub>-driven reactions depend on a "priming" reduction of the LPMO and can, once activated, carry out multiple reactions (Bissaro et al., 2017). In other words, O<sub>2</sub>-driven reactions necessitate stoichiometric amounts of reductant relative to the amount of product formed, while H<sub>2</sub>O<sub>2</sub>-driven reactions mostly require only priming amounts of reductant. Nonetheless, H<sub>2</sub>O<sub>2</sub>-driven reactions still need reductant throughout the process, as LPMOs may be sporadically re-oxidized (Eijsink et al., 2019; Kuusk et al., 2019). Additionally, H<sub>2</sub>O<sub>2</sub>-driven reactions occur more rapidly than O<sub>2</sub>-driven reactions (Eijsink et al., 2019).

As of now, both  $O_2$  and  $H_2O_2$  are generally accepted as viable oxygen co-substrates for LPMOs. However, the debate surrounding the nature of the LPMO oxygen co-substrate persists. A major obstacle in determining the true nature of the LPMO co-substrate is that, in the absence of a substrate,  $O_2$  participates in reactions that produce  $H_2O_2$ , either by reacting with a reduced LPMO protein not currently bound to a substrate molecule or by reactions between molecular oxygen and reductant (Loose et al., 2018; Stepnov et al., 2021). In conclusion, it is important to note that the general consensus is that both  $O_2$  and  $H_2O_2$  can serve as legitimate co-substrates for LPMOs, with each being favored under different circumstances. The ongoing debate underscores the need for further research to better understand the nature of LPMO co-substrates and their role in catalysis.

### **1.3.6 LYTIC POLYSACCHARIDE MONOOXYGENASES MECHANISM**

Enzyme mechanisms provide a detailed roadmap of the chemical reactions that facilitate the transformation of a substrate into a product. This process typically involves the substrate's initial binding to the enzyme at the active site, leading to the formation of an enzyme-substrate complex, which then undergoes a series of chemical alterations. When it comes to LPMOs, the sequence of these reactions remains a topic of ongoing scientific debate. The primary hurdle to reaching a consensus is the elusive nature of the oxygen substrate. Thus, despite numerous propositions and extensive review, a definitive mechanism for LPMO catalysis has yet to be established (Chylenski et al., 2019).

However, we can still outline a generalized sequence of events. Before a LPMO can function as a catalyst, it must undergo an activation process. This process, which I have previously detailed, begins with the incorporation of a  $Cu(II)$ -ion from the solution into the active site's T-shaped histidine brace. This incorporation forms an LPMO- $Cu(II)$  complex, which is then reduced by an electron donor to LPMO- $Cu(I)$  (Bissaro et al., 2020). Beyond this point, the specific reactions and sequence of events become less definitive.

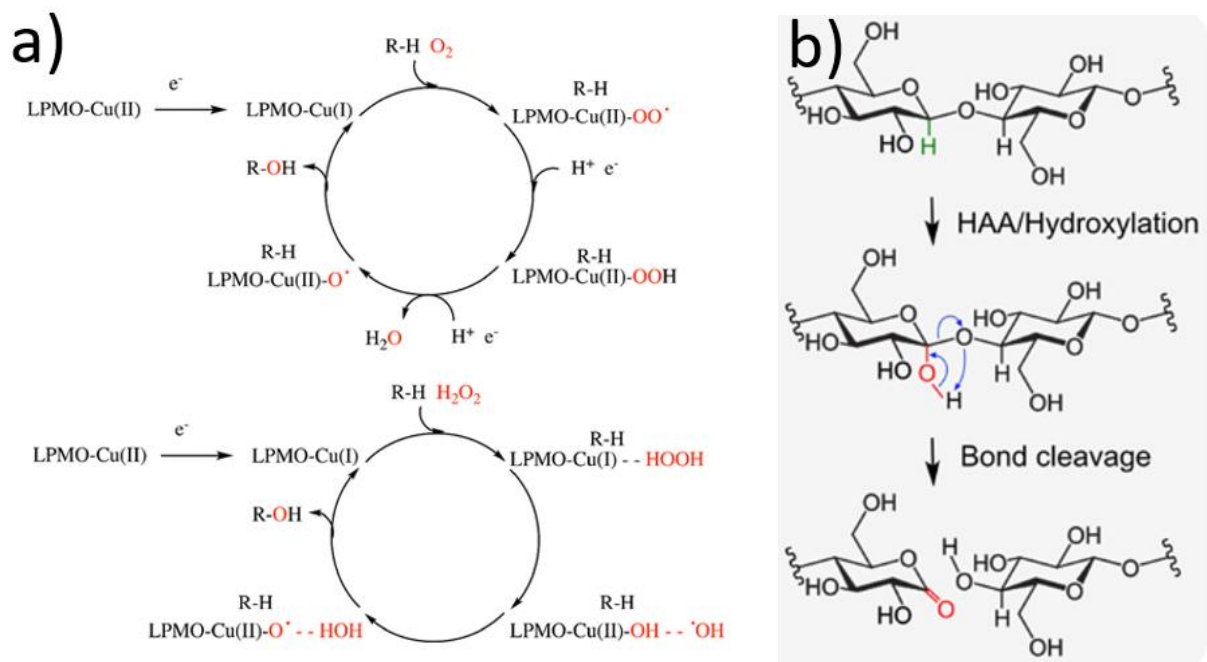


Figure 1-4 **LPMO mechanisms.** *a) Schematic summaries of proposed mechanisms for hydrogen atom abstraction by an LPMO using  $O_2$  (top) or  $H_2O_2$  (bottom) as the co-substrate. Figure and text taken from (Chylenski et al., 2019). b) Schematic presentation of the mechanism of bond cleavage of the scissile glycoside bond after the C1 carbon is attacked by the LPMOs oxygen radical. Figure and text taken from (Eijsink, 2019).*

Two proposed mechanisms under consideration have been included here as examples. One mechanism involves  $O_2$  acting as the co-substrate, while the other involves  $H_2O_2$  in the same role. Both mechanisms are outlined in Fig. 1.4 a, for reference. Notably, both mechanisms result in the creation of an oxygen radical species. These radical leverages potent chemistry to attack either the C1 or C4 carbon in a polysaccharide. The subsequent mechanism for the cleavage of the glycosidic bond in polysaccharides, following the attack of the oxygen radical, is also delineated in Fig. 1.4 b.

### 1.3.7 LYTIC POLYSACCHARIDE MONOOXYGENASE INACTIVATION

The progress curve of an LPMO reaction frequently exhibits nonlinearity, a result of the susceptibility of LPMOs, like other metalloenzymes, to oxidative damage under non-optimal conditions, leading to enzyme inactivation. Separate studies conducted by Loose *et al.*, and Bissaro *et al.*, using O<sub>2</sub> and H<sub>2</sub>O<sub>2</sub> as co-substrates respectively, have concluded that LPMO inactivation generally coincides with oxidative damage to amino acid residues near the copper site (Bissaro *et al.*, 2017; Loose *et al.*, 2018). Moreover, given the ongoing debate on the role of O<sub>2</sub> vs H<sub>2</sub>O<sub>2</sub> in LPMO catalysis, it is crucial to note that the autocatalytic inactivation of LPMOs occurs regardless of the reaction fuel (Chylenski *et al.*, 2019). As mentioned in the earlier section on electron donors, reduced LPMOs have a Cu(I) ion. However, when the reduced LPMO is not bound to a substrate, the Cu(I) ion becomes exposed to the solvent. One theory proposes that this reduced transition metal will, in the absence of a substrate, participate in reactions with O<sub>2</sub> or H<sub>2</sub>O<sub>2</sub>, leading to the eventual formation of reactive oxygen species, possibly including harmful species such as hydroxyl radicals (Chylenski *et al.*, 2019). In the absence of a bound substrate, these species are likely to react with other elements near the catalytic center, such as the copper-coordinating histidine, a phenomenon that was observed by Bissaro *et al.*, (Bissaro *et al.*, 2017).

In line with these observations, Bissaro *et al.*, found that the presence of a substrate indeed protects LPMOs from oxidative inactivation (Bissaro *et al.*, 2017). Further studies have revealed a strong correlation between a LPMO's affinity for its substrate and its stability (Chylenski *et al.*, 2019). It has also been demonstrated that higher substrate concentrations promote LPMO stability (Courtade *et al.*, 2018). Therefore, LPMOs should ideally be in environments with a substantial surplus of substrate to minimize the likelihood of autocatalytic oxidative damage. However, achieving this in practice, especially during industrial bioprocessing of lignocellulosic biomass, can be challenging. Both the quantity and nature of the substrate change throughout the reaction, accelerating enzyme inactivation. Regrettably, in a "typical" bioprocessing reaction catalyzed by an LPMO-containing commercial cellulase cocktail, an LPMO may become inactive during the final stage of the process. This inactivation is particularly unfortunate as the most recalcitrant parts of the substrate remain at this point, marking the time when the LPMO would be most beneficial (Chylenski *et al.*, 2019).

### 1.3.8 PURPOSE OF THIS THESIS

The crux of this master thesis is to expand our understanding of the active site in lytic polysaccharide monooxygenases (LPMOs), where our current knowledge remains limited. Our understanding of the roles of the histidine's in the histidine brace is well established at this point, as is the roles of alanine, tyrosine, and phenylalanine to a lesser degree. However, there is one glutamate /glutamine residue that is structurally conserved throughout the LPMO superfamily, but that is significantly understudied in comparison. This “gatekeeper residue” is hypothesized to regulate access to the active site and “caging” H<sub>2</sub>O<sub>2</sub> positioning during reactions with Cu(I) (Vaaje-Kolstad et al., 2017). The gap in our understanding necessitates further investigation to unravel the molecular mechanism of LPMOs and to explore their potential utility in biotechnological processes. In this context, this thesis will delve into the roles of the conserved Glu/Gln gatekeeper residue in fungal *NcAA9C* from *Neurospora crassa* and bacterial *SmAA10A* from *Serratia marcescens*.

*SmAA10A* also known as CBP21 was chosen for our model enzyme as it is utilized in several studies, including mutational studies focusing on conserved residues in the active site (Bissaro et al., 2020). Therefore, by selecting *SmAA10A*, we are provided with fundamental knowledge and relevant research, that will be invaluable when analyzing our results. In *SmAA10A* the gatekeeper residue is a glutamate (Glu60/E60), that is hypothesized to mediate access to the active site and “caging” the oxygen co-substrate in reactions with Cu(I) (Bissaro et al., 2020).

To investigate the functionality of the gatekeeper we utilized site-directed mutagenesis to produce different *SmAA10A* mutants. The glutamate (Glu/E) in *SmAA10A* was mutated into glutamine (Gln/Q), asparagine (Asn/N), or aspartate (Asp/D). Giving us the *SmAA10A*-E60 mutants, *SmAA10A*-E60Q, *SmAA10A*-E60D and *SmAA10A*-E60N. Notably, both aspartate and asparagine have a shorter carbon chain (one -CH<sub>2</sub>- less) than glutamate and glutamine, thereby placing the polar side-group further away.

Glutamate and aspartate also have an extra carboxyl group on its side chain that tends to lose a proton (H<sup>+</sup> ion) and become negatively charged at physiological pH, classifying both glutamate and aspartate as an acidic amino acid. Glutamine and asparagine both have side chains that contain an amide group (-CONH<sub>2</sub>) and are considered neutral amino acid because the amide group does not lose or gain protons at physiological pH. We mutated the gatekeeper to

investigate if changing the nature of the residue would (i) impact the catalytic potential of the enzyme, or (ii) increase the likelihood of enzyme inactivation.

Due to unforeseen circumstances arising from the COVID-19 pandemic, our *SmAA10A* mutants were lost. This necessitated a shift of focus to premade *NcAA9C* variants from our laboratory supply. In *NcAA9C*-Q164, glutamine (Q) had been mutated into glutamate (E), asparagine (N), or aspartate (D), mirroring the mutations performed on *SmAA10A*. The sole difference was the alteration of Q to E, instead of vice versa. Moreover, enzyme activity assays with different reductants was a target on the *NcAA9C* variants to assess whether a change in the electron donor could influence the catalytic activity. Overall, this thesis aims to significantly augment our understanding of the LPMOs active site by examining the importance of the Glu/Gln “gatekeeper residue”, as well as the implications of electron donor selection on enzyme activity which may have profound implications for biotechnological applications.

## 2 MATERIALS

Table 2-1 Laboratory equipment

<i>EQUIPMENT</i>	<i>SPECIFICATIONS</i>	<i>SUPPLIER</i>
Autoclave	Sterilizer GmbH	CertoClav
Autoclave tape		VWR
Automatic pipettes	0.2-2µl, 1-10µl, 2-20µl, 20-200µl, 100-1000µl, 0.5-5ml, 1-10 ml	Thermo Scientific
Biosafety cabinet	Model: AV-100	Telstar
Blue-cap bottles	1000 ml, 500 ml, 250 ml, 100 ml	VWR, PYREX, SCHOTT DURAN
Bottle top filters	Steritop™ 0,22 µm Steritop™ 0,45 µm	Millipore
Cell density meter	ULTROSPEC® 10	Biochrom
Centrifuge	Centrifuge 5418 R Heraeus multifuge X1R centrifuge Allegra X-30R centrifuge Avanti J-26S XP centrifuge	Eppendorf Thermo scientific Beckman coulter
Centrifuge rotors	JA 10, JA 12,5, JA 25	Beckman
Centrifuge tubes	250 ml, 500 ml, 35 ml	Nalgene
Cryotubes	2 ml	Sarstedt
Culture flasks	2000 ml, 1000 ml	Nalgene
Culture Tube	Glass	
Dry Bath	Mini Dry Bath	Fisher Scientific
Electrophoresis equipment	Vertical electrophoresis tank Power supply	VWR Bio-Rad
Filter plate	96 wells	Thermo Scientific
Freezer (-20 °C)		Bosch, Siemens, Whirlpool
Freezer (-80 °C)	Ultra-Low	SANYO
Fume hood	Zafe 81	Zystm
Gel imager	Gel Doc EZ Imager	Bio-Rad
Glass equipment		Pyrex Schott

Gloves	Nitrile, vinyl	VWR
Greiner tubes	15 ml, 50 ml	VWR
Hot plate magnetic stirrer	IKA® RCT classic safety control	IKA
HPLC system	ICS 3000 ICS 5000	Thermo Scientific
HPLC-columns	CarboPac PA200	Thermo Scientific
HPLC-vail cap	11 mm Snap Ring Cap, tr., Silic. white/PTFE red, 45°C, 1.3mm	VWE
	11 mm combination Seal: PE Snap ring Cap, blue, center hole; silicone white/PTFEblue, 55° shore A, 1.0mm, cross-slitted	Fisher brand
HPLC-vails	0.3ml PP Snap Ring Micro-Vail, 32x11.6mm, transparent	VWR
Ice maker	KF 145	PORKKA
Incubator		Termaks
Inoculation loops	Plastic: 1µl, 10µl	Sarstedt
Liquid chromatography- system	BioLogic LP System	Bio-Rad
Microbalance	CP224S	Sartorius
Parafilm		VWR
Pasteur Pipettes	5 ml	VWR
Petri dish	9 cm	Heger
pH benchtop meter	FiveEasy Plus	Mettler Toledo
Pipette tips	Next Generation Tip Refill	VWR
Protein Concentrators	Amicon® Ultra-15 Centrifugal Filter Unit	Millipore
Reaction tube with conical bottom	1.5 ml, 2 ml, 5 ml	VWR
Refrigerator (4 °C)		Whirlpool
Shaking incubator	INFORS HT Innova®44	VWR Brunswick scientific
Sonicator bath	3510	Branson
Spatula	Metal, plastic	

Spectrophotometer	Cary 8454 UV-Vis	Agilent Technologies
	BioPhotometer D30	Eppendorf
Stain-Free Gels	Any kD, 10-well comb, 30 $\mu$ l	Bio-Rad
	Any kD, 15-well comb, 15 $\mu$ l	
Syringes		
Tabletop centrifuge		Eppendorf
	Mini Star	VWR
	Scanspeed mini	Labogene
Thermomixer	Thermomixer comfort	Eppendorf
	ThermoMixer C	
UVettes	50-2000 $\mu$ L	Eppendorf
Vacuum manifold		Millipore
Water bath	3510	Branson
Weighing boats	Plastic 4x4 cm (S)	VWR
	Plastic 9x9 cm (M)	
	Plastic 14x14 cm (L)	
Weighing scales		Sartorius
Whirlmixer	MS 3 basic	IKA®
	Vortex-genie 2	Scientific industries

Table 2-2 Software for analysis

SOFTWARE	APPLICATION	SUPPLIER
Chromeleon	HPLC	Chromeleon
Chromatography Studio		
ImageLab	Gel visualization	BioRad
LP Data View	LC	BioRad
UV-Visible ChemStation	Spectroscopy	Agilent Technologies

Table 2-3Chemicals

CHEMICAL		SUPPLIER
Acetic acid	CH <sub>3</sub> COOH	Sigma-Aldrich?
Agar-agar		Merck Millipore
Ampicillin sodium salt	C <sub>16</sub> H <sub>18</sub> N <sub>3</sub> NaO <sub>4</sub> S	
β-chitin (72-100 nm particle size)	(C <sub>8</sub> H <sub>13</sub> O <sub>5</sub> N) <sub>n</sub>	
Cellobiose	C <sub>12</sub> H <sub>22</sub> O <sub>11</sub>	Megazyme
Cellopentaose	C <sub>30</sub> H <sub>52</sub> O <sub>26</sub>	Megazyme
Cellotriose	C <sub>18</sub> H <sub>32</sub> O <sub>16</sub>	Megazyme
Chitin beads		
Cystine	C <sub>4</sub> H <sub>5</sub> N <sub>3</sub> O	Sigma-Aldrich
Distilled water, dH <sub>2</sub> O (Milli-Q quality)	H <sub>2</sub> O	Merck Millipore
Ethanol	C <sub>2</sub> H <sub>5</sub> OH	
Ethylenediaminetetraacetic acid (EDTA)	C <sub>10</sub> H <sub>16</sub> N <sub>2</sub> O <sub>8</sub>	Sigma-Aldrich
Gallic acid	C <sub>6</sub> H <sub>2</sub> (OH) <sub>3</sub> COOH	Sigma-Aldric
Hydrogen chloride	HCl	Sigma-Aldric
Hydrogen peroxide	H <sub>2</sub> O <sub>2</sub>	
Imidazole	C <sub>3</sub> H <sub>4</sub> N <sub>2</sub>	
Isopropyl β-D-1-thiogalactopyranoside (IPTG)	C <sub>9</sub> H <sub>18</sub> O <sub>5</sub> S	
Kanamycin	C <sub>18</sub> H <sub>38</sub> N <sub>4</sub> O <sub>15</sub> S	
Sodium chloride	NaCl	VWR
Sodium hydroxide	NaOH	VWR?
Sucrose	C <sub>12</sub> H <sub>22</sub> O <sub>11</sub>	
Super Optimal broth with Catabolite repression (SOC media)	2% tryptone, 0.5% yeast extract, 10 mM NaCl, 2.5 mM KCl, 10 mM MgCl <sub>2</sub> , 10 mM MgSO <sub>4</sub> , and 20 mM glucose.	
Trizma base	C <sub>4</sub> H <sub>11</sub> NO <sub>3</sub>	Sigma-Aldrich
Tryptone		Merck Millipore
Ultra clean water	Milli-Q	Direct16
Yeast extracts		Invitrogen

Table 2-4 Self-made media and buffer

<b>MEDIA</b>	<b>CONTENT</b>
Lysogeny broth (LB) media	20 g Tryptone 5g Yeast extract 10 g NaCl Add dH <sub>2</sub> O to a total volume of 1 L and Autoclave the solution.
Lysogeny broth (LB) media with agar agar added ampicillin for petri dishes	5 g Tryptone 2.5 g Yeast extract 2.5 g NaCl 7.5 g agar Add dH <sub>2</sub> O to a total volume of 500 mL and autoclave the solution. When the solution has cold down adequately (about 50 °C) move it to a biosafety cabinet and add 0.5 mL of 100 mg/mL ampicillin. Lastly, distribute the solution into petri dishes before it solidifies. Store then the petri dishes at 4 °C.
Spheroplast Buffer	10 mL Tris-HCl pH 8.0 17.1 g sucrose 100 µL 0.5 EDTA pH 8.0 1 cOmplete™ Protease Inhibitor Cocktail Tablet, from Roche Add ice-cold dH <sub>2</sub> O to 100 mL

Table 2-5 Bacteria strains

<b>BACTERIA STRAIN</b>	<b>SPECIFICATION</b>	<b>SUPPLIER</b>
Escherichia coli One Shot® BL21 Star™ (DE3)	Chemical competent cells for protein expression	Life Technologies

Table 2-6 Enzymes

ENZYME	SPECIFICATION	SUPPLIER
Lytic polysaccharide monooxygenase (LPMOs)	<i>NcAA9C</i> -WT	Enzymes were produced in <i>Pichia pastoris</i> , and expression strains were made as described by Rieder et al. 2020, unpublished.
	<i>NcAA9C</i> -Q164D	
	<i>NcAA9C</i> -Q164E	
	<i>NcAA9C</i> -Q164N	
	<i>SmAA10A</i> -WT	Self-produced, E-coli strains from strain collection form pep-group, (Bissaro et al., 2020)
	<i>SmAA10A</i> -E60D	
	<i>SmAA10A</i> -E60N	
	<i>SmAA10A</i> -E60Q	
Glycoside Hydrolase	Lysozyme	Provided form the general in-house supply Pep-floor, NMBU.
	<i>SmGH20</i>	Provided form the general in-house supply PEP research group, NMBU. , E-coli strains from strain collection form pep-group.

## 3 METHODS

### 3.1 TRANSFORMING COMPETENT CELLS WITH PLASMID CARRYING *SmAA10A* VARIANTS

Materials:

- Chemical competent *E. coli* cells (One Shot<sup>®</sup> BL21 Star<sup>™</sup> (DE3))
- Plasmid DNA of the *SmAA10A* variants; *SmAA10A-E60*, *SmAA10A-E60Q*, *SmAA10A-E60D* and *SmAA10A-E60N* produced by Bissaro.
- SOC-media
- IPTG
- LB agar plates with ampicillin (100 µg/mL)
- Ampicillin (100 mg/mL)

Method:

Our aim was to generate four variants of the *SmAA10A* protein: the wild type enzyme and three mutants featuring alterations in the gatekeeper residue. The protein production methodology largely followed the protocol outlined by Vaaje-Kolstad *et al.*, (Vaaje-Kolstad *et al.*, 2005b).

Each of the four *SmAA10A* genes, inserted in a pRSETB vector, was independently transformed into a specific strain of competent *Escherichia coli* cells. We employed One Shot<sup>®</sup> BL21 Star (DE3) chemically competent *E. coli* cells, renowned for their proficiency in protein expression.

The competent *E. coli* cells were initially thawed on ice, after which 1 µL of plasmid DNA was gently introduced. The cell-vials were then subjected to an ice bath for a period of 30 minutes to ensure complete absorption. The transformation was subsequently initiated via heat shock. The procedure involved a brief, 30-second incubation at 42 °C followed by an immediate return to the ice bath. Following the thermal treatment, 250 µL of pre-warmed SOC medium was incorporated with the cells.

To stimulate transcription of the *SmAA10A* variant genes, regulated by the lac operator, IPTG was added to the cell solution. Acting as a molecular analogue of allolactose, IPTG promotes the transcription of the lac operon by inhibiting the repression of the β-galactosidase coding gene lacZ (Sigma-Aldrich, 2020). Allolactose is a lactose metabolite integral to this process.

Following the procedures described earlier, the vials containing the cells were placed in a shaking incubator at 37 °C with a shaking speed of 300 rpm for an hour. As a final step, we

dispersed two distinct volumes of the transformed cells - 50 $\mu$ L and the remaining volume - onto separate LB agar plates imbued with ampicillin (concentration: 100  $\mu$ g/mL). The plates were then inverted and incubated overnight at 37 °C in a warming cabinet.

On the subsequent day, a single bacterial colony from each agar plate was carefully isolated and transferred to a fresh set of LB agar plates also containing ampicillin at a concentration of 100  $\mu$ g/mL. These plates were similarly inverted and incubated overnight at 37 °C in the warming cabinet, thereby setting the stage for the next phase of experimentation.

## 3.2 EXPRESSION AND PURIFICATION OF *SmAA10A* VARIANTS

Materials:

- *E. coli* Glycerol stocks with strains expressing *SmAA10A* variants (*SmAA10A-E60*, *SmAA10A-E60Q*, *SmAA10A-E60D*, and *SmAA10A-E60N*)
- LB media
- Ampicillin (100 mg/mL)

Method:

Our objective was to cultivate bacteria that had successfully incorporated vectors harboring the *SmAA10A* variant genes, and subsequently stimulate them to express the encoded LPMO. First, the transformed cells from Section 3.1 were introduced into approximately 300 mL of LB media fortified with ampicillin at a concentration of 100 mg/mL. The pRSET vector is designed to also incorporate an antibacterial resistance gene, thereby ensuring survival only of those cells which have successfully integrated one of the pRSET vectors in the ampicillin-infused medium.

The bacterial culture was then incubated at 37 °C with a shaking speed of 200 rpm for an uninterrupted duration of 20 hours. Following incubation, the cells were harvested through a centrifugation process using a JA10 rotor. The centrifuge was set to 8000rpm at a temperature of 4 °C and the procedure lasted for 10 minutes. Subsequently, the supernatant was carefully decanted, and the resultant cell pellet was stored at -20 °C for future processing.

### 3.3 PERIPLASMIC EXTRACTION

#### Materials:

- Cell pellets (referring to Section 3.2)
- Spheroplast buffer
  - 10 mL 1 M Tris-HCl pH 8.0
  - 17.1 g sucrose
  - 100  $\mu$ L 0.5 M EDTA pH 8.0
  - 1 cOmplete<sup>TM</sup> Protease Inhibitor Cocktail Tablet, from Roche
  - Add ice-cold dH<sub>2</sub>O to 100 mL
- 20 mM MgCl<sub>2</sub>
- Ice-cold dH<sub>2</sub>O

#### Method:

To extract the *SmAA10A* proteins from the *E. coli* cells, a periplasmic extraction procedure was performed. The pRSET B\_*SmAA10A* vectors carry a signal peptide attached to the *SmAA10A* variant gene, which prompts the translocation of *SmAA10A* variant from the cytoplasm to the periplasmic space. This periplasmic space refers to the area sandwiched between the cytoplasmic membrane and the outer membrane in Gram-negative bacteria, such as *E. coli*. The proteins residing in the periplasmic space were then released by applying a "cold osmotic shock" process, resulting in the elimination of the outer membrane.

Each cell pellet was first resuspended in 25 mL of spheroplast buffer. Subsequently, the suspensions were transferred to 35 mL centrifuge tubes and briefly incubated on ice for 5 minutes. The tubes were then centrifuged at 8000 rpm (4 °C) for 10 minutes. After centrifugation, the cell pellets were left to stand at room temperature for another 10 minutes. Each pellet was then resuspended in 15 mL of ice-cold deionized water (dH<sub>2</sub>O). Following this, the tubes were subjected to a brief 45-second incubation period on ice prior to the addition of 1.5 mL of MgCl<sub>2</sub> (20 mM). After this, the tubes underwent another round of centrifugation at 8000 rpm (4 °C) for 10 minutes. The resulting supernatant was then filtered (0.45 $\mu$ m), and the resultant extract was stored at 4 °C for subsequent purification steps.

### 3.4 CHITIN BEAD AFFINITY CHROMATOGRAPHY

#### Materials:

- Periplasmic extracts (referring to Section 3.3)
- Ammonium sulfate (3 M)
- Chitin beads
- Column
- Buffer A: Tris-HCL (50 mM pH 8.0), Ammonium sulfate (1M)
- Buffer B: Acetic acid (20 mM)
- 20 % ethanol

#### Method:

The *SmAA10A* proteins were isolated using chitin affinity chromatography, leveraging the inherent chitinolytic properties of *SmAA10A* variants to distinguish them from residual cellular material. The periplasmic extracts were initially adjusted to Buffer A, and care was taken to administer ammonium sulfate gradually to prevent sample compromise. Our chromatographic setup consisted of a column packed with 10 mL of chitin beads, linked to a UV detector. Data collection and visualization of chromatographic readings were facilitated by the BioLogic LP Data View software. Prior to initiating the chromatographic process, the UV lamp was activated, and the flow rate set to 2.5 mL/min.

The protocol began with washing the column with Buffer A until a stable UV baseline was achieved. Subsequently, the periplasmic extract solution was applied to the column. The chitinolytic *SmAA10A* enzymes were then retained within the chitin bead packing material. At this juncture in the chromatogram, a broad peak indicative of impurities was observed. Next, the column was rinsed again with Buffer A until a new UV baseline was established, indicating the removal of impurities. The enzyme was dislodged from the stationary phase when the column was flushed with Buffer B. In the chromatograms, the eluted proteins emerged as a tall, narrow peak. The volume corresponding to this peak, which encompassed the *SmAA10A* variant proteins, was collected separately. The flow-through preceding the application of periplasmic extract onto the column and the post-application flow-through until Buffer B was run were collected separately. As a final step, the column was washed with 20% ethanol for about 10 minutes to eradicate any lingering impurities and was then stored at 4 °C. This entire process was individually repeated with new columns for each *SmAA10A* variant.

### 3.5 SODIUM DODECYL SULFATE-POLYACRYLAMIDE GEL ELECTROPHORESIS (SDS-PAGE)

#### Materials:

- Purified protein (referring to Section 3.4)
- SDS-PAGE working solution
  - 6.3  $\mu\text{L}$  NuPAGE<sup>®</sup> LDS Sample Buffer (4x)
  - 2.5  $\mu\text{L}$  NuPAGE<sup>®</sup> Reducing Agent (10x)
  - 11.2  $\mu\text{L}$  dH<sub>2</sub>O
- NuPAGE<sup>®</sup> 10 % Bis-Tris Gel 1.0 mm x 10 wells or - NuPAGE<sup>®</sup> 10 % Bis-Tris Gel 1.0 mm x 15 wells
- BenchMark<sup>™</sup> Protein Ladder
- SDS Running buffer (Tris/Glycine/SDS Buffer)

#### Method:

To assess the success of the purification process, we performed sodium dodecyl sulfate-polyacrylamide gel electrophoresis (SDS-PAGE). This discontinuous electrophoretic system is specialized in separating proteins based on their molecular mass. Generally, the process comprises gel preparation, sample preparation, electrophoresis, protein staining or Western blotting, and analysis of the resultant banding pattern. In this case, we utilized a pre-made gel, thus eliminating the need for gel preparation. However, comprehensive sample preparation was performed.

Initially, 5  $\mu\text{L}$  of the sample solution was combined with a working solution made up of 6.3  $\mu\text{L}$  NuPAGE<sup>®</sup> LDS Sample Buffer, 2.5  $\mu\text{L}$  NuPAGE<sup>®</sup> Reducing Agent, and 11.2  $\mu\text{L}$  deionized water (dH<sub>2</sub>O). The mixed solution was then heated to 95 °C for 5 minutes using a thermomixer. This heating disrupted the protein's secondary and tertiary structures by breaking hydrogen bonds and elongating the molecules. The NuPAGE<sup>®</sup> Reducing Agent assisted in dismantling disulfide bridges. Once the solution cooled to room temperature, approximately 20  $\mu\text{L}$  of each sample was pipetted into separate wells in the pre-submerged gel contained within an electrophoresis apparatus. In addition, a 12  $\mu\text{L}$  protein ladder, used to approximate the mass of fragments during electrophoresis, was also loaded onto the gel. The gel was subsequently connected to a power source with positive and negative terminals.

Upon application of a 220V voltage, electrophoresis commenced. This process enabled the migration of negatively charged molecules through the gel towards the positively charged electrode, with the molecules moving at varying speeds based on their sizes. Smaller molecules

traversed the gel more quickly, as they navigated the gel matrix more effectively than larger molecules. The electrophoresis proceeded for 32 minutes at 400 mA. Following electrophoresis, the gel was rinsed and submerged in water on a green tray. We utilized the Bio-Rad gel documentation system for imaging. This system produced an image illustrating fragment distribution by size, where band intensity correlated to fragment concentration. Given that *SmAA10A* has a molecular weight of 18.8 kDa, a successful purification would manifest as a single intense band around this marker.

### 3.6 DETERMINING PROTEIN CONCENTRATION - $A_{280}$

Material:

- Isolated *SmAA10A* variants (referring to Section 3.5)
- Buffer
- UVette

Method:

The determination of protein concentration was accomplished using a UV spectrophotometer. The principle of UV spectroscopy is based on the property of specific compounds to absorb UV light at particular wavelengths. Through quantifying the absorption of light ( $A$ ), the molar concentration ( $c$ ) can be inferred by employing Beer-Lambert's law,

$$A = \epsilon cl$$

where  $\epsilon$  is the molar absorbance coefficient and  $l$  is the optical path length.

The three aromatic amino acids, phenylalanine, tyrosine, and tryptophan, all absorb UV light and exhibit absorption maxima at 257 nm, 274 nm, and 280 nm, respectively. We utilized a spectrophotometer set to the wavelength of 280 nm to evaluate the protein concentration. Before measuring absorbance, however, the samples required dilution to avoid surpassing the instrument's detection range. The exact dilution factor varied slightly and needed to be determined experimentally. Instrument preparation began with running a blank, comprised solely of the buffer. This blank enabled the spectrophotometer to account for and negate the extra absorbance introduced by the solution in which the protein was suspended. Following this, each sample's absorbance was measured. The obtained absorbance values were then multiplied by the dilution factor. The protein concentrations could subsequently be determined by incorporating these absorbance values into Beer-Lambert's law.

### 3.7 COPPER-SATURATING *SmAA10A* VARIANTS

Material:

- Isolated *SmAA10A* variants (referring to Section 3.4)
- $\text{CuSO}_4$
- Protein Concentrator 10K MWCO
- Bis-Tris 50 mM

Method:

The activity of LPMOs are contingent on the availability of a copper ion in its active site. To ensure that each enzyme in the solution is activated, we saturated the purified samples from Section 3.4 with copper.  $\text{CuSO}_4$  was initially added to the samples to achieve a final  $\text{CuSO}_4$  concentration three times that of the initial LPMO concentration. The samples were then chilled on ice for an hour. Since excess copper could initiate unintended side reactions, it was necessary to eliminate the surplus copper from the solution. To achieve this, we utilized Protein Concentrators, single-use ultrafiltration centrifugal devices with a molecular weight cutoff membrane. Given that *SmAA10A* has a molecular weight of 18.8 kDa, we used Protein Concentrators with a MWCO of 10,000.

The first step was to rinse the Protein Concentrator with 15 mL of 50 mM Bis-Tris buffer by centrifuging at 3500 rpm at 4 °C for 20-30 minutes, discarding the run-through afterward. The sample was then transferred into the Protein Concentrator. If required, the volume was adjusted to approximately 15 mL with the addition of Bis-Tris buffer (50 mM). The Protein Concentrator was centrifuged (3500 rpm, 4°C) until only about 1 mL remained in the upper chamber. If the sample volume exceeded 15 mL, this step was repeated. Subsequently, the solution was washed by adding buffer to the upper chamber and concentrating it. This process was repeated thrice. The remaining solution in the upper chamber was then collected and stored at 4 °C. The run-through from all but the first wash was also collected and stored at 4°C. To confirm that the protein remained in the upper chamber, we performed an SDS-PAGE (like we did in Section 3.5) with the proteins and their run-throughs. Finally, UV-spectroscopy was used to determine the protein concentrations (in the same way as in Section 3.6).

### 3.8 PRE-CULTURE CULTURE OF TRANSFORMED *E. coli* BL21 (DE3) WITH PLASMID CARRYING *SmAA20* GENE

Material:

- Glycerol stock with *SmGH20 E.coli* BL21. DE3, pET – 30Xa/ LIC, kanamycin /IPTG okt 2016 from the lab supply
- LB-medium
- Kaanmycin (50 mg/mL)
- Shaking incubator

Method:

*SmGH20* is an enzyme from *Serratia marcescens* that belongs to family 20 of the glycosidic hydrolases. *SmGH20* is one of the last enzymes in the chitin degradation pathway of *S. marcescens*. The pre-culture of *E. coli* BL21 (DE3) was initiated in a sterile biosafety cabinet. The process involved preparing a sterile culture tube, to which 5 mL of LB medium and 5  $\mu$ L of kanamycin (50 mg/mL) was added. A sterile inoculation loop was then employed to transfer cells from the glycerol stock containing the mutant *E. coli* strain into the LB medium fortified with 100  $\mu$ g/mL kanamycin. The prepared pre-culture was subsequently incubated overnight at 37 °C with agitation set to 150 rpm in a shaking incubator.

### 3.9 CULTIVATION OF *E.coli* IN SHAKER FLASK AND EXPRESSION OF *SmGH20*

Material:

- Pre-culture (from Section 3.8)
- IPTG (Isopropyl  $\beta$ -D-1-thiogalactopyranoside), 1M

Method:

To commence the cultivation in a shaker flask, 2.5 mL of the pre-culture was transferred into a flask containing 250 mL of LB medium supplemented with kanamycin (100  $\mu$ g/mL). The flask was then placed in a shaking incubator and incubated at 37 °C until the optical density reached 0.5. This was followed by the addition of IPTG (1M) to a final concentration of 0.1 mM, thereby triggering the expression of *SmGH20*. Finally, the culture was allowed to incubate further at 30 °C for a duration of 3 hours.

### 3.10 HARVEST OF *SmGH20*

#### Material:

- Culture from (Section 3.9)
- Tris-HCl (100 mM, pH 8)
- Tris-HCl (100 mM, pH 8) with lysozyme (1 mg/mL)
- Microfluidizer
- 20 % Ethanol
- dH<sub>2</sub>O
- Bis-tris (50 mM)
- Ni-NTA column
- Tris-HCl (100 mM, pH 8), with Imidazole (20mM)
- Tris-HCl (100 mM, pH 8), with Imidazole (1M)
- Sanke skin tube – thermo scientific (10 kD cutoff)

#### Method:

Cells from the culture (from Section 3.9) were subjected to centrifugation at 8000 rpm for 10 minutes. The cell pellets were then resuspended in Tris-HCl (100 mM, pH 8), with lysozyme (1 mg/mL) to a total volume of 20 mL and incubated at room temperature for 20 minutes. Following this, Tris-HCl (100 mM, pH 8) was added to increase the total volume to 100 mL. The solution was then chilled on ice.

Subsequently, the cells were lysed using a microfluidizer, a high-pressure homogenization instrument that disrupts cell structures by guiding the material through microchannels under high pressure (1500 psi for *E. coli*). This process exposes the material to forces such as shear, impact, and energy dissipation. A chamber with a Z-geometry was used for this process as it is particularly effective for cell disruption (Microfluidics, 2020). The system was rinsed with dH<sub>2</sub>O before sample introduction and with 20% ethanol after the sample was collected, after which the sample was placed back on ice.

Next, the sample was centrifuged at 1100 rpm for 20 minutes, after which the supernatant was filtered using a 0.22 µm filter. The concentration of *SmGH20* in the sample was determined using UV-spectroscopy, prior to proceeding to purification via affinity chromatography. The method followed for this was similar to that for *SmAA10A* purification (Section 3.4), but with a few differences. The columns used were instead packed with Ni-NTA, the washing buffer

consisted of Tris-HCl (100 mM, pH 8), with Imidazole (20mM), and the elution buffer comprised of -Tris-HCl (100 mM, pH 8), with Imidazole (1M). The sample was loaded at a flow rate of 0.5 ml/min.

The purified sample was then concentrated using protein concentrators. Despite the sample's slight viscosity making this process challenging, it was successfully completed. Following this, the sample was dialyzed. This should ideally have been done immediately after microfluidization, but it was inadvertently skipped. The sample was poured into a "snake skin" tube and submerged in Bis-Tris buffer (50 mM) overnight. This process was carried out at 4 °C with two changes of buffer during the dialysis. The sample was then concentrated once more. To assess the purity and concentration of the sample, SDS-PAGE and UV-spectroscopy were performed respectively (as described in Sections 3.5 and 3.6 respectively).

### 3.11 CONFIRMING ACTIVITY IN THE *SmAA10A* WILD TYPE AND GATEKEEPER MUTANTS.

Material:

- Thermomixer
- Vacuum manifold
- dH<sub>2</sub>O
- *SmAA10A*-E60/wild type, *SmAA10A*-E60D, *SmAA10A*-E60N, *SmAA10A*-E60Q (50 mM) from Section 3.7
- Bis-Tris buffer (500 mM)
- β-chitin (50 g/L)
- Ascorbic acid (50 mM)
- NaOH (200 mM)
- *SmGH20* (50 μM) from lab supply.
- Chitobionic acid (A2<sup>ox</sup>) standards (10-300 μM)

Method:

Our study initiated with the execution of time course activity assays, designed to confirm the functionality and viability of the *SmAA10A* variants for subsequent investigations. Time course activity assays are scientific methods employed to evaluate enzyme activity, thereby signifying the amount of active enzyme available. In biochemical terms, enzyme activity refers to the amount of substrate transformed per unit time, essentially computed as the product of rate and reaction volume. The setup for our time course activity assay reactions was deliberately

consistent, designed to maintain a concentration of 50 mM BisTris, 1  $\mu$ M LPMO, 1 mM ascorbic acid, and a substrate concentration in the range of 15-2.5 g/L  $\beta$ -chitin. The total volume for these reactions was held constant at 200  $\mu$ L. The experiments were designed with two variables: the type of LPMO (*SmAA10A-E60* (wild type), *SmAA10A-E60D*, *SmAA10A-E60N*, or *SmAA10A-E60Q*), and the substrate concentration of  $\beta$ -chitin (15 g/L, 7.5 g/L, and 2.5 g/L).

The reaction mixture was initially formulated by blending 4  $\mu$ L of LPMO (50 $\mu$ M) with 20  $\mu$ L of BisTris (500 mM). Depending on the designated substrate concentration, 60  $\mu$ L, 30  $\mu$ L, or 10  $\mu$ L of  $\beta$ -chitin (50 g/L) was added, followed by 122  $\mu$ L, 142  $\mu$ L, or 161  $\mu$ L of dH<sub>2</sub>O, respectively. Both the prepared reaction mixture and the negative control were placed in a thermomixer set at 37 °C and 1000 rpm. The reaction was then initiated by the addition of 4  $\mu$ L of ascorbic acid (50 mM). We paused the reaction at 5 min, 10 min, 20 min, 60 min and 180-minute intervals, extracting 25  $\mu$ L aliquots which were then heat-inactivated at 100 °C for 10 minutes.

Subsequently, we introduced 5  $\mu$ L of *SmGH20* (50  $\mu$ M) to each 25  $\mu$ L aliquot, incubating them at 37 °C over-night. This was followed by the addition of 70  $\mu$ L of NaOH (200 mM), after which the aliquots were filtered using a vacuum manifold. We then transferred 80  $\mu$ L of each reaction into HPLC vials, which were then preserved at -20 °C for subsequent high-performance liquid chromatography (HPLC) analysis.

Prior to the ion chromatographic analysis, we prepared standards of oxidized dimers (A2<sup>ox</sup>) at concentrations of 300  $\mu$ M, 150 $\mu$ M, 75  $\mu$ M, 50  $\mu$ M, and 10  $\mu$ M. Each HPLC vial, set aside for standard solutions, contained 50  $\mu$ L of the specific concentration diluted in 200  $\mu$ L of NaOH (200 mM).

### 3.12 DETERMINING THE OPTIMAL SUBSTRATE CONCENTRATION FOR *SMAA10A* VARIANTS

#### Material:

- *SmAA10A*-E60 /wild type (50 mM)
- Thermomixer
- Vacuum manifold
- dH<sub>2</sub>O
- Bis-Tris buffer (500 mM)
- $\beta$ -chitin (50 g/L)
- Ascorbic acid (50 mM)
- NaOH (200 mM)
- *SmGH20* (27  $\mu$ M)
- Chitobionic acid (A2<sup>ox</sup>) standards 10-300  $\mu$ M

#### Method:

In order to ascertain the optimal substrate concentration for subsequent experiments with *SmAA10A*, we conducted time course activity assays using the *SmAA10A*-E60 (wild type) and four different concentrations of  $\beta$ -chitin. The methodological framework applied here paralleled the one detailed in Section 3.11, albeit with some distinctions. The first variance is that our scope was limited to the *SmAA10A*-E60/wild type protein only. Secondly, we experimented with distinct  $\beta$ -chitin concentrations, namely 15 g/L, 10 g/L, 6 g/L, and 2.5 g/L.

The reaction mixture was prepared by combining 4  $\mu$ L of 50 $\mu$ M LPMO with 20  $\mu$ L of 500 mM BisTris. The  $\beta$ -chitin and dH<sub>2</sub>O quantities were adjusted according to the required  $\beta$ -chitin concentration. For a concentration of 15 g/L  $\beta$ -chitin, we added 60  $\mu$ L of 50 g/L  $\beta$ -chitin and 112  $\mu$ L of dH<sub>2</sub>O. For a concentration of 10 g/L  $\beta$ -chitin, the blend included 40  $\mu$ L of 50 g/L  $\beta$ -chitin and 132  $\mu$ L of dH<sub>2</sub>O. To achieve a concentration of 6 g/L  $\beta$ -chitin, we combined 24  $\mu$ L of 50 g/L  $\beta$ -chitin with 148  $\mu$ L of dH<sub>2</sub>O. Lastly, for a concentration of 2.5 g/L  $\beta$ -chitin, we mixed 10  $\mu$ L of 50 g/L  $\beta$ -chitin and 162  $\mu$ L of dH<sub>2</sub>O. Also, 5  $\mu$ L of 27 $\mu$ M *SmGH20* was added to each aliquot, and incubated over-night at 37 °C.

The time points for halting the reactions were also altered, and we opted for intervals of 30 min, 60min, 90min, 120min, and 150 minutes. Aside from these modifications, the rest of the procedure mirrored the methodology laid out in Section 3.11.

### 3.13 DETERMINING *SmAA10A* VARIANT ACTIVITY WITHOUT ELECTRON DONOR

#### Material:

- Thermomixer
- Vacuum manifold
- dH<sub>2</sub>O
- *SmAA10A*-E60/wild type, *SmAA10A*-E60D, *SmAA10A*-E60N, *SmAA10A*-E60Q (50 mM).
- Bis-Tris buffer (500 mM)
- $\beta$ -chitin (50 g/L)
- NaOH (200 mM)
- *SmGH20* (50  $\mu$ M)
- Chitobionic acid (A2<sup>ox</sup>) standards 10-300  $\mu$ M

#### Method:

Time course activity assays with *SmAA10A* variants were performed without added electron donor, to evaluate the electron donor dependency of LPMOs. The methodological framework applied here paralleled the one detailed in section 3.11, albeit with some distinctions. The first variance is that we did not add ascorbic acid. Each reaction had had a total volume of 200 $\mu$ L containing 10 g/L  $\beta$ -chitin, 1 $\mu$ M LPMO and 50mM Bis Tris buffer.

The time points for halting the reactions were also altered, and we opted for intervals 30 min, 60 min, 90 min, 120 min and 150 min. Aside from these modifications, the rest of the procedure mirrored the methodology laid out in section 3.11.

### 3.14 DETERMINING THE ACTIVITY OF *SmAA10A* VARIANTS UNDER *in-situ* PEROXIDASE CONDITIONS

#### Material:

- Thermomixer
- Vacuum manifold
- dH<sub>2</sub>O
- *SmAA10A*-E60/wild type (50 mM)
- Bis-Tris buffer (500 mM)
- $\beta$ -chitin (50 g/L)
- Ascorbic acid (50 mM)
- NaOH (200 mM)
- *SmGH20* (27  $\mu$ M)
- Chitobionic acid (A2<sup>ox</sup>) standards 10-300  $\mu$ M

#### Method:

To determine the activity of *SmAA10A* variants under *in-situ* peroxidase conditions time course activity assays was performed as described in section 3.11, but with some differences. Firstly  $\beta$ -chitin (10 g/L) and ascorbic acid (1mM) in Bis-tris buffer (50 mM, pH 6.5) was incubated with *SmAA10A* variant (1 $\mu$ M) at 37 °C in a thermomixer (1000 rpm), for varying amounts of time (30 min, 60 min, 90 min, 120 min, and 150 min). Aside from these modifications, the rest of the procedure mirrored the methodology laid out in section 3.11.

### 3.15 DETERMINING ACTIVITY FOR *SmAA10A* WILD TYPE AND GATEKEEPER MUTANTS WITH ADDED H<sub>2</sub>O<sub>2</sub> – FIRST SETUP.

#### Material:

- *SmAA10A*-E60, *SmAA10A*-E60Q, *SmAA10A*-E60D, *SmAA10A*-E60N (5 μM)
- Thermomixer
- Vacuum manifold
- dH<sub>2</sub>O
- Bis-Tris buffer (500 mM)
- β-chitin (50 g/L)
- Ascorbic acid (500 μM)
- H<sub>2</sub>O<sub>2</sub> (1 mM)
- NaOH (200 mM)
- *SmGH20* (50 μM)
- Chitobionic acid (A2<sup>ox</sup>) standards 10-300 μM

#### Method:

Time course activity assays with *SmAA10* variants were performed with different added concentrations of hydrogen peroxide, to evaluate the second of the oxygen co-substrates of LPMOs. The methodological framework applied here paralleled the one detailed in Section 3.11, albeit with some distinctions. The first variance is that we add H<sub>2</sub>O<sub>2</sub> (5μM, 10μM, 20μM, 50μM and 100μM).

Each reaction had had a total volume of 200μL containing β-chitin (6 g/L), LPMO (0.1μM), ascorbic acid (500 μM), Bis-Tris buffer (50mM, pH 6.5), and H<sub>2</sub>O<sub>2</sub> (5μM, 10μM, 20μM, 50μM and 100μM). The time points for halting the reactions were also altered, and we opted for intervals of 60 sec, 90 sec, 120 sec, 150 sec, and 180 seconds. Aside from these modifications, the rest of the procedure mirrored the methodology laid out in section 3.11.

### 3.16 DETERMINING ACTIVITY FOR *SmAA10A* WILD TYPE AND GATEKEEPER MUTANTS WITH ADDED H<sub>2</sub>O<sub>2</sub>-SECOND SETUP.

#### Material:

- *SmAA10A*-E60, *SmAA10A*-E60Q, *SmAA10A*-E60D, *SmAA10A*-E60N (50 μM)
- Thermomixer
- Vacuum manifold
- dH<sub>2</sub>O
- Bis-Tris buffer (500 mM)
- β-chitin (50 g/L)
- Ascorbic acid (500 μM)
- H<sub>2</sub>O<sub>2</sub> (1 mM)
- NaOH (200 mM)
- *SmGH20* (50 μM)
- Chitobionic acid (A2<sup>ox</sup>) standards 10-300 μM

#### Method:

Time course activity assays with *SmAA10A* variants were performed with hydrogen peroxide. The experimental framework was similar to what was described in Section 3.11, but with some differences. Individual reactions with *SmAA10A* wild type and the gatekeeper mutant (E60Q, E60D, and E60N) was performed. The reaction setup was that H<sub>2</sub>O<sub>2</sub> (100μM), β-chitin (10 g/L), Ascorbic acid (20μM) in Bis-tris (50mM, pH 6.5) was incubated with *SmAA10A* variant (1μM) at 37 ° C. The reaction volume was 200 μl. Another difference was that we used the time points, 30 sec, 60 sec, 90 sec, 120 sec, and 150 seconds. Other than that the reaction setup is identical to the one described in Section 3.11.

### 3.17 *SmAA10A* WILD TYPE AND GATEKEEPER MUTANTS ACTIVITY IN THE PRESENCE OF HRP UNDER IN-SITU PEROXYGENASE CONDITIONS.

#### Material:

- Thermomixer
- Vacuum manifold
- dH<sub>2</sub>O
- *SmAA10A*-E60, *SmAA10A* E60D, *SmAA10A* E60N, *SmAA10A* E60Q (50 mM)
- Bis-Tris buffer (500 mM)
- $\beta$ -chitin (50 g/L)
- Ascorbic acid (50 mM)
- HRP (11.36  $\mu$ M)
- NaOH (200 mM)
- Amplex<sup>TM</sup> red
- *SmGH20* (50  $\mu$ M)
- Chitobionic acid (A2<sup>ox</sup>) standards 10-300  $\mu$ M

#### Method:

In our endeavor to investigate the oxygen co-substrate of *SmAA10A*, we introduced an additional enzyme, horseradish peroxidase (HRP), into our experimental setup. This enzyme competes for hydrogen peroxide with the LPMO, thus allowing us to evaluate its influence.

To conduct this study, we employed time course activity assays with *SmAA10A* variants and HRP, emulating the methodology outlined in Section 3.11, albeit with some modifications. Our experiment was designed to comprise four reaction setups. Each setup maintained consistent conditions of  $\beta$ -chitin (10 g/L), BisTris (50 mM), LPMO (1  $\mu$ M), with varying HRP concentrations (2  $\mu$ M, 1  $\mu$ M, 0.5  $\mu$ M and 0.25  $\mu$ M). Lastly, 4  $\mu$ L each of AcsA (50 mM), and Amplex<sup>TM</sup> Red was and mixed, an added last to initiate the reaction. These reactions were balanced with dH<sub>2</sub>O to attain a total volume of 200  $\mu$ M. Reaction aliquots of 25  $\mu$ L were extracted at regular intervals of 30 min, 60 min, 90 min, 120 min, and 150 minutes. This methodology was implemented for both the *SmAA10A* wild type and the gatekeeper mutants. Other than that, the reaction setup is identical to the one described in Section 3.11.

### 3.18 *NcAA9C* WILD TYPE AND GATEKEEPER MUTANTS ACTIVITY IN THE PRESENCE OF DIFFERENT ELECTRON DONORS UNDER IN-SITU PEROXYGENASE CONDITIONS.

#### Material:

- Thermomixer
- dH<sub>2</sub>O
- *NcAA9C*-Q164, *NcAA9C*-Q164D, *NcAA9C*-Q164E, *NcAA9C*-Q164N (10 μM)
- Bis-Tris (500 mM)
- Cellopentaose (10 mM)
- Ascorbic acid (5 mM)
- Gallic acid (5 mM)
- Cystine (5 mM)
- NaOH (200 mM)
- Cellobiose (DP2<sup>ox</sup>) standards
- Cellotriose (DP3<sup>ox</sup>) standards

#### Method:

We conducted time course activity assays to examine the influence of the active site's gatekeeper residue mutation on enzyme activity and reductant selectivity. Time course activity assays are lab procedures used to measure enzyme activity, indicating the quantity of active enzyme present. Enzyme activity is the quantity of substrate transformed per time unit, calculated as rate multiplied by reaction volume.

The activity assay reactions were consistently set up with cellopentaose (1mM), Bis-Tris buffer (50mM, pH 6.5), LPMO (1 μM) and reductant (1 mM), with a total volume of 200 μL. The reactions were prepared with two variables: the Reductant (Ascorbic acid, Gallic acid, and cystine) and the LPMO (*NcAA9C*-Q164/wild type, *NcAA9C*-Q164D, *NcAA9C*-Q164E, and *NcAA9C*-Q164N).

Initially, we mixed 116 μL dH<sub>2</sub>O, 20 μL BisTris (500 mM), 20 μL cellopentaose (10 mM), and 4 μL LPMO (50 μM). Then, 20 μL of this solution was transferred to a new vial with 5 μL H<sub>2</sub>O as a negative control. This control was used to check for any enzyme activity independent of the reductant. Both the reaction mixture and the negative control were placed on a thermomixer at 37 °C and 750 rpm. To start the reaction, we added 35 μL of the reductant to the reaction mixture. At the time intervals of 10 min, 30 min, 60 min, 120 min, and 180 min, we added 25 μL of the reaction mixture to 175 μL of NaOH (200 mM) in an HPLC vial, thus stopping the

reaction. The same process was applied to the negative control after 180 min. The reactions were then stored at -20 °C.

Before ion chromatographic analysis, we prepared cellobiose (DP2<sup>ox</sup>) and cellotriose (DP3<sup>ox</sup>) standards with concentrations of 450 μM, 300 μM, 150 μM, 75 μM, and 25 μM. One HPLC-vial with the standard contained 25 μL cellobiose and 25 μL cellotriose of the same concentration in 200 μL of NaOH (200 mM).

### 3.19 PRODUCT ANALYSIS BY ION CHROMATOGRAPHIC SYSTEM (ICS)

Materials:

- LPMO reactions (from Sections, 3.11-3.18)
- Dionex Bio-LC (ICS 3000) equipped with a CarboPac 200 column
- Pulsed amperometric detector (PAD)
- Gold electrode
- Eluents for oligosaccharide analysis:
  - Buffer A: Degassed NaOH (0.1 M)
  - Buffer B: Degassed NaOH (0.1 M), NaCH<sub>3</sub>COOH (1 M)
  - Buffer C: Degassed dH<sub>2</sub>O

Method:

Our primary tool for quantifying the concentration of oxidized product was high performance anion exchange chromatography monitored by a pulsed amperometric detector (HPAEC-PAD). This technique capitalizes on the principle of anion exchange chromatography, wherein substances are separated based on their charge. The column of the HPAEC houses a strong anion-exchange stationary phase which retains negatively charged ions.

Given that carbohydrates, similar to other weak acids, transform into oxyanions at high pH levels, HPAEC-PAD demonstrates exceptional efficiency in their separation (Corradini et al., 2012). Furthermore, the magnitude of a carbohydrate's negative charge scales with the number of sugar units present in an oligosaccharide, consequently leading to staggered retention times for dimers, trimers, tetramers, pentamers, and so on.

To prepare for the HPLC run, we prepared and degassed three buffers with nitrogen: Buffer A consisting of NaOH (0.1 M), Buffer B with NaOH (0.1) M and NaCH<sub>3</sub>COOH (1 M), and Buffer C composed of dH<sub>2</sub>O. Subsequently, we created a new sequence in the Chromeleon Chromatography Studio. The sequence began with three blanks, followed by the first set of three standards, the first half of the samples, the second set of standards, the second half of the samples, the third set of standards, and a final blank. The instrument's flow was calibrated to 0.5 ml/min.

During each run, weak acids yield H<sup>+</sup> to NaOH and transition into oxyanions. The oligosaccharides, based on their charge, separate at this stage. These weak acid carbohydrates are then subjected to forced electrocatalytic oxidation at the gold electrode through the application of a positive potential. The carbohydrates are detected by quantifying the electrical current emanating from their oxidation at the surface of the gold electrode (Rohrer, 2013). The concentration of oxidized products was ascertained by generating a standard curve from the three standard runs. Upon elution of the sample, a peak is discernible on the chromatogram. Leveraging the software, we identify the area beneath this peak and input this value into the equation derived from the standard curve. This yields the concentration of the product at the given time. This process was implemented for all the samples across the time course activity assays previously described.

## 4 RESULTS

### 4.1 PURIFICATION OF *SmAA10A*

The *SmAA10A* wild type (WT) enzyme was successfully extracted and isolated via a process known as periplasmic extraction. The resultant extract, enriched with *SmAA10A*, was then subjected to an initial phase of purification employing chitin beads affinity chromatography. The resulting chromatogram provided a visual confirmation of this purification stage, with an in-depth procedural description available in Section 3.4. Alas, the original chromatogram corresponding to this purification could not be recovered as a consequence of the relocation of the instrument in conjunction with the Covid-19-pandemic and the extended timeframe of this thesis. However, an example chromatogram that visualizes the purification of a *SmAA10A* wild type is included in Fig.4.1.

The isolated *SmAA10A*'s molecular integrity post-purification was then ascertained via gel electrophoresis. The purification protocol for the gatekeeper mutants (*SmAA10A*-E60Q, *SmAA10A*-E60D, and *SmAA10A*-E60N) was consistent with that employed for the wild type *SmAA10A*-E60. Accordingly, a singular chromatogram has been utilized herein to represent the purification trajectory of all *SmAA10A* variants. Worth noting is the suboptimal viability of the initial transformant stock, which necessitated the iterative execution of the transformation procedure thrice prior to obtaining a viable stock of *SmAA10A* wild type and the gatekeeper mutants.

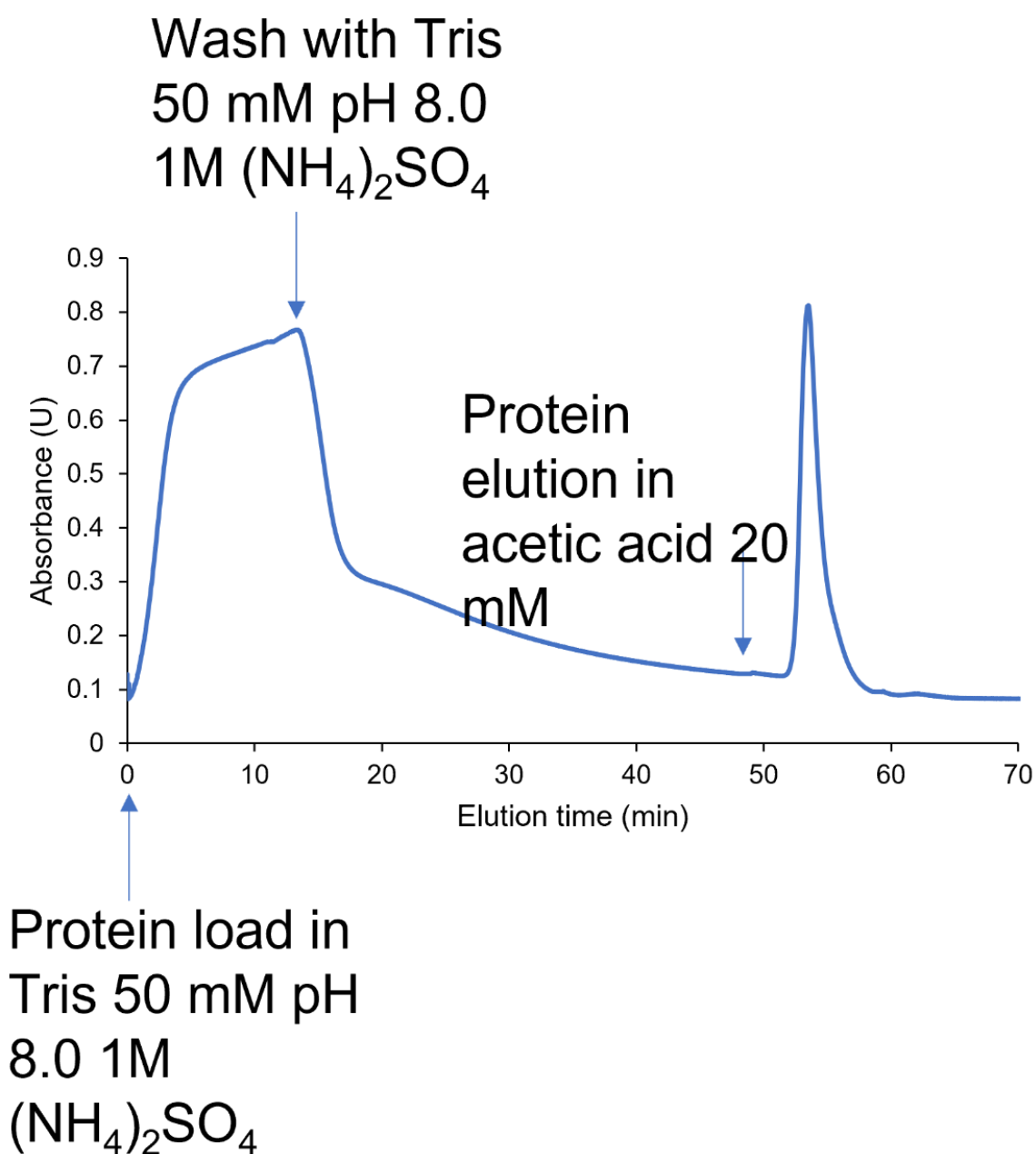


Figure 4-1 **Chromatogram for purifying SmAA10A -Wild type on a Chitin Column.** As the periplasmic extract is applied to the column, a broad peak arises at the start of the chromatogram that contains contamination and undesired proteins. The tall peak, from when acetic acid was loaded on the column, contains SmAA10A. This chromatogram was supplied by the lab group.

#### 4.1.1 OVERALL RESULTS OF PURIFICATION.

To confirm successful isolation of *SmAA10A* variants, fractions from the chitin bead affinity chromatography were analyzed using SDS-PAGE (Fig 4.2). A distinct band in well 2, aligned with *SmAA10A* expected molecular weight (18.8 kDa), provides evidence of successful extraction. This band parallels a previously validated sample (well 1) from the lab supply, strengthening the conclusion. The absence of bands in the flow-through indicates minimal enzyme loss during purification, highlighting the efficient and effective isolation of *SmAA10A*.



Figure 4-2 SDS-PAGE gel electrophoresis of the fractions containing *SmAA10A* wild type from chitin bead affinity chromatography. The figure represents an SDS-PAGE gel electrophoresis demonstrating the different fractions obtained from the affinity chromatography of *SmAA10A* wild type, having a molecular weight of 18.8 kDa. On the left, a band corresponds to the Benchmark Ladder, used as a molecular weight reference. Well 1 is populated with a comparative sample of *SmAA10A* from the lab supply. Well 2 houses the periplasmic extract containing our isolated *SmAA10A* wild type. The last lane, well 3, contains the flow-through fraction from the purification process.

The purification of *SmAA10A* gatekeeper mutants followed the same protocol as the wild type *SmAA10A* (Fig. 4.3). Noticeable bands were observed in wells 1, 3, and 5, corresponding to the enzyme's predicted molecular weight of 18.8 kDa. However, SDS-PAGE analysis revealed substantial enzyme presence in the flow-through for *SmAA10A-E60D* and *SmAA10A-E60Q* gatekeeper mutants, and trace amounts for *SmAA10A-E60N* mutant, indicating inadequate efficiency in the initial purification.

A second purification cycle was conducted, and the assessment (Fig. 4.4) showed detectable *SmAA10A* variants in most fractions, indicating incomplete segregation of the enzyme. *SmAA10A-E60D* and *SmAA10A-E60Q* still had residual enzymes in their flow-throughs, but with reduced concentrations compared to the first purification cycle. Notably, the *SmAA10A-E60N* mutant exhibited no enzyme presence in its flow-through, suggesting higher efficacy in its isolation throughout both purification rounds.

The consistent use of columns for both purifications led to speculation that inefficiencies in enzyme removal for *SmAA10A-E60D* and *SmAA10A-E60Q* gatekeeper mutants might be due to potential column defects. Using new columns for these mutants could potentially improve the results. Despite incomplete purification success, further purification efforts were terminated as the acquired enzyme quantity was deemed sufficient for subsequent experiments.

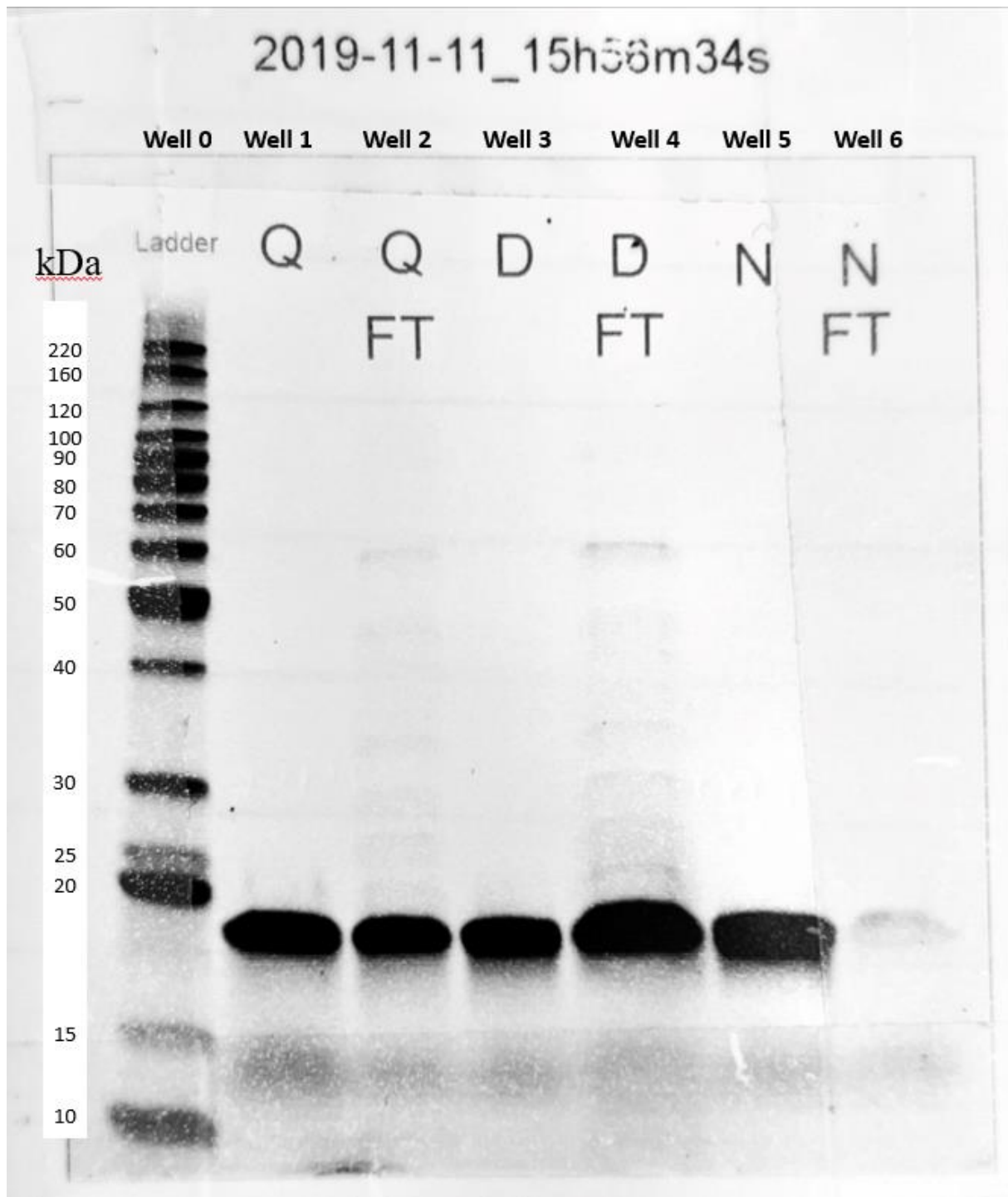


Figure 4-3 SDS-PAGE gel electrophoresis on fractions containing *SmAA10A* gatekeeper mutants (E60D, E60N, E60Q) obtained from the first chitin bead affinity chromatography. The gel shows distinct bands representing the mutants with a molecular weight of about 18.8 kDa. The Benchmark Ladder serves as the molecular weight standard on the far left. Wells 1-6 represent different purification stages for each mutant: 1 and 2 for E60Q, 3 and 4 for E60D, and 5 and 6 for E60N. The first is the isolate post purification, the second the flow-through.

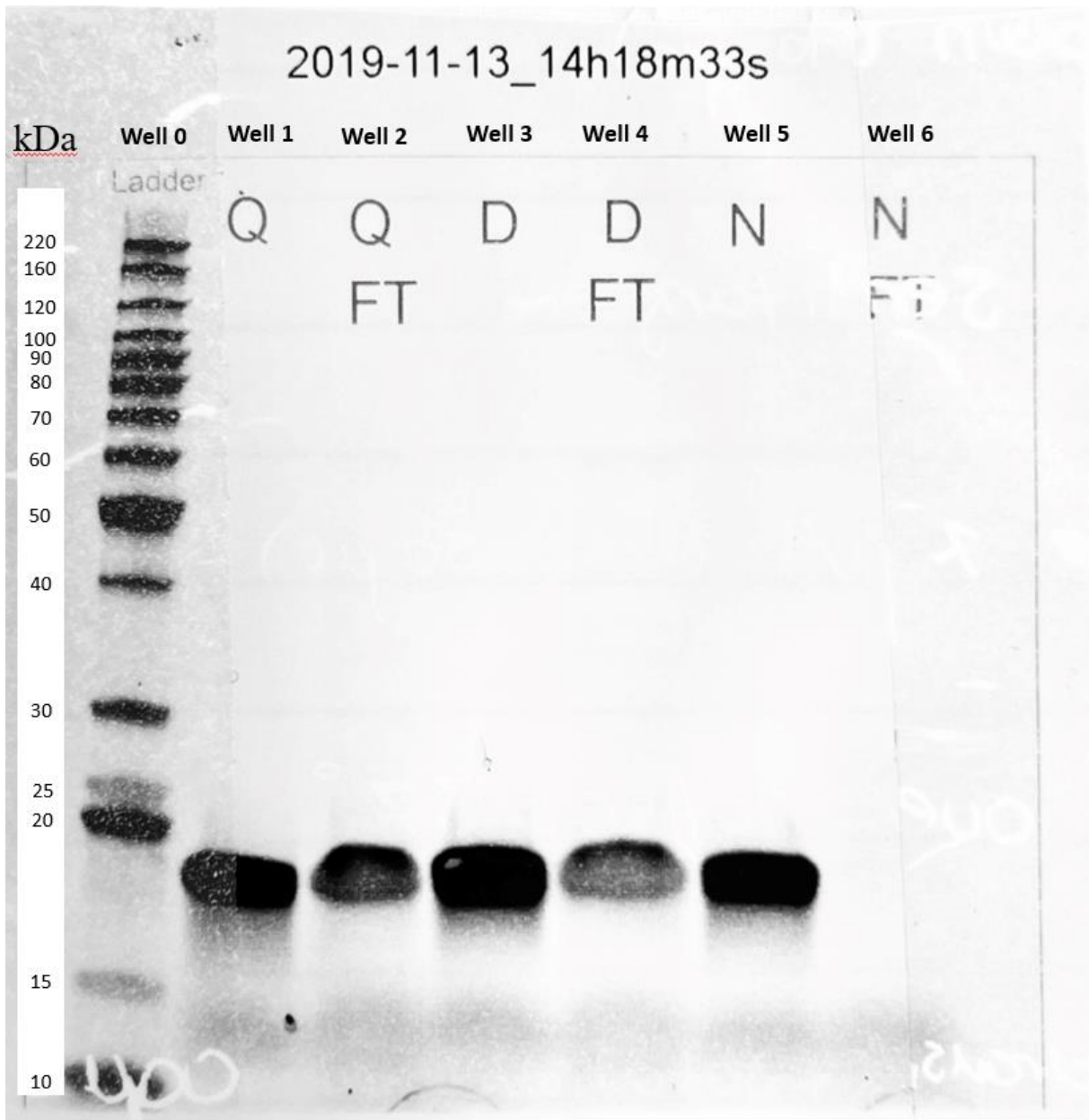


Figure 4-4 SDS-PAGE Gel electrophoresis on fractions containing SmAA10A gatekeeper mutants (E60D, E60N, E60Q) obtained from the second chitin bead affinity chromatography. The gel shows distinct bands representing the mutants with a molecular weight of about 18.8 kDa. The Benchmark Ladder serves as the molecular weight standard on the far left. Wells 1-6 represent different purification stages for each mutant: 1 and 2 for E60Q, 3 and 4 for E60D, and 5 and 6 for E60N. The first is the isolate post purification, the second the flow-through.

#### 4.1.2 CONCENTRATION OF ISOLATED *SMAA10A* VARIANTS- $A_{280}$

After purification and up-concentration, the concentration of the LPMO was determined by measuring the absorbance at 280 nm using UV/vis spectroscopy ( $A_{280}$ ). The final concentrations are collected in Table 4.1. The exact volume acquired of each *SmAA10A* variant was impossible to recover as it was noted on the enzyme's containers, with was lost under Covid-19-lockdown.

Table 4-1 **Finale enzyme concentration measured in  $\mu\text{M}$  after purification of the *SmAA10A* variants.**

<b>Enzyme</b>	<b>Concentration (<math>\mu\text{M}</math>)</b>
Wild type	423.1
E60D	74.2
E60Q	21.1
E60N	61.4

#### 4.2 PURIFICATION OF *SmGH20*

The *E. coli* bacteria harboring *SmGH20* was proliferated from glycerol stock from the lab supply. Following this, the enzyme was liberated from the bacterial cells by microfluidization, a technique used to disrupt cell membranes. The resultant extract was subsequently dialyzed to remove unwanted small molecules and ions. Following dialysis, purification of the extract was carried out using a Ni-NTA column, a common technique for the purification of His-tagged proteins.

Further confirmation of successful purification was obtained through SDS-PAGE analysis. However, we encountered issues with the activity of *SmGH20*. The batch was suspected to be inactive, but we soon realized that a dialysis stage following microfluidization had been skipped. Dialysis was then performed to rectify this and the SDS-PAGE analysis corresponding to this purified batch is provided in Figure 4.5. At the time, the production of a third batch was underway but was put on hold due to restrictions related to the COVID-19 pandemic.

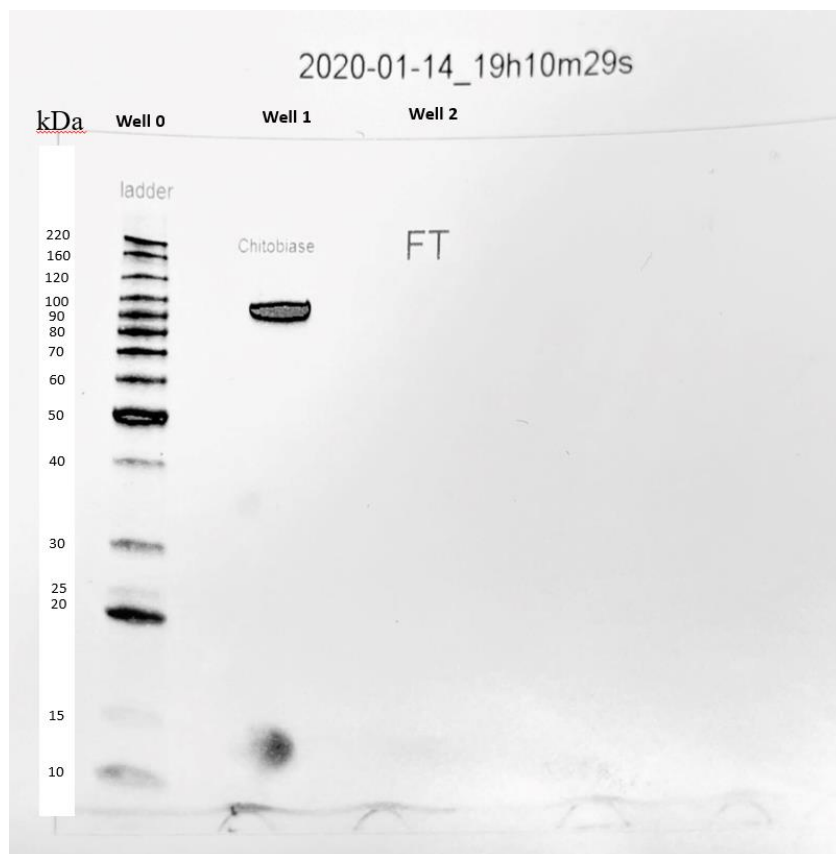


Figure 4-5 SDS-PAGE gel electrophoresis of the fractions containing *SmGH20* from following purification on Ni-NTA column. Well 0 contains the Benchmark Ladder, well 1 holds the periplasmic extract containing *SmGH20*, and well 3 hold the flow through from the purification.

## 4.3 TIME COURSE ACTIVITY ASSAYS WITH THE *SmAA10A* WILD TYPE AND GATEKEEPER MUTANTS

### 4.3.1 EVALUATING THE FUNCTIONAL ACTIVITY OF *SMAA10A* VARIANTS

To determining whether our *SmAA10A* enzymes were functional, we tried to determine enzymatic activity by conducting time course activity assays with the *SmAA10A* wild type and gatekeeper mutants; *SmAA10A*-E60Q, *SmAA10A*-E60D, and *SmAA10A*-E60N, under *in-situ* peroxygenase conditions. As such, the *SmAA10A* variant was mixed with diverse amount of  $\beta$ -chitin (2.5 g/L, 7.5 g/L and 15 g/L) for varying amounts of time (5 min, 10 min, 20 min, 60 min and 180 min) before terminating the reaction by heat inactivation. Next, *SmGH20* was added to the reaction aliquots to convert oxidized products to soluble chitobionic acid ( $A2^{ox}$ ). However, to complicate matters, the *SmGH20* enzymes appear to be inactive. Furthermore, the chitobionic

acid standards associated with these reactions were also compromised, making it impossible to convert our measurements to concentrations of  $A2^{ox}$ . However, to determine the functional activity of the enzymes, only observing the presence of oxidized products is required, which can be accomplished without functioning *SmGH20* and Standards. Figures 4.6, visualize the reactions of the *SmAA10A* variants with the different  $\beta$ -chitin concentrations of 15 g/L, 7.5 g/L and 2.5 g/L. Oxidized products are observed in all reaction aliquots, indicating that *SmAA10A* wild type and mutants are all indeed active on  $\beta$ -chitin concentrations between 2.5-15 g/L. In the appendix, Figure S4-S9, shows the reactions for the individual concentration of  $\beta$ -chitin. In summary, we observe that high levels of substrate (15 mg/ml) is beneficial.

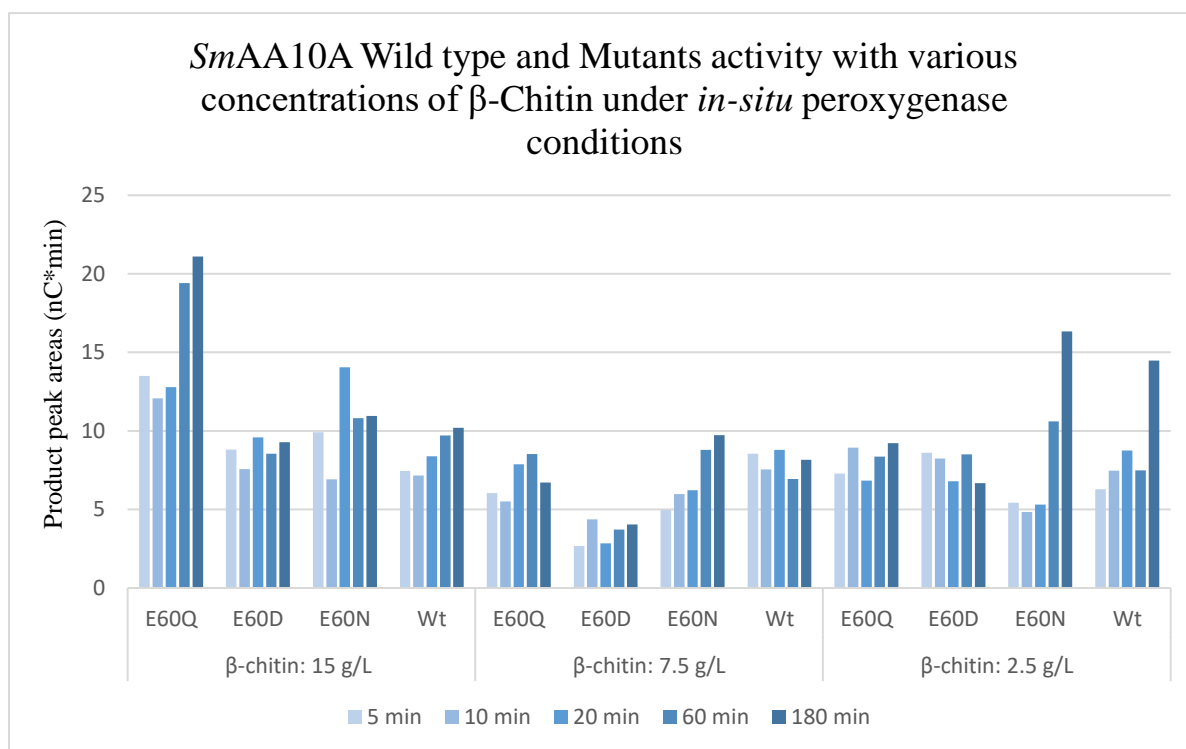


Figure 4-6 Time course activity assays with *SmAA10A* wild type and gatekeeper mutants in varying concentrations of  $\beta$ -chitin under *in-situ* peroxygenase conditions. For each experiment, a suspension of  $\beta$ -chitin (15 g/L, 7.5 g/L and 2.5 g/L), ascorbic acid (1mM) in Bis-tris buffer (50 mM, pH 6.5) was incubated with *SmAA10A* variant (1  $\mu$ M); wt, E60Q, E60D, and E60N, at 37 °C in a thermomixer (1000 rpm), for varying amounts of time (5 min, 10 min, 20 min, 60 min, and 180min). The reaction is shown in a bar chart, where the amount of oxidized products is represented by product peak areas (nC\*min) on the y-axis.

### 4.3.2 SUBSTRATE SATURATION ANALYSIS: *SmAA10A* WILD TYPE RESPONSE TO B-CHITIN

Time course activity assays with *SmAA10A* wild type were performed to ascertain the optimal range of substrate concentrations for use in later experiments. *SmAA10A* wild type was mixed with different amount of  $\beta$ -chitin (2.5 g/L, 6 g/L, 10 g/L and 15 g/L) for varying amounts of time (30 min, 60 min, 90 min, 120 min, and 150 min) before terminating the reaction by heat inactivation. Newly cultivated *SmGH20* (27 $\mu$ M) was then introduced to the reaction aliquots to convert oxidized products to soluble chitobionic acid ( $A2^{ox}$ ). Figure 4.7 visualizes the results of the reactions with the different concentrations of the  $\beta$ -chitin. The y-axis quantifies the concentration of  $A2^{ox}$  in  $\mu$ M, and the x-axis represents the progression of time since commencement of the reaction measured in minutes. In the appendix, Figure S1, show the first standard curve form this experiment as an example of  $A2^{ox}$ -standard curves. Again, we observe that high substrate concentration is beneficial for *SmAA10A* catalysis.

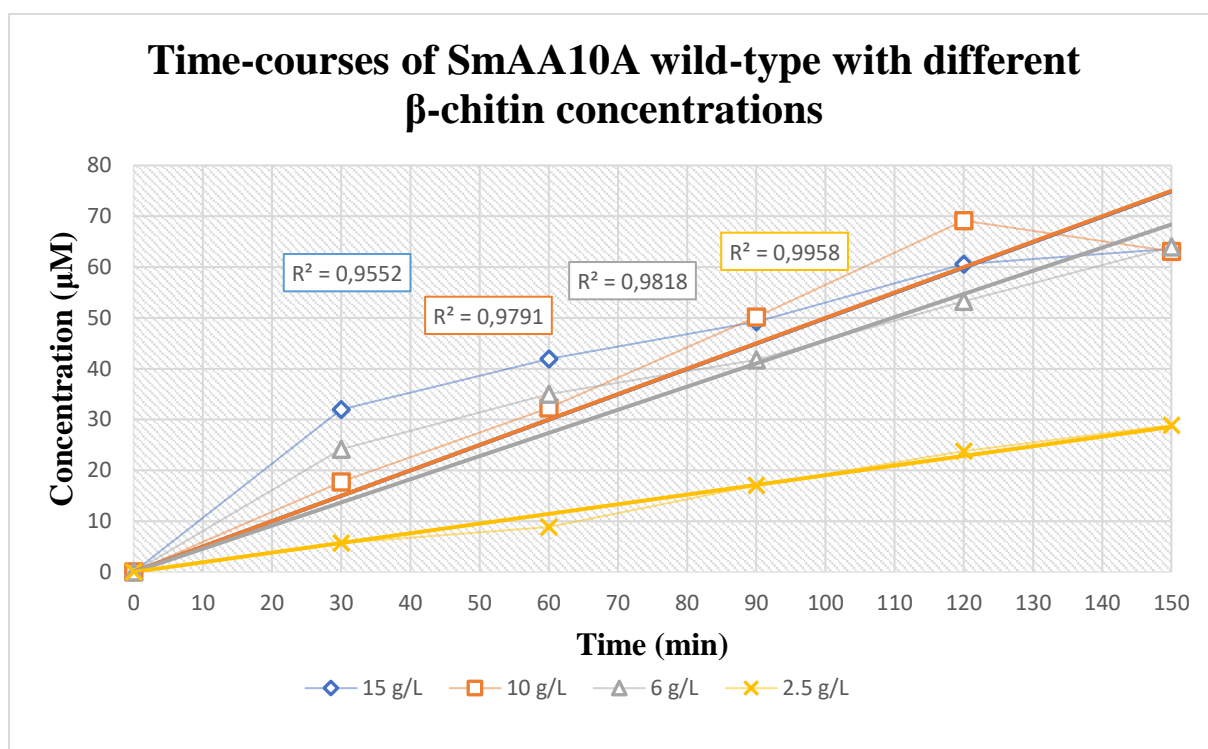


Figure 4-7 Time course activity assays of *SmAA10A* wild type with varying  $\beta$ -chitin concentrations under *in-situ* peroxygenase conditions. For each experiment, a suspension of  $\beta$ -chitin and ascorbic acid (1mM) in Bis-tris buffer (50 mM, pH 6.5) was incubated with *SmAA10A* wild type (1  $\mu$ M) at 37 °C in a thermomixer (1000 rpm), for varying amounts of time (30 min, 60 min, 90 min, 120 min and 150 min). The graph visualizes the concentration of oxidized products (y-axis) detected in the final reaction mixture (expressed as  $A2^{ox}$ ), at the time of enzyme heat inactivation (x-axis) and flowed by break down of substrate with *SmGH20*. There are four unique reactions with the  $\beta$ -chitin concentrations: 15 g/L (blue), 10 g/L (orange), 6 g/L (gray) and 2.5 g/L (yellow), and a linear trend line and complementary  $R^2$  value is included for each reaction.

### 4.3.3 INVESTIGATING ELECTRON DONOR INDEPENDENCE IN *SmAA10A* VARIANT REACTIONS

LPMO activity is dependent on an externally supplied electron donor, so to investigating electron donor dependence in *SmAA10A* wild type and gatekeeper mutants (E60Q, E60D, and E60N), we performed time course activity assays without the presence of external electron donors, situating our experiments under *in-situ* peroxygenase conditions. *SmAA10A* variants (1  $\mu$ M) was incubated together with  $\beta$ -chitin (10 g/L) in Bis-Tris buffer for varying amounts of time (30 min, 60 min, 90 min, 120 min, and 150 min) before terminating the reaction by heat inactivation. Next, *SmGH20* was added to the reaction aliquots to convert oxidized products to soluble chitobionic acid ( $A2^{ox}$ ) over night. Figure 4.8 visualize the product ( $A2^{ox}$ ) concentration within the reaction milieu, measured in  $\mu$ M, and the progression of time since the reaction's commencement, measured in minutes, on the y-axis and x-axis, respectively. In the Appendix, Figure S10 and S11, show the reactions for each individual parallel. It is not clear why products, albeit at low concentrations, are detected. The chitin may contain some innate oxidized groups.

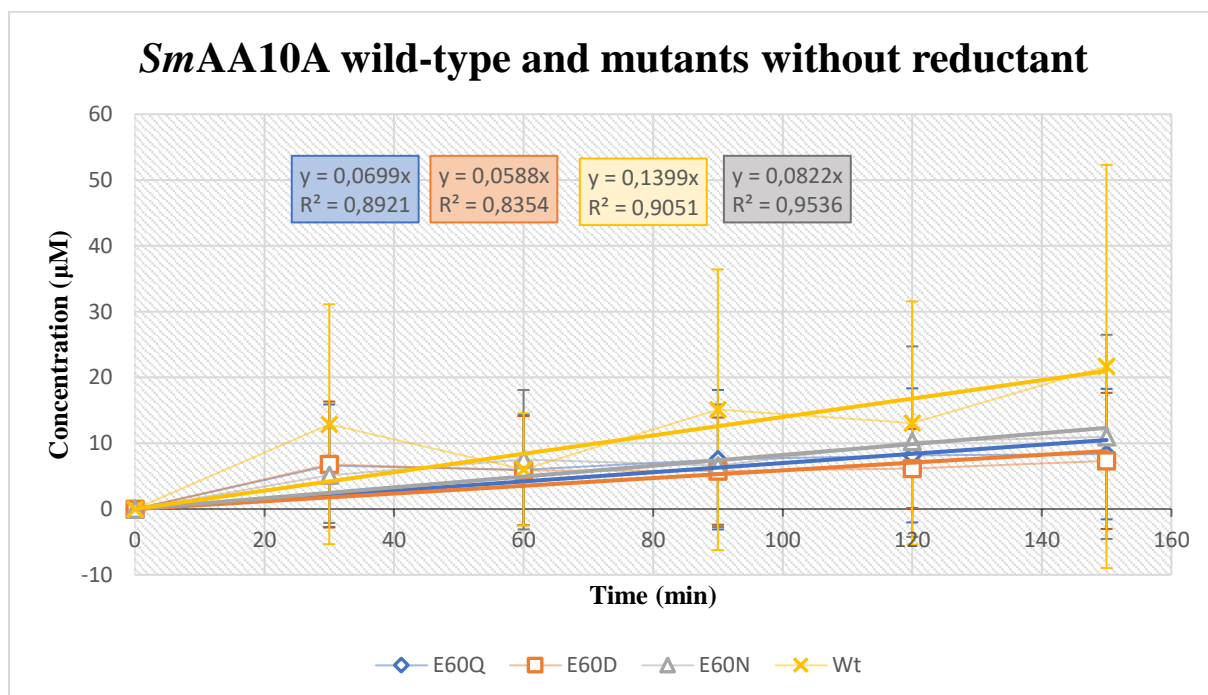


Figure 4-8 **Time course activity assays of *SmAA10A* wild type and mutants without added electron donor.** For each experiment, a suspension of  $\beta$ -chitin (10 g/L) in Bis-tris buffer (50 mM, pH 6.5) was incubated with *SmAA10A* variant (1  $\mu$ M) at 37  $^{\circ}$ C in a thermomixer (1000 rpm), for varying amounts of time (30 min, 60 min, 90 min, 120 min, and 150 min). The graph visualizes the concentration of oxidized products (y-axis) detected in the final reaction mixture (expressed as  $A2^{ox}$ ), at the time of enzyme heat inactivation (x-axis). There are four unique reactions with the *SmAA10A* variants: E60Q (blue), E60D (orange), E60N (gray) and wt (yellow). Trendline and R-squared is also supplied for each of the runs with the different *SmAA10A* variant. Furthermore, the standard deviation of each data point is visualized as in brackets.

#### 4.3.4 ACTIVITY ANALYSIS OF *SmAA10A* VARIANTS UNDER *IN-SITU* PEROXYGENASE CONDITIONS.

To study the importance of the glutamate gatekeeper residue in *SmAA10A*, we performed duplicate time course activity assays with *SmAA10A* wild type and gatekeeper mutants (E60Q, E60D, and E60N) under *in-situ* peroxygenase conditions. A *SmAA10A* variant (1  $\mu$ M) was incubated together with  $\beta$ -chitin (10 g/L) in bis-tris buffer (50 mM, pH 6.5) for different amounts of time (30 min, 60 min, 90 min, 120 min, and 150 min) before terminating the reaction by heat inactivation. Next, *SmGH20* was added to the reaction aliquots to convert oxidized products to soluble chitobionic acid ( $A2^{ox}$ ) over night. Figure 4.9 visualize the product ( $A2^{ox}$ ) concentration within the reaction milieu, measured in  $\mu$ M, and the progression of time since the reaction's commencement, measured in minutes, on the y-axis and x-axis, respectively. For all variants, product concentrations are higher in the presence of reductant than in the absence of reductant.

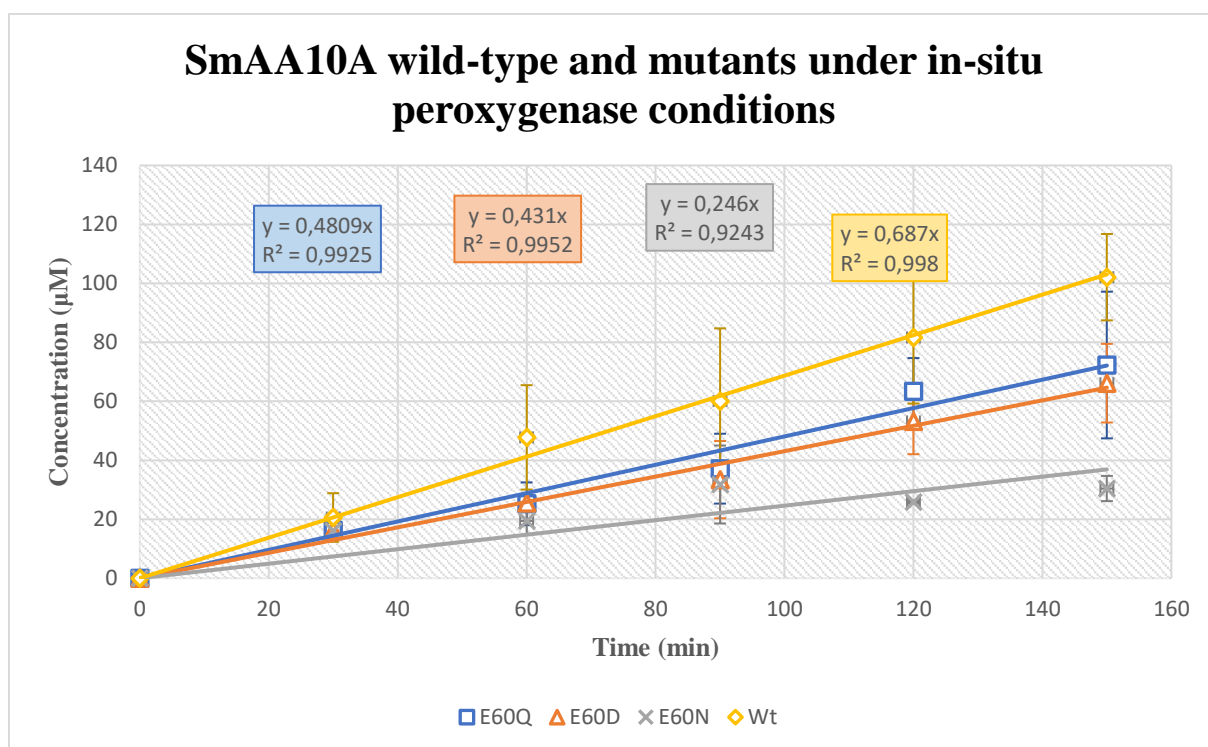


Figure 4-9 **Time course activity assays of *SmAA10A* wild type and mutants under *in-situ* peroxygenase condition.** For each experiment, a suspension of  $\beta$ -chitin (10 g/L) and ascorbic acid (1mM) in Bis-tris buffer (50 mM, pH 6.5) was incubated with *SmAA10A* variant (1 $\mu$ M) at 37 °C in a thermomixer (1000 rpm), for varying amounts of time (30 min, 60 min, 90 min, 120 min and 180 min). The graph visualizes the concentration of oxidized products (y-axis) detected in the final reaction mixture (expressed as  $A2^{ox}$ ), at the time of enzyme heat inactivation (x-axis). There are four unique reactions with the *SmAA10A* variants: E60Q (blue), E60D (orange), E60N (gray) and Wt (yellow). Trendline and R-squared is also supplied for each of the runs with the different *SmAA10A* variant. Furthermore, the standard deviation of each data point is visualized as in brackets.

### 4.3.5 ACTIVITY ANALYSIS OF *SmAA10A* VARIANTS WITH ADDED HYDROGEN PEROXIDE.

Time course activity assays with the *SmAA10A* wild type and gatekeeper mutants (E60Q, E60D, and E60N) were performed to study the activity of *SmAA10A* variants when unique amounts of hydrogen peroxide were added to the reaction. The experimental framework included was that *SmAA10A* wild type and mutants (0.1  $\mu\text{M}$ ) was mixed with various amount of  $\text{H}_2\text{O}_2$  (5 $\mu\text{M}$ , 10 $\mu\text{M}$ , 20 $\mu\text{M}$ , 50 $\mu\text{M}$  and 100 $\mu\text{M}$ ) for varying amounts of time (60sec, 90sec, 120sec, 150sec, and 180sec) before terminating the reaction by heat inactivation. Next, *SmGH20* was added to the reaction aliquots to convert oxidized products to soluble chitobionic acid ( $\text{A2}^{\text{ox}}$ ) over night. From Figure 4.13, it looks like all of the *SmAA10A* variants were inactivated shortly after the initiation of reaction demonstrated through no significant increase of detection oxidized product ( $\text{A2}^{\text{ox}}$ ) with time. However, we do have reason to believe that the *SmGH20* used for these experiments was inactive at the time of the experiments. The *SmGH20* had been newly cultivated from glycerol stock, then isolated by microfluidization. The viscous sample was not dialyzed prior to down concentration, something that might have reduced the activity of *SmGH20*. These experiments need to be performed again, but they do show that we have peroxygenase activity for all four enzymes.

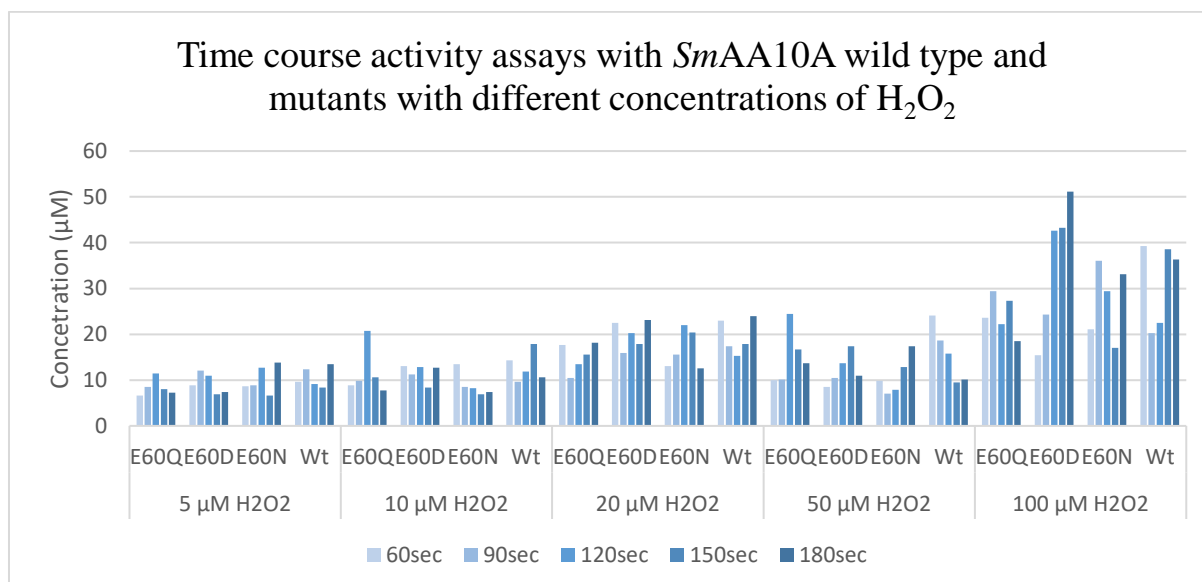


Figure 4-10 Time course activity assays with *SmAA10A* wild type and mutants in varying concentrations of  $\text{H}_2\text{O}_2$ . For each experiment, a suspension of *b*-chitin (6 g/L), ascorbic acid (20  $\mu\text{M}$ ) and  $\text{H}_2\text{O}_2$  (5 $\mu\text{M}$ , 10 $\mu\text{M}$ , 20 $\mu\text{M}$ , 50 $\mu\text{M}$  or 100 $\mu\text{M}$ ) in Bis-tris buffer (50 mM, pH 6.5) was incubated with *SmAA10A* variants (0.1  $\mu\text{M}$ ) at 37 °C in a thermomixer (1000 rpm), for varying amounts of time (60s, 90s, 120s, 150s and 180s). The reaction is shown in a bar chart, where the concentration of chitobionic acid ( $\text{A2}^{\text{ox}}$ ) in  $\mu\text{M}$  represented by the y-axis.

Following dialysis of *SmGH20*, a second time course activity assays with  $H_2O_2$  ( $100\mu M$ ) was performed using a different reaction setup. *SmAA10A* variant ( $1\mu M$ ) was incubated with  $H_2O_2$  ( $100\mu M$ ),  $\beta$ -chitin ( $10\text{ g/L}$ ), ascorbic acid ( $20\mu M$ ) in Bis-tris buffer ( $50\text{ mM}$ ,  $pH\ 6.5$ ). This reaction is visualized in Figure 4.11.

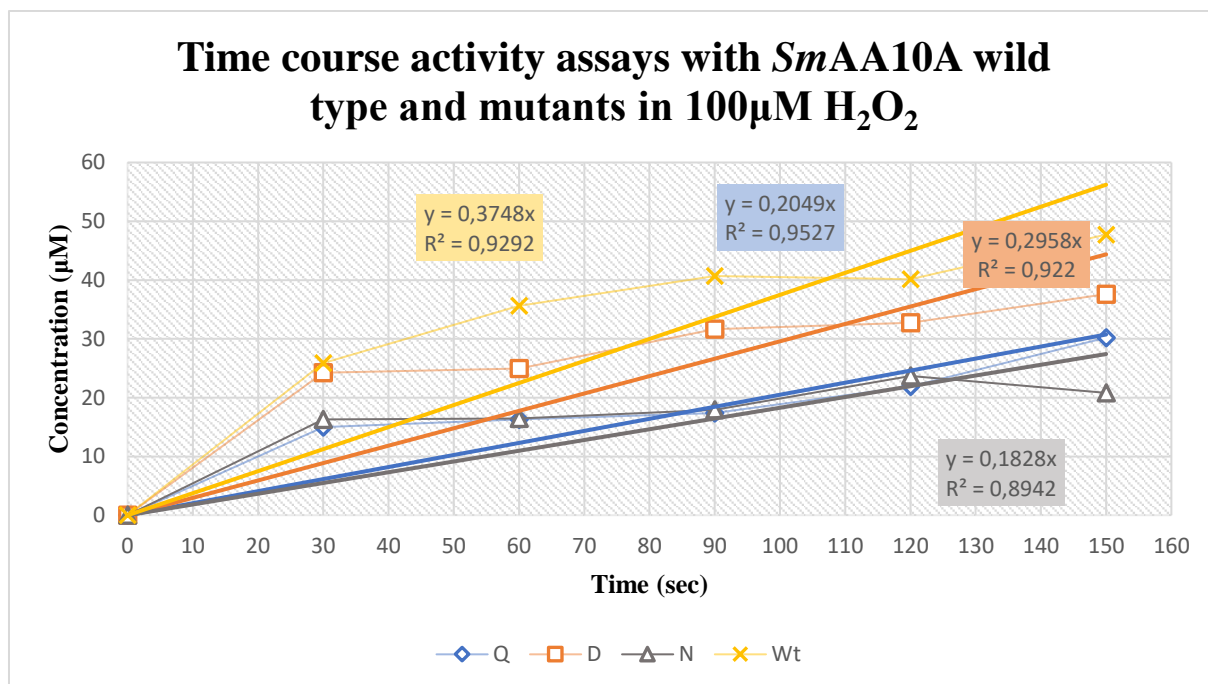


Figure 4-11 **Time course activity assays with *SmAA10A* wild type and mutants in  $100\mu M H_2O_2$ .** For each experiment, a suspension of  $\beta$ -chitin ( $10\text{ g/L}$ ), ascorbic acid ( $20\mu M$ ) and  $H_2O_2$  ( $100\mu M$ ) in Bis-tris buffer ( $50\text{ mM}$ ,  $pH\ 6.5$ ) was incubated with *SmAA10A* variants ( $1\mu M$ ) at  $37\text{ }^\circ C$  in a thermomixer ( $1000\text{ rpm}$ ), for varying amounts of time ( $30s$ ,  $60s$ ,  $90s$ ,  $120s$ , and  $150s$ ). The graph visualizes the concentration of oxidized products (y-axis) detected in the final reaction mixture (expressed as  $A_{2^{ox}}$ ), at the time of enzyme heat inactivation (x-axis). There are four unique reactions with the *SmAA10A* variants: *E60Q* (blue), *E60D* (orange), *E60N* (gray) and wt (yellow), and a linear trend line and complementary  $R^2$  value is included for each reaction.

In general, we observe that the wild type catalyzed reaction provides more product with time than the mutants.

#### **4.3.6 ACTIVITY ANALYSIS OF *SMAA10A* VARIANTS IN THE PRESENCE OF HRP UNDER *IN-SITU* PEROXYGENASE CONDITIONS.**

We performed time course activity assays with *SmAA10A* variants in the presence of ascorbic acid and different concentrations of the hydrogen peroxide-consuming enzyme horseradish peroxidase (HRP) to assess if this would abolish or inhibit the reaction. It is postulated that the Glu-residue hydrogen bonds to hydrogen peroxide during catalysis (Bissaro et al PNAS 2020). A change of this residue may affect this interaction and result in an increase or decrease of affinity, and activity may, hence, increase or decrease in the presence of HRP compared to the wild type.

The experimental framework was that *SmAA10A* variants (1 $\mu$ M) was mixed with divers amounts of HRP (0.25  $\mu$ M, 0.5  $\mu$ M, 1  $\mu$ M, and 2  $\mu$ M) for varying amounts of time (30 min, 60 min, 90 min, 120 min, and 150 min) before terminating the reaction by heat inactivation. Next, *SmGH20* was added to the reaction aliquots to convert oxidized products to soluble chitobionic acid (A2<sup>ox</sup>) over night. For more detailed description of the reaction setup see Section 3.17 Figures 4.12-4.15 visualize the product (A2<sup>ox</sup>) concentration within the reaction milieu, measured in  $\mu$ M, and the progression of time since the reaction's commencement, measured in minutes, on the y-axis and x-axis, respectively.

In general, increased HRP concentration resulted in less product formation. Moreover, the wild type was less affected than the mutants. At 0.25  $\mu$ M HRP, product concentration was reduced to 60 % for the wild type, 20 % for E60Q, 15 % for E60D, and 27 % for E60N. The latter displayed the smallest activity on  $\beta$ -chitin in the absence of HRP. The results suggest that Glu participates in binding hydrogen peroxide during turnover.

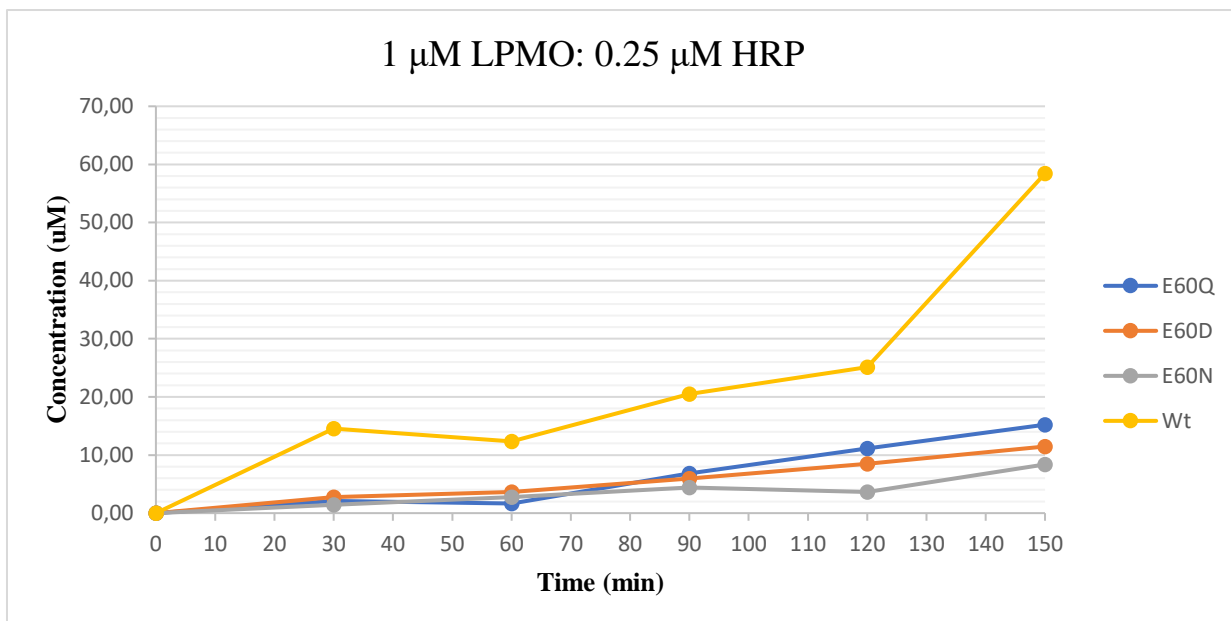


Figure 4-12 **Time course activity assays of *SmAA10A* variants under in-situ peroxygenase conditions with 0.25 μM HRP.** For each experiment, a suspension of HRP (0.25μM), β-chitin (10 g/L), ascorbic acid (1mM) and Amplex Red™ in Bis-tris buffer (50 mM, pH 6.5) was incubated with *SmAA10A* variant (1 μM) at 37 °C in a thermomixer (1000 rpm), for varying amounts of time (30 min, 60 min, 90 min, 120 min, and 150 min). The graph visualizes the concentration of chitobionic acid (A2<sup>ox</sup>) detected in the final reaction mixture (y-axis), at the time of enzyme heat inactivation (x-axis). There are four unique reactions with the *SmAA10A* variants: E60Q (blue), E60D (orange), E60N (gray) and wild type (yellow).

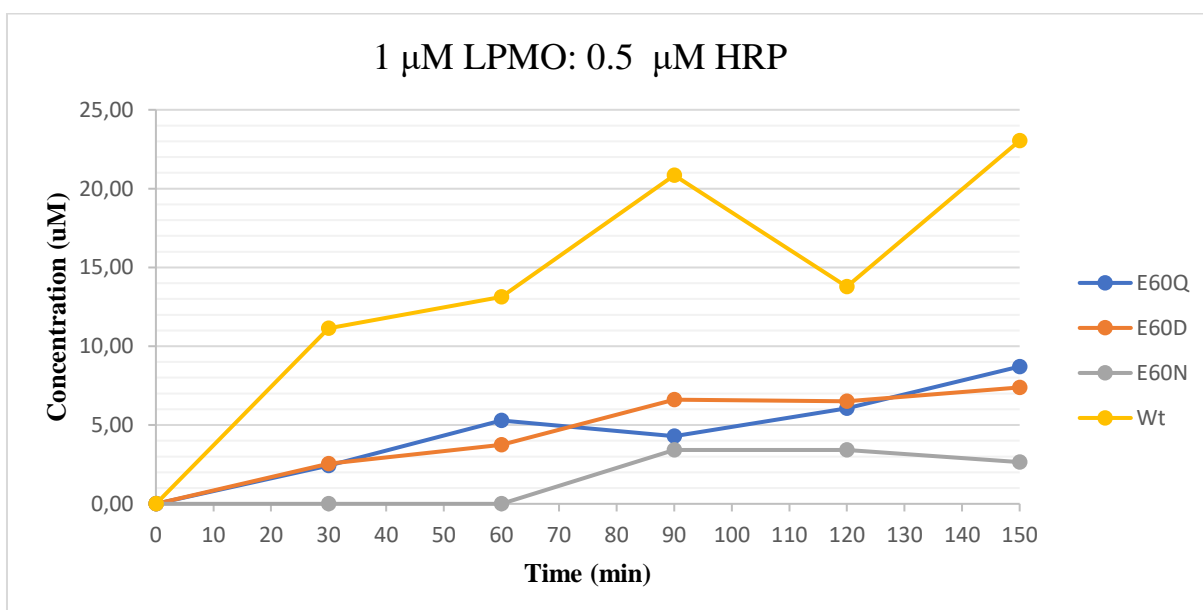


Figure 4-13 **Time course activity assays of *SmAA10A* variants under in-situ peroxygenase conditions with 0.5μM HRP.** For each experiment, a suspension of HRP (0.5μM), β-chitin (10 g/L), ascorbic acid (1mM) and Amplex Red™ in Bis-tris buffer (50 mM, pH 6.5) was incubated with *SmAA10A* variant (1 μM) at 37 °C in a thermomixer (1000 rpm), for varying amounts of time (30 min, 60 min, 90 min, 120 min, and 150 min). The graph visualizes the concentration of chitobionic acid (A2<sup>ox</sup>) detected in the final reaction mixture (y-axis), at the time of enzyme heat inactivation (x-axis). There are four unique reactions with the *SmAA10A* variants: E60Q (blue), E60D (orange), E60N (gray) and wild type (yellow).

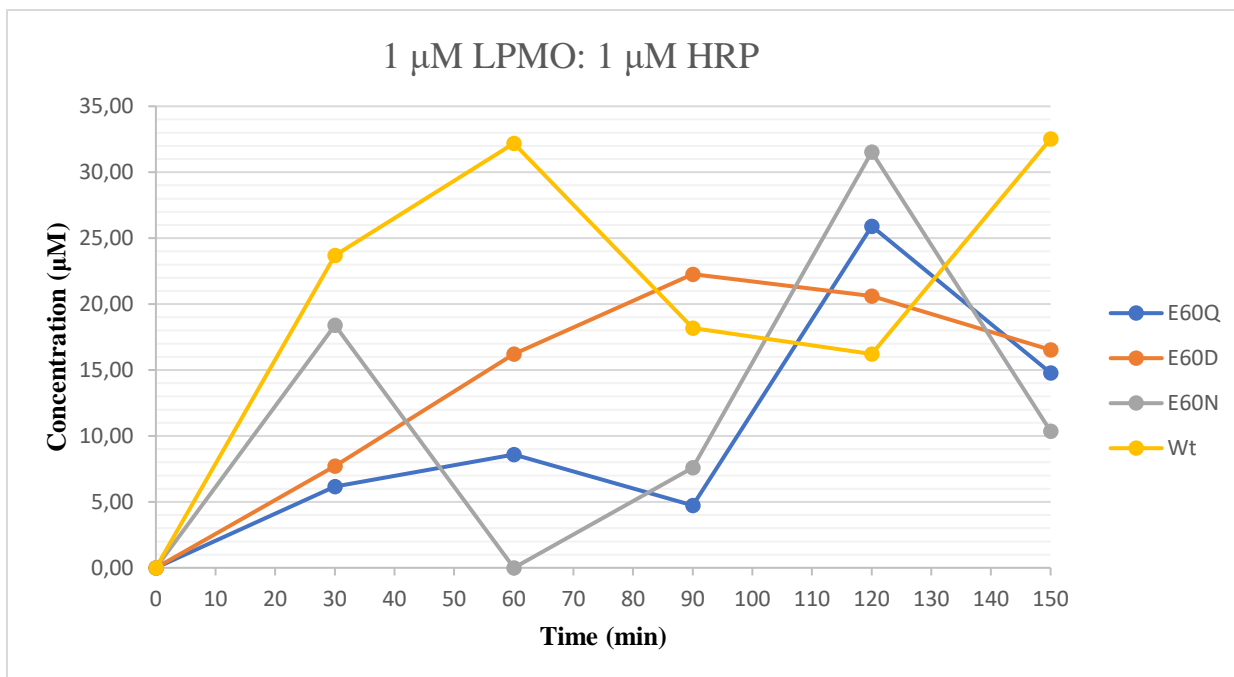


Figure 4-14 **Time course activity assays of *SmAA10A* variants under in-situ peroxygenase conditions with 1μM HRP.** For each experiment, a suspension of HRP (1μM), *b*-chitin (10 g/L), ascorbic acid (1mM) and Amplex Red™ in Bis-tris buffer (50 mM, pH 6.5) was incubated with *SmAA10A* variant (1 μM) at 37 °C in a thermomixer (1000 rpm), for varying amounts of time (30 min, 60 min, 90 min, 120 min, and 150 min). The graph visualizes the concentration of chitobionic acid (A2<sup>ox</sup>) detected in the final reaction mixture (y-axis), at the time of enzyme heat inactivation (x-axis). There are four unique reactions with the *SmAA10A* variants: E60Q (blue), E60D (orange), E60N (gray) and wild type (yellow).

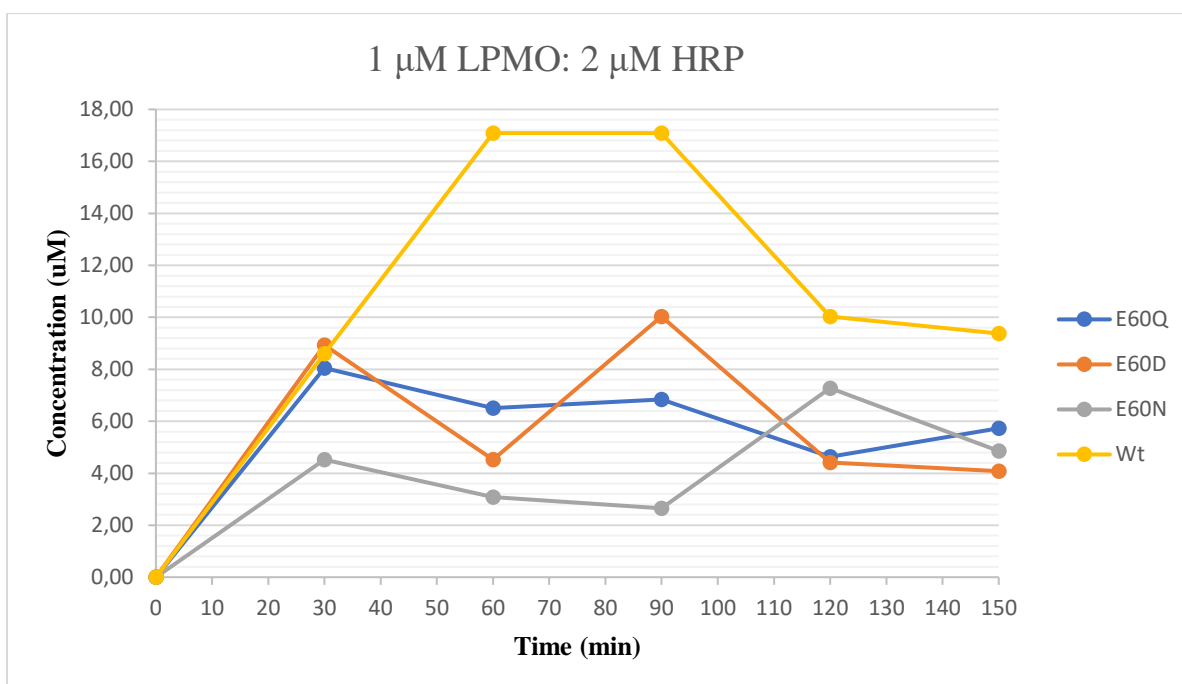


Figure 4-15 **Time course activity assays of *SmAA10A* variants under in-situ peroxygenase conditions with 2μM HRP.** For each experiment, a suspension of HRP (2μM), *b*-chitin (10 g/L), ascorbic acid (1mM) and Amplex Red™ in Bis-tris buffer (50 mM, pH 6.5) was incubated with *SmAA10A* variant (1 μM) at 37 °C in a thermomixer (1000 rpm), for varying amounts of time (30 min, 60 min, 90 min, 120 min, and 150 min). The graph visualizes the concentration of chitobionic acid (A2<sup>ox</sup>) detected in the final reaction mixture (y-axis), at the time of enzyme heat inactivation (x-axis). There are four unique reactions with the *SmAA10A* variants: E60Q (blue), E60D (orange), E60N (gray) and wild type (yellow).

## 4.4 REDIRECTED FOCUS FROM *SmAA10A* TO *NcAA9C*

Due to a series of unforeseen events, including disruptions caused by the COVID-19 pandemic and an unfortunate incident of prolonged improper storage leading to the degradation of our enzyme samples, our original research trajectory focused on *SmAA10A* was significantly derailed. Additional complications arose from an extended sick leave, further fragmenting the continuity of our investigations. As a consequence, our research emphasis pivoted towards investigating the role of the gatekeeper residue in the enzyme *NcAA9C*, as replication of prior experiments with *SmAA10A* was rendered infeasible. Opportunely, our research group had previously secured pure batches of these mutant enzymes, providing a mitigating factor to the research interruptions experienced. These enzyme samples, graciously contributed by Dr. Lukas Rieder, became instrumental in our redirected focus. The ensuing sections of the results will thus expound upon our discoveries concerning the role of the glutamine (*NcAA9C*-Q164) gatekeeper residue in *NcAA9C*.

## 4.5 TIME COURSE ACTIVITY ASSAYS WITH THE *NcAA9C* WILDTYPE AND GATEKEEPER MUTANTS

Intrigued by the potential impact of gatekeeper glutamine (Q164) mutations in *NcAA9C*, we delved into a systematic analysis. Using time course activity assays, we explored the activity variations between *NcAA9C* wild type and its mutants (Q164E, Q164D, Q164N) in the presence of electron donors like ascorbic acid, gallic acid, and cystine. The substrate for these reactions was cellopentose (DP5), as such standards of oxidized cellobiose (DP2<sup>ox</sup>) and cellotriose (DP3<sup>ox</sup>) were prepared. In the Appendix, Figure S3, an example standard calibration curve is shown. Meanwhile, Figures 4.16-4.19 present the results of these assays. Figure 4.16 shows the time course activity assays with the wild type enzyme and each of the reductants, Figure 4.17 showcases the same for the *NcAA9C*-Q164D mutant, Figure 4.18 features the *NcAA9C*-Q164N mutant, and Figure 4.19 highlights the *NcAA9C*-Q164E mutant. The y-axis represents the combined concentration cellobiose (DP2<sup>ox</sup>) and cellotriose (DP3<sup>ox</sup>) reaction solution, measured in  $\mu\text{M}$ , while the x-axis denotes the time elapsed since the reaction was initiated measured in minutes.

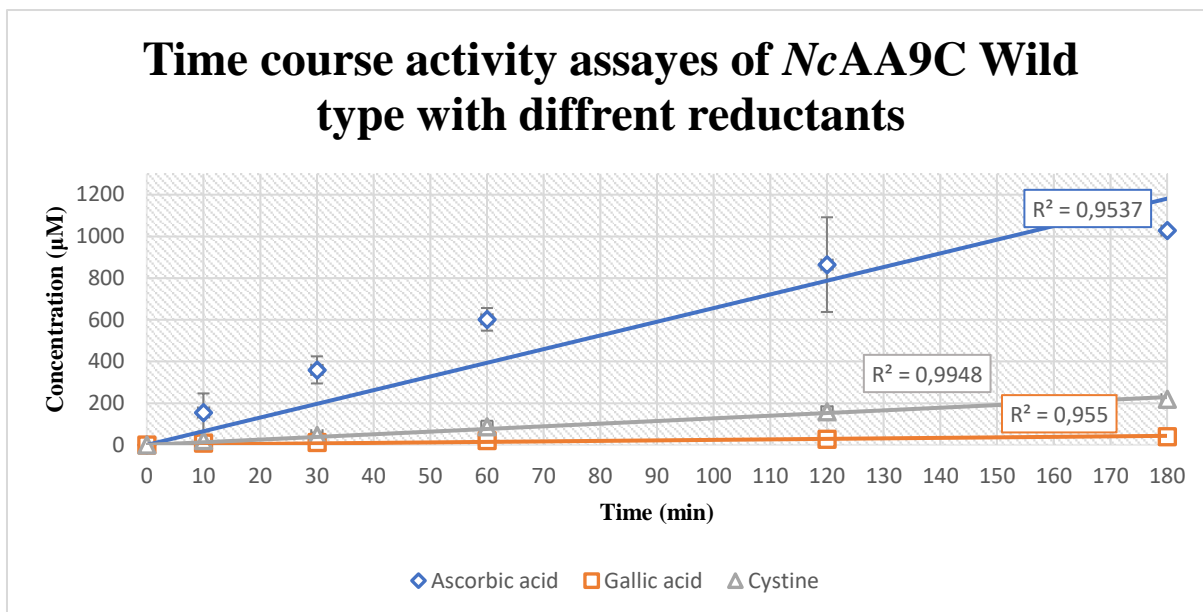


Figure 4-16 Time course activity assays of *NcAA9C* wild type with diverse electron donors. For each experiment, a suspension of cellopentose (1mM g/L) and electron donor (1mM) in Bis-tris buffer (50 mM, pH 6.5) was incubated with *NcAA9C* wild type (1 µM) at 37 °C in a thermomixer (750 rpm), for varying amounts of time (10 min, 30 min, 60 min, 120 min, and 180 min). The graph visualizes the concentration (µM) of oxidized products; cellobiose (DP2<sup>ox</sup>) and cellotriose (DP3<sup>ox</sup>) detected in the final reaction mixture (y-axis), at the time of inactivation with NaOH (x-axis). There are three reactions, one each for the different electron donors Ascorbic Acid (blue), Gallic Acid (orange) and cystine (gray). Trendlines and R-squared are also supplied for each of the experiments for the different reactions. Furthermore, the standard deviation of each data point is visualized as black brackets.

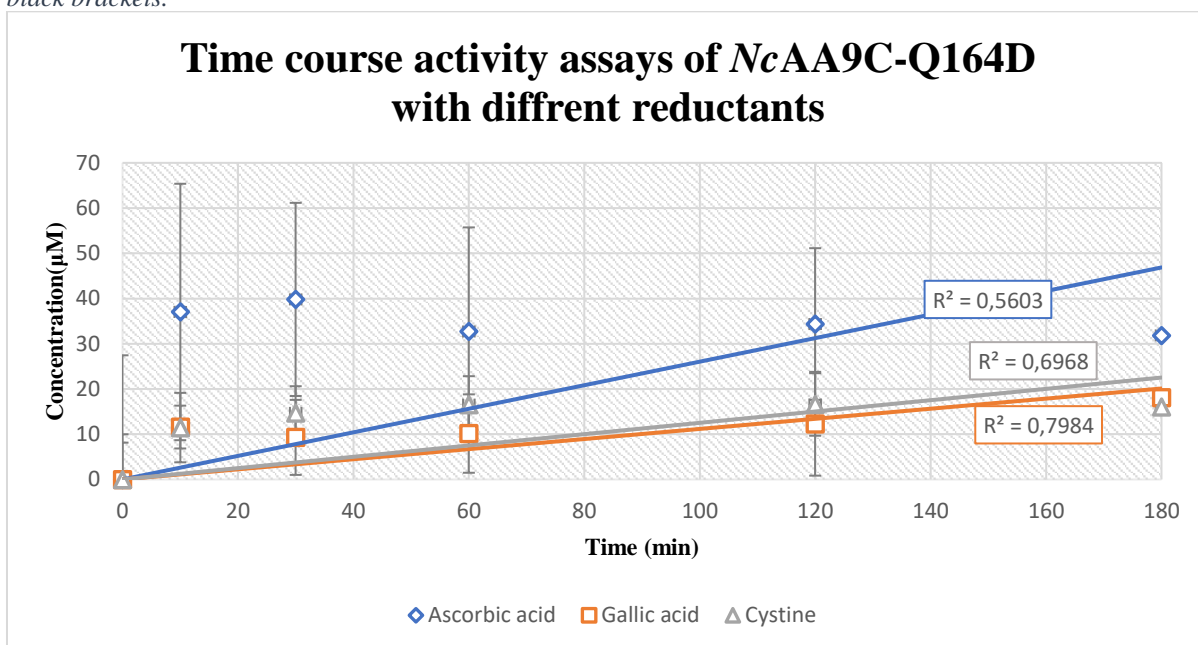


Figure 4-17 Time course activity assays of *NcAA9C-Q164D* with diverse reductants, For each experiment, a suspension of cellopentose (1mM g/L) and electron donor (1mM) in Bis-tris buffer (50 mM, pH 6.5) was incubated with *NcAA9C-Q164D* (1 µM) at 37 °C in a thermomixer (750 rpm), for varying amounts of time (10 min, 30 min, 60 min, 120 min, and 180 min). The graph visualizes the concentration (µM) of oxidized products; cellobiose (DP2<sup>ox</sup>) and cellotriose (DP3<sup>ox</sup>) detected in the final reaction mixture (y-axis), at the time of inactivation with NaOH (x-axis). There are three reactions, one each for the different electron donors Ascorbic Acid (blue), Gallic Acid (orange) and cystine (gray). Trendlines and R-squared are also supplied for each of the experiments for the different reactions. Furthermore, the standard deviation of each data point is visualized as black brackets.

### Time course activity assays of NcAA9C-Q164N with different reductants

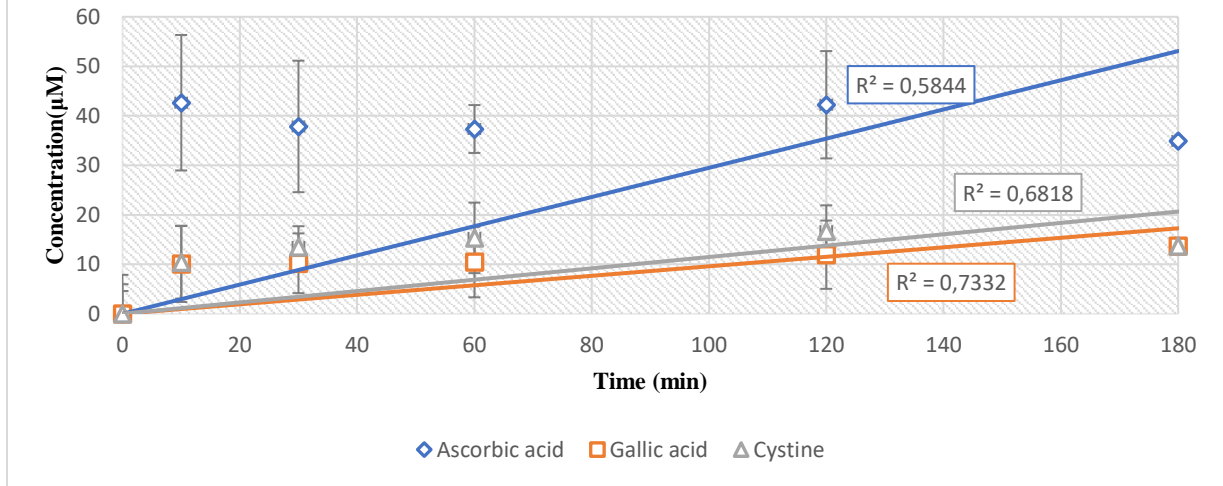


Figure 4-18 Time course activity assays of NcAA9C-Q164N with diverse reductants. For each experiment, a suspension of cellopentose (1mM g/L) and electron donor (1mM) in Bis-tris buffer (50 mM, pH 6.5) was incubated with NcAA9C-Q164N (1 µM) at 37 °C in a thermomixer (750 rpm), for varying amounts of time (10 min, 30 min, 60 min, 120 min, and 180 min). The graph visualizes the concentration (µM) of oxidized products; cellobiose (DP2<sup>ox</sup>) and cellotriose (DP3<sup>ox</sup>) detected in the final reaction mixture (y-axis), at the time of inactivation with NaOH (x-axis). There are three reactions, one each for the different electron donors Ascorbic Acid (blue), Gallic Acid (orange) and cystinee (gray). Trendlines and R-squared are also supplied for each of the experiments for the different reactions. Furthermore, the standard deviation of each data point is visualized as black brackets.

### Time course activity assays of NcAA9C-Q164E with different reductants

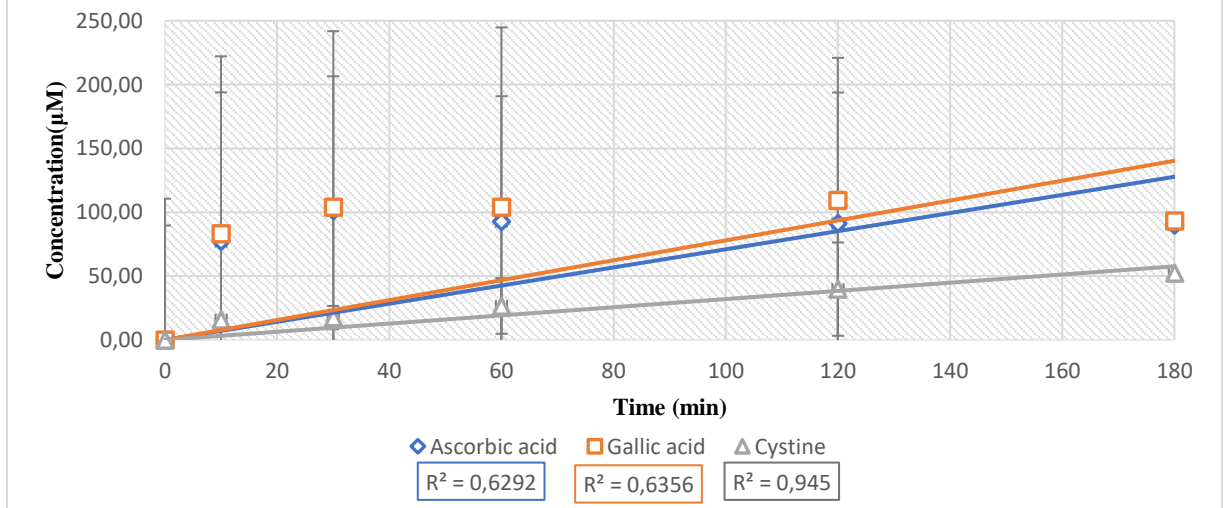


Figure 4-19 Time course activity assays of NcAA9C-Q164E with diverse reductants. For each experiment, a suspension of cellopentose (1mM g/L) and electron donor (1mM) in Bis-tris buffer (50 mM, pH 6.5) was incubated with NcAA9C-Q164E (1 µM) at 37 °C in a thermomixer (750 rpm), for varying amounts of time (10 min, 30 min, 60 min, 120 min, and 180 min). The graph visualizes the concentration (µM) of oxidized products; cellobiose (DP2<sup>ox</sup>) and cellotriose (DP3<sup>ox</sup>) detected in the final reaction mixture (y-axis), at the time of inactivation with NaOH (x-axis). There are three reactions, one each for the different electron donors Ascorbic Acid (blue), Gallic Acid (orange) and cystine (gray). Trendline and R-squared are also supplied for each of the experiments for the different reactions. Furthermore, the standard deviation of each data point is visualized as black brackets.

Figures 4.20-4.22 illustrate the same time course activity assays with *NcAA9C* variants but with the focus on the reductants used rather than the enzymes. Figure 4.20 shows reactions with ascorbic acid, Figure 4.21 showcases reactions using gallic acid, and Figure 4.22 highlights cysteine-assisted reactions. The y-axis represents the product concentration in the reaction solution, measured in  $\mu\text{M}$ , while the x-axis denotes the time elapsed since the enzyme's introduction into the solution, measured in minutes. Additionally, each reaction is accompanied by a trend line.

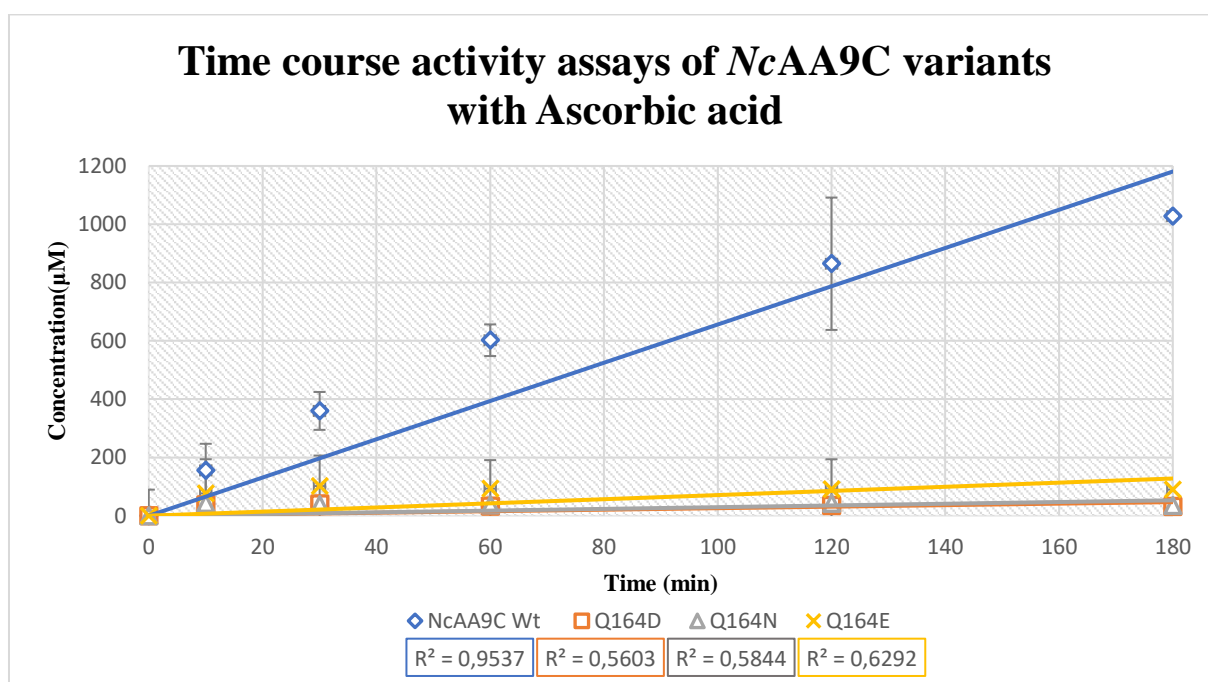


Figure 4-20 **Time course activity assays of *NcAA9C* variants with ascorbic acid as electron donor.** The figure visualize the release of oxidized cellobiose ( $DP2_{ox}$ ) and cellotriose ( $DP3_{ox}$ ) after incubation of LPMO ( $1 \mu\text{M}$ ) with cellopentaose ( $10 \text{ mM}$ ) and ascorbic acid ( $1 \text{ mM}$ ) in BisTris buffer ( $50 \text{ mM}$ ). The y-axis denotes the combined concentration of  $DP2_{ox}$  and  $DP3_{ox}$ , while the x-axis represents time (minutes) elapsed since the initiation of the reaction. There are four reactions, one each for the different *NcAA9C* variants: wild type (blue), Q164D (orange) Q164N (gray), and Q164E (yellow). Each reaction has six-time measurements at the time points (0 min, 10 min, 30 min, 60 min, 120 min and 180 min). Trendline and R-squared are also supplied for each of the experiments for the different reactions. Furthermore, the standard deviation of each data point is visualized as black brackets.

## Time course activity assays of NcAA9C variants with Gallic acid

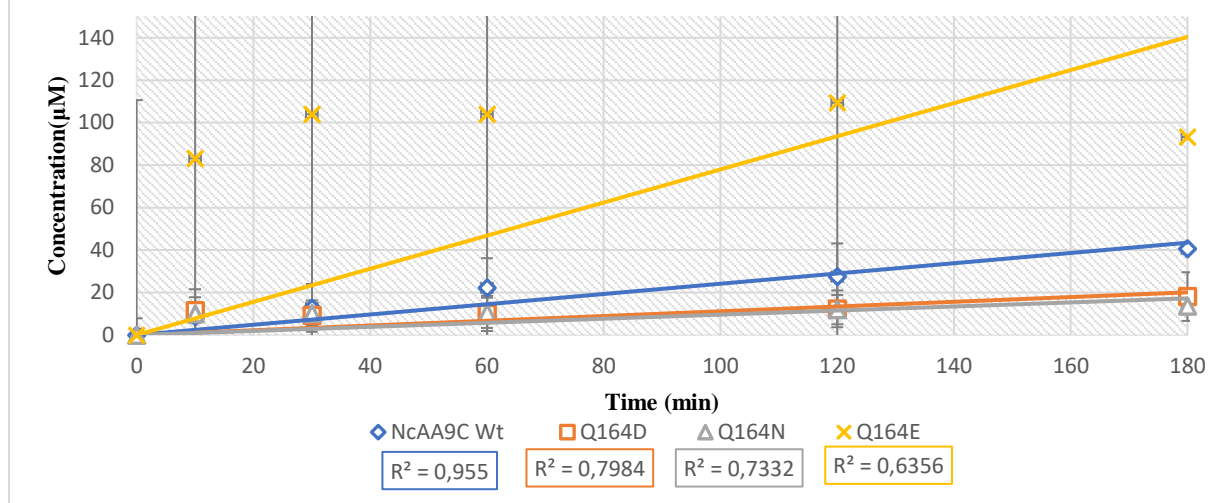


Figure 4-21 Time course activity assays of NcAA9C variants with gallic acid as electron donor. The figure visualize the release of oxidized cellobiose (DP2<sub>ox</sub>) and cellotriose (DP3<sub>ox</sub>) after incubation of LPMO (1 µM) with cellopentaose (10 mM) and gallic acid (1 mM) in BisTris buffer (50 mM). The y-axis denotes the combined concentration of DP2<sub>ox</sub> and DP3<sub>ox</sub>, while the x-axis represents time (minutes) elapsed since the initiation of the reaction. There are four reactions, one each for the different NcAA9C variants: wild type (blue), Q164D (orange) Q164N (gray), and Q164E (yellow). Each reaction has six-time measurements at the time points (0 min, 10 min, 30 min, 60 min, 120 min and 180 min). Trendline and R-squared are also supplied for each of the experiments for the different reactions. Furthermore, the standard deviation of each data point is visualized as black brackets

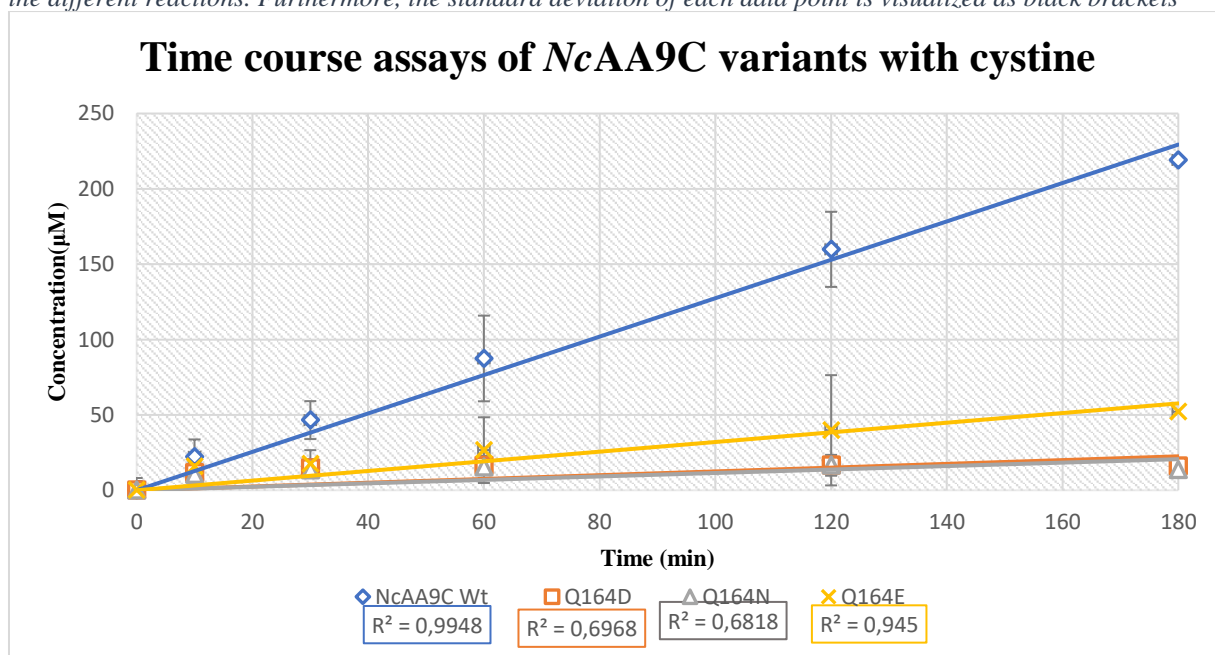


Figure 4-22 Time course activity assays of NcAA9C variants with cystine as electron donor. The figure visualize the release of oxidized cellobiose (DP2<sub>ox</sub>) and cellotriose (DP3<sub>ox</sub>) after incubation of LPMO (1 µM) with cellopentaose (10 mM) and ascorbic acid (1 mM) in BisTris buffer (50 mM). The y-axis denotes the combined concentration of DP2<sub>ox</sub> and DP3<sub>ox</sub>, while the x-axis represents time (minutes) elapsed since the initiation of the reaction. There are four reactions, one each for the different NcAA9C variants: wild type (blue), Q164D (orange) Q164N (gray), and Q164E (yellow). Each reaction has six-time measurements at the time points (0 min, 10 min, 30 min, 60 min, 120 min and 180 min). Trendline and R-squared are also supplied for each of the experiments for the different reactions. Furthermore, the standard deviation of each data point is visualized as black brackets.

In summary, *NcAA9C* wild type and mutants have the highest activity when ascorbic acid is the reductant. Moreover, the wild type has higher activity and stability than the mutants with ascorbic acid as the reductant. There are only small differences in the activities between gallic acid and cysteine as the reductant. The mutants are relatively slow in their presence but appear to be relatively more stable compared to when ascorbate is used.

#### 4.5.1 DETERMINING THE INITIAL RATES OF *NcAA9C* ACTIVITY

The initial rate of enzyme activity refers to the rate at which an enzyme-catalyzed reaction occurs when the substrate concentration is saturating, and the reaction has just started. The initial rates of enzyme activity for *NcAA9C*, a lytic polysaccharide monooxygenase active on cellulose, and its three mutants (Q164D, Q164N, and Q164E) were investigated using activity assays. Three different reductants—ascorbic acid, gallic acid, and cysteine—were then employed in the assays. The initial rates of activity for *NcAA9C* were consistently determined by performing time course activity assays using cellopentaose (Glc5) as the substrate.

Cellopentaose was primary chosen because it yields only two oxidized products when degraded by *NcAA9C*; cellobionic acid (DP2<sub>ox</sub>) and cellotronic acid (DP3<sub>ox</sub>), both of which are soluble. Standards for both DP2<sub>ox</sub> and DP3<sub>ox</sub> were prepared in the concentration range of 25-450  $\mu$ M. The oxidized products concentrations were determined individually by plotting the formation of product with respect to time, then combined to calculate the initial activity rates for the *NcAA9C* variants, as presented in Table 4.2.

Table 4-2 Starting rates in  $\mu$ M/min for *NcAA9C* wild type and mutant catalysis of oxidation by (Glc)5.

<b>Enzyme</b>	<b>Wild type</b>	<b>Q164D</b>	<b>Q164N</b>	<b>Q164E</b>
<b>Ascorbic acid</b>	9.8 $\pm$ 0.9 <sup>a</sup>	3.7 $\pm$ 2.7 <sup>b</sup>	4.26 $\pm$ 0.6 <sup>b</sup>	7.7 $\pm$ 9.0 <sup>b</sup>
<b>Gallic acid</b>	0.24 $\pm$ 0.02	1.16 $\pm$ 0.9 <sup>b</sup>	1.01 $\pm$ 0.8 <sup>b</sup>	8.3 $\pm$ 13 <sup>b</sup>
<b>Cystine</b>	1.27 $\pm$ 0.05	1.15 $\pm$ 0.8 <sup>b</sup>	1.0 $\pm$ 0.5 <sup>b</sup>	0.26 $\pm$ 0.03

a Initial rate in the linear region the first 60 min.

b No new products formed after 10 min. The numbers presented are taken as the concentration of product formed at 10 min and divided by 10 min to present a rough estimation of the initial rate in this time window.

## 4.5.2 DETERMINING MAXIMUM PRODUCT FORMATION FOR NCAA9C

The “Maximum product formation” is a measure of the total amount of oxidized product formed during a reaction. “Maximum product formation” gives a simple comparison of the effectiveness of the different reaction setups described in 3.18 and is shown in Table 4.3.

Table 4-3 Maximum product formation ( $\mu\text{M}$ ) for NCAA9C wild-type and mutant catalysis of oxidation of (Glc)5 during the time period of the experiment

<b>Enzym</b>	<b>Wild type</b>	<b>Q164D</b>	<b>Q164N</b>	<b>Q164E</b>
<b>Ascorbic acid</b>	1028	40 <sup>a</sup>	43 <sup>c</sup>	101 <sup>a b</sup>
<b>Gallic acid</b>	41	18 <sup>a</sup>	14 <sup>a</sup>	109 <sup>a</sup>
<b>Cystine</b>	219	16 <sup>a b</sup>	17 <sup>a</sup>	52 <sup>a</sup>

a Inside the standard deviation the other data points.

b average timepoints 60, 120 and 180 min.

c 10 min, all following time points concentration

## 5 DISCUSSION

### Mutational Effects on *SmAA10A* and *NcAA9C* during Catalysis

Lytic polysaccharide monooxygenases have garnered substantial global research interest due to their unique ability to cleave crystalline polysaccharides. However, the roles of individual amino acids in the catalytic process are not thoroughly understood. Bissaro *et al.* clearly demonstrated the importance of a Glu-residue near the active site in *SmAA10A* for successful and stable catalysis. From calculations, it was proposed that this residue is important by hydrogen bonding to hydrogen peroxide during the catalysis (Bissaro *et al.*, 2020). All LPMOs contain either a glutamate or glutamine residue in the active site. Another computational study concluded that a Gln in *LsAA9A* was important in “caging” a formed hydroxyl radical during catalysis, hence, enabling this to participate in the formation of the Cu(II)-oxyl species responsible for C-H hydroxylation in the cellulose substrate (Wang *et al.*, 2018). In this work, we are further investigating the role of the Gln-residue in *NcAA9C* and the Glu-residue in *SmAA10A*. We investigated the activities of the wild types and selected mutants under various conditions to assess, reactivity, inactivation of catalysis, and ability to bind hydrogen peroxide. Our findings aim to establish a foundational understanding for the molecular basis of LPMO activity.

### Mutant Variants of *SmAA10A-E60* and *NcAA9C-Q164*

To delve into this, we used site-directed mutagenesis on the Glu/Gln residue of *SmAA10A* (Glu60/E60) and *NcAA9C* (Gln164/Q164) and we mutated the glutamate (E60) in *SmAA10A* into glutamine (E60Q), aspartate (E60D), or asparagine (E60N). Simultaneously, for *NcAA9C-Q164*, we mutated glutamine into glutamate (Q164E), aspartate (Q164D), and asparagine (Q164N). Glutamine and glutamate are utilized by different LPMOs. However, the primary difference lies in the side chain; glutamine has an amide group (CONH<sub>2</sub>), whereas glutamate possesses a carboxylic acid group (COOH). By switching between glutamine and glutamate, we aim to ascertain if these two amino acids can be interchangeably used or if they fulfill distinct functions in various LPMOs. Lastly, aspartate and asparagine, having shorter carbon chains (one -CH<sub>2</sub>- less) than glutamate and glutamine, position the carboxylate group further from the copper ion. This provides an opportunity to investigate the implications of residues interactions and their effects on positioning.

Figure 4.9 presents the outcomes of the *SmAA10A* reactions with ascorbic acids. The mutants *SmAA10A-E60Q*, *SmAA10A-E60D*, and *SmAA10A-E60N* all display diminished activity in

comparison to the *SmAA10A* wild type. Notably, *SmAA10A-E60N* produced the fewest oxidized products, indicating this mutant might be the most susceptible to inactivation. The mutants *SmAA10A-E60Q* and *SmAA10A-E60D* demonstrate comparable activity levels, falling between the wild type and *SmAA10A-E60N*. These findings align with previous research by Bissaro *et al.*, 2020, on *SmAA10A*.

Interestingly, the experiments performed with the hydrogen peroxide quenching HRP show clear differences for the four variants. Here, clearly the wild type was less inhibited by the presence of HRP than the three mutants. This suggests that Glu is better in hydrogen bonding to hydrogen peroxide than the three other amino acids. This provides support to the calculations performed by Bissaro *et al.*

As depicted in Figure 4.20, *NcAA9C-Q164E*, *NcAA9C-Q164D*, and *NcAA9C-Q164N* mutants are all active, albeit significantly less so than the wild type. *NcAA9C-Q164E* ranks as the second most active mutant, while *NcAA9C-Q164D* and *NcAA9C-Q164N* show comparable activity levels, being the least effective. A comparison between Figure 4.9 (*SmAA10A*) and Figure 4.20 (*NcAA9C*) demonstrates a consistent trend: mutants are less active than the wild types. Nevertheless, *NcAA9C-Q164* appears significantly more effective, and its mutants seem more prone to inactivation than those of *SmAA10A*. Thus, we propose that glutamate (E60, *SmAA10A*) and glutamine (Q164, *NcAA9C*) coordinate the substrate towards the copper ion for the formation of oxygen radical, catalyzing the oxidative cleavage on cellulose and chitin.

However, they do not appear to be interchangeable, as both the *SmAA10A-E60Q* and *NcAA9C-Q164E* mutants displayed reduced activity compared to the wild types. We then hypothesize, that in changing the structure of the residue the superoxide is not as restrained allowing the radical to react with the enzyme itself. This damage might then inactivate the enzyme, explaining why the mutant's activity declined with time. Our results also point to that there are likely other so called second-sphere residues that are important for "caging" the reactive intermediates in LPMO catalysis. In *NcAA9A*, a proposed candidate is His155 and Asn185 in *SmAA10A* (Dr. Kelsi Hall personal communication).

### **Electron Donor**

Electron donors are pivotal for LPMO functionality. They prepare the enzyme for action by reducing its copper active site. Many studies have shown that without an electron donor LPMO catalysis cannot occur (Kuusk *et al.*, 2019). Figure 4.8 presents results of *SmAA10A* reactions without a reductant. To evaluate the dependence of LPMO catalysis on external electron donors,

we conducted time course activity assays on *SmAA10A* wild type and its gatekeeper mutants without exogenous reductants under *in-situ* peroxygenase conditions. Intriguingly, as Figure 4.8 illustrates, all *SmAA10A* variants demonstrated some oxidative activity. A detailed analysis of the data however showed significant standard deviations. Only the initial parallel exhibited notable activity (see Figure S.10), while the majority of readings from the subsequent parallel (Figure S.11) detected no oxidized product formation. Suspecting contamination of our  $\beta$ -chitin supply with minor reductant traces or other oxidized products we used fresh  $\beta$ -chitin for the next parallel. While three readings from this latter parallel indicated oxidized product formation, most showed no product creation. As conducting a third parallel to confirm our hypothesis proved impractical, we can't draw any conclusions on this point.

In experiments involving *NcAA9C* and three reductants (ascorbic acid, gallic acid, and cystine), shown in Figures 4.16-4.22, it becomes evident that all reactants can activate *NcAA9C*. Stepnov *et al.* and Rieder *et al.* Have demonstrated that *in-situ* hydrogen peroxide production needed for catalysis depends on both the nature of the LPMO as well as the reductant (Rieder *et al.*, 2021; Stepnov *et al.*, 2021). The extent of oxidative cleavage, however, is reductant dependent. Data from Figure 4.16 suggests *NcAA9C* wild type recognizes ascorbic acid as the primary reductant, followed by cystine and then gallic acid. Figures 4.17 and 4.18, representing *NcAA9C*-Q164D and *NcAA9C*-Q164N, generally reflect this pattern. For *NcAA9C*-Q164E, both ascorbic acid and gallic acid functioned similarly as reductants, with cystine following. Yet, upon reviewing the data we notice significant standard deviations in most mutant reactions. Interestingly, as noted in Table 4.2, no new products appeared after 10 minutes, indicating the mutants were inactive prior to this moment. A notable exception was the *NcAA9C*-Q164E reactions with cystine, which produced modest oxidized product amounts but showed no marked inactivation trends during the study. An interesting observation is that when gallic acid and cysteine are used as reductants, all mutants appear to be less prone for inactivation. The reduced catalytic speed appears to improve catalytic stability. This implies that reductant selection is an important parameter in LPMO catalysis.

## **Concluding Remarks and Perspectives**

The identification of LPMOs, proficient in cleaving crystalline substrates, has revolutionized our understanding of enzymatic carbohydrate degradation, offering novel enzymatic tools for biotechnology. However, several facets of LPMO's molecular mechanism remain a mystery. For LPMOs to be effectively utilized in large-scale lignocellulosic biofuel production, deeper insights are necessary. This thesis lays the groundwork for future research on LPMO's molecular mechanisms and the influence of reductants on LPMO catalysis. The data highlights the indispensable roles of the conserved glutamate/glutamine residue in LPMO activity and the consequential effects of reductant choice on LPMO performance. Our results point also towards that there are other second-sphere residues that likely play important roles in LPMO catalysis. A natural target for future research is to look at how the Glu/Gln residues interact with these, i.e., the proposed His and Asn, in "caging" reactive intermediates formed during catalysis.

## 6 REFERENCES

- Beeson, W. T., Vu, V. V., Span, E. A., Phillips, C. M. & Marletta, M. A. (2015). Cellulose Degradation by Polysaccharide Monooxygenases. *Annual Review of Biochemistry*, Vol 84, 84: 923-946. doi: 10.1146/annurev-biochem-060614-034439.
- Bissaro, B., Forsberg, Z., Ni, Y., Hollmann, F., Vaaje-Kolstad, G. & Eijsink, V. G. H. (2016). Fueling biomass-degrading oxidative enzymes by light-driven water oxidation. *Green Chemistry*, 18 (19): 5357-5366. doi: 10.1039/c6gc01666a.
- Bissaro, B., Rohr, A. K., Muller, G., Chylenski, P., Skaugen, M., Forsberg, Z., Horn, S. J., Vaaje-Kolstad, G. & Eijsink, V. G. H. (2017). Oxidative cleavage of polysaccharides by monocopper enzymes depends on H<sub>2</sub>O<sub>2</sub>. *Nature Chemical Biology*, 13 (10): 1123+. doi: 10.1038/nchembio.2470.
- Bissaro, B., Streit, B., Isaksen, I., Eijsink, V. G. H., Beckham, G. T., DuBois, J. L. & Rohr, A. K. (2020). Molecular mechanism of the chitinolytic peroxygenase reaction. *Proceedings of the National Academy of Sciences of the United States of America*, 117 (3): 1504-1513.
- Cannella, D., Mollers, K. B., Frigaard, N. U., Jensen, P. E., Bjerrum, M. J., Johansen, K. S. & Felby, C. (2016). Light-driven oxidation of polysaccharides by photosynthetic pigments and a metalloenzyme. *Nature Communications*, 7. doi: ARTN 11134  
10.1038/ncomms11134.
- Cantarel, B. L., Coutinho, P. M., Rancurel, C., Bernard, T., Lombard, V. & Henrissat, B. (2009). The Carbohydrate-Active EnZymes database (CAZy): an expert resource for Glycogenomics. *Nucleic Acids Research*, 37: D233-D238. doi: 10.1093/nar/gkn663.
- CAZy. (2020). GH1 Family Glycoside Hydrolase family classification. Université d'Aix-Marseille online database (The Carbohydrate-Active EnZymes database). Available at: <http://www.cazy.org/Glycoside-Hydrolases.html> (accessed: 2020-11-01).
- Chylenski, P., Bissaro, B., Sorlie, M., Rohr, A. K., Varnai, A., Horn, S. J. & Eijsink, V. G. H. (2019). Lytic Polysaccharide Monooxygenases in Enzymatic Processing of Lignocellulosic Biomass. *Acs Catalysis*, 9 (6): 4970-4991. doi: 10.1021/acscatal.9b00246.
- Ciano, L., Davies, G. J., Tolman, W. B. & Walton, P. H. (2018). Bracing copper for the catalytic oxidation of C-H bonds. *Nature Catalysis*, 1 (8): 571-577. doi: 10.1038/s41929-018-0110-9.
- Corradini, C., Cavazza, A. & Bignardi, C. (2012). High-Performance Anion-Exchange Chromatography Coupled with Pulsed Electrochemical Detection as a Powerful Tool to Evaluate Carbohydrates of Food Interest: Principles and Applications. *International Journal of Carbohydrate Chemistry*, 2012: 487564. doi: 10.1155/2012/487564.
- Courtade, G., Forsberg, Z., Heggset, E. B., Eijsink, V. G. H. & Aachmann, F. L. (2018). The carbohydrate-binding module and linker of a modular lytic polysaccharide monooxygenase promote localized cellulose oxidation. *Journal of Biological Chemistry*, 293 (34): 13006-13015. doi: 10.1074/jbc.RA118.004269.
- Couturier, M., Ladeveze, S., Sulzenbacher, G., Ciano, L., Fanuel, M., Moreau, C., Villares, A., Cathala, B., Chaspoul, F., Frandsen, K. E., et al. (2018). Lytic xylan oxidases from wood-decay fungi unlock biomass degradation. *Nature Chemical Biology*, 14 (3): 306+. doi: 10.1038/nchembio.2558.
- Danneels, B., Tanghe, M., Joosten, H. J., Gundinger, T., Spadiut, O., Stals, I. & Desmet, T. (2017). A quantitative indicator diagram for lytic polysaccharide monooxygenases reveals the role of aromatic surface residues in H<sub>1</sub>LPMO9A regioselectivity. *Plos One*, 12 (5).

- Drula, E., Garron, M. L., Dogan, S., Lombard, V., Henrissat, B. & Terrapon, N. (2022). The carbohydrate-active enzyme database: functions and literature. *Nucleic Acids Research*, 50 (D1): D571-D577. doi: 10.1093/nar/gkab1045.
- Eijsink, V. (2019). *Bio335 – Enzymology*. Canvas. p. 88.
- Eijsink, V. G. H., Petrovic, D., Forsberg, Z., Mekasha, S., Rohr, A. K., Varnai, A., Bissaro, B. & Vaaje-Kolstad, G. (2019). On the functional characterization of lytic polysaccharide monoxygenases (LPMOs). *Biotechnology for Biofuels*, 12. doi: ARTN 58  
10.1186/s13068-019-1392-0.
- Eriksson, K. E., Pettersson, B. & Westermark, U. (1974). Oxidation - Important Enzyme Reaction in Fungal Degradation of Cellulose. *Febs Letters*, 49 (2): 282-285. doi: Doi 10.1016/0014-5793(74)80531-4.
- Filiatrault-Chastel, C., Navarro, D., Haon, M., Grisel, S., Herpoel-Gimbert, I., Chevret, D., Fanuel, M., Henrissat, B., Heiss-Blanquet, S., Margeot, A., et al. (2019). AA16, a new lytic polysaccharide monoxygenase family identified in fungal secretomes. *Biotechnology for Biofuels*, 12: 15. doi: 10.1186/s13068-019-1394-y.
- Forsberg, Z., Sorlie, M., Petrovic, D., Courtade, G., Aachmann, F. L., Vaaje-Kolstad, G., Bissaro, B., Rohr, A. K. & Eijsink, V. G. H. (2019). Polysaccharide degradation by lytic polysaccharide monoxygenases. *Current Opinion in Structural Biology*, 59: 54-64.
- Garcia-Santamarina, S., Probst, C., Festa, R. A., Ding, C., Smith, A. D., Conklin, S. E., Brander, S., Kinch, L. N., Grishin, N. V., Franz, K. J., et al. (2020). A lytic polysaccharide monoxygenase-like protein functions in fungal copper import and meningitis. *Nature Chemical Biology*, 16 (3): 337-+. doi: 10.1038/s41589-019-0437-9.
- Hemsworth, G. R., Henrissat, B., Davies, G. J. & Walton, P. H. (2014). Discovery and characterization of a new family of lytic polysaccharide monoxygenases. *Nature Chemical Biology*, 10 (2): 122-126.
- Hemsworth, G. R. (2023). Revisiting the role of electron donors in lytic polysaccharide monoxygenase biochemistry. *Essays in Biochemistry*, 67 (3): 585-595. doi: 10.1042/Ebc20220164.
- Horn, S. J., Vaaje-Kolstad, G., Westereng, B. & Eijsink, V. G. H. (2012). Novel enzymes for the degradation of cellulose. *Biotechnology for Biofuels*, 5. doi: Artn 45  
10.1186/1754-6834-5-45.
- Kuusk, S., Kont, R., Kuusk, P., Heering, A., Sorlie, M., Bissaro, B., Eijsink, V. G. H. & Valjamae, P. (2019). Kinetic insights into the role of the reductant in H<sub>2</sub>O<sub>2</sub>-driven degradation of chitin by a bacterial lytic polysaccharide monoxygenase. *Journal of Biological Chemistry*, 294 (5): 1516-1528. doi: 10.1074/jbc.RA118.006196.
- Labourel, A., Frandsen, K. E. H., Zhang, F., Brouilly, N., Grisel, S., Haon, M., Ciano, L., Ropartz, D., Fanuel, M., Martin, F., et al. (2020). A fungal family of lytic polysaccharide monoxygenase-like copper proteins. *Nature Chemical Biology*, 16 (3): 345-+. doi: 10.1038/s41589-019-0438-8.
- Levasseur, A., Drula, E., Lombard, V., Coutinho, P. M. & Henrissat, B. (2013). Expansion of the enzymatic repertoire of the CAZy database to integrate auxiliary redox enzymes. *Biotechnology for Biofuels*, 6. doi: Artn 41  
10.1186/1754-6834-6-41.
- Loose, J. S. M., Vaaje-Kolstad, G. & Eijsink, V. (2018). *Biochemical investigation of catalysis by lytic polysaccharide monoxygenases*. Biokjemiske undersøkelser av katalyse i lytiske polysakkarid-monooksygenaser: Norwegian University of Life Sciences, ?s.  
Microfluidics. (2020). *How our Microfluidizer® Processors work*. In Microfluidics (ed.). Available at: <https://www.microfluidics-mpt.com/microfluidics-technology/how-it-works>.

- Quinlan, R. J., Sweeney, M. D., Lo Leggio, L., Otten, H., Poulsen, J. C. N., Johansen, K. S., Krogh, K. B. R. M., Jorgensen, C. I., Tovborg, M., Anthonsen, A., et al. (2011). Insights into the oxidative degradation of cellulose by a copper metalloenzyme that exploits biomass components. *Proceedings of the National Academy of Sciences of the United States of America*, 108 (37): 15079-15084. doi: 10.1073/pnas.1105776108.
- Reese, E. T., Siu, R. G. H. & Levinson, H. S. (1950). The Biological Degradation of Soluble Cellulose Derivatives and Its Relationship to the Mechanism of Cellulose Hydrolysis. *Journal of Bacteriology*, 59 (4): 485-497.
- Rieder, L., Ebner, K., Glieder, A. & Sørli, M. (2021). Novel molecular biological tools for the efficient expression of fungal lytic polysaccharide monoxygenases in *Pichia pastoris*. *Biotechnology for Biofuels*, 14 (1): 122. doi: 10.1186/s13068-021-01971-5.
- Rohrer, J. (2013). Analysis of Carbohydrates by High-Performance Anion-Exchange Chromatography with Pulsed Amperometric Detection (HPAE-PAD).
- Sabbadin, F., Hemsworth, G. R., Ciano, L., Henrissat, B., Dupree, P., Tryfona, T., Marques, R. D. S., Sweeney, S. T., Besser, K., Elias, L., et al. (2018). An ancient family of lytic polysaccharide monoxygenases with roles in arthropod development and biomass digestion. *Nature Communications*, 9: 12. doi: 10.1038/s41467-018-03142-x.
- Sabbadin, F., Urresti, S., Henrissat, B., Avrova, A. O., Welsh, L. R. J., Lindley, P. J., Csukai, M., Squires, J. N., Walton, P. H., Davies, G. J., et al. (2021). Secreted pectin monoxygenases drive plant infection by pathogenic oomycetes. *Science*, 373 (6556): 774+. doi: 10.1126/science.abj1342.
- Saloheimo, M., Nakari-Setälä, T., Tenkanen, M. & Penttilä, M. (1997). cDNA cloning of a *Trichoderma reesei* cellulase and demonstration of endoglucanase activity by expression in yeast. *Eur J Biochem*, 249 (2): 584-91. doi: 10.1111/j.1432-1033.1997.00584.x.
- Sigma-Aldrich. (2020). *IPTG*. Available at: [https://www.sigmaaldrich.com/catalog/product/sial/i6758?lang=en&region=NO&gclid=Cj0KCQjwk8b7BRCaARIsAARRTL51KHbm2e5Ufp8CfZ6FAKunlrgH3ucZSm7TGPJiyJ3-GU8vifp8yJYaAkDUEALw\\_wcB](https://www.sigmaaldrich.com/catalog/product/sial/i6758?lang=en&region=NO&gclid=Cj0KCQjwk8b7BRCaARIsAARRTL51KHbm2e5Ufp8CfZ6FAKunlrgH3ucZSm7TGPJiyJ3-GU8vifp8yJYaAkDUEALw_wcB) (accessed: 28.10.2020).
- Stepnov, A. A., Forsberg, Z., Sorlie, M., Nguyen, G. S., Wentzel, A., Rohr, A. K. & Eijsink, V. G. H. (2021). Unraveling the roles of the reductant and free copper ions in LPMO kinetics. *Biotechnology for Biofuels*, 14 (1). doi: ARTN 28  
10.1186/s13068-021-01879-0.
- Sun, P. C., Huang, Z. Y., Banerjee, S., Kadowaki, M. A. S., Veersma, R. J., Magri, S., Hilgers, R., Muderspach, S. J., Laurent, C. V. F. P., Ludwig, R., et al. (2023). AA16 Oxidoreductases Boost Cellulose-Active AA9 Lytic Polysaccharide Monoxygenases from *Myceliophthora thermophila*. *Acs Catalysis*, 13 (7): 4454-4467. doi: 10.1021/acscatal.3c00874.
- Sunna, A., Gibbs, M. D. & Bergquist, P. L. (2000). A novel thermostable multidomain 1,4-beta-xylanase from '*Caldibacillus cellulovorans*' and effect of its xylan-binding domain on enzyme activity. *Microbiology (Reading)*, 146 ( Pt 11): 2947-2955. doi: 10.1099/00221287-146-11-2947.
- Vu, V. V., Beeson, W. T., Span, E. A., Farquhar, E. R. & Marletta, M. A. (2014). A family of starch-active polysaccharide monoxygenases. *Proceedings of the National Academy of Sciences of the United States of America*, 111 (38): 13822-13827. doi: 10.1073/pnas.1408090111.
- Vaaje-Kolstad, G., Horn, S. J., van Aalten, D. M. F., Synstad, B. & Eijsink, V. G. H. (2005a). The non-catalytic chitin-binding protein CBP21 from *Serratia marcescens* is essential for chitin degradation. *Journal of Biological Chemistry*, 280 (31): 28492-28497. doi: 10.1074/jbc.M504468200.

- Vaaje-Kolstad, G., Houston, D. R., Riemen, A. H. K., Eijsink, V. G. H. & van Aalten, D. M. F. (2005b). Crystal structure and binding properties of the *Serratia marcescens* chitin-binding protein CBP21. *Journal of Biological Chemistry*, 280 (12): 11313-11319. doi: 10.1074/jbc.M407175200.
- Vaaje-Kolstad, G., Westereng, B., Horn, S. J., Liu, Z. L., Zhai, H., Sorlie, M. & Eijsink, V. G. H. (2010). An Oxidative Enzyme Boosting the Enzymatic Conversion of Recalcitrant Polysaccharides. *Science*, 330 (6001): 219-222. doi: 10.1126/science.1192231.
- Vaaje-Kolstad, G., Forsberg, Z., Loose, J. S. M., Bissaro, B. & Eijsink, V. G. H. (2017). Structural diversity of lytic polysaccharide monooxygenases. *Current Opinion in Structural Biology*, 44: 67-76. doi: 10.1016/j.sbi.2016.12.012.
- Wang, B., Johnston, E. M., Li, P., Shaik, S., Davies, G. J., Walton, P. H. & Rovira, C. (2018). QM/MM Studies into the H<sub>2</sub>O<sub>2</sub>-Dependent Activity of Lytic Polysaccharide Monooxygenases: Evidence for the Formation of a Caged Hydroxyl Radical Intermediate. *ACS Catalysis*, 8 (2): 1346-1351. doi: 10.1021/acscatal.7b03888.
- Yu, X. R., Zhao, Y., Yu, J. H. & Wang, L. S. (2023). Recent advances in the efficient degradation of lignocellulosic metabolic networks by lytic polysaccharide monooxygenase. *Acta Biochimica Et Biophysica Sinica*, 55 (4): 529-539. doi: 10.3724/abbs.2023059.
- Aachmann, F. L., Sorlie, M., Skjak-Braek, G., Eijsink, V. G. H. & Vaaje-Kolstad, G. (2012). NMR structure of a lytic polysaccharide monooxygenase provides insight into copper binding, protein dynamics, and substrate interactions. *Proceedings of the National Academy of Sciences of the United States of America*, 109 (46): 18779-18784. doi: 10.1073/pnas.1208822109.

## APPENDIX

### Standard curves:

To determine the concentration of the oxidized product from experiments, we utilized standards of varying concentrations to create standard curves. B-chitin was used as a substrate for reactions involving both *SmAA10A* wild-type and mutants. Subsequently, *SmGH20* was then added to the reaction aliquots and incubated at 37 °C overnight. *SmGH20* gains access to the substrate through the openings in the crystal structure introduced by the LPMO. It can then break down  $\beta$ -chitin to Chitobionic acid ( $A2^{OX}$ ), a soluble oxidized dimer that can be quantified. Therefore, we used standards of Chitobionic acid ( $A2^{OX}$ ) in the concentration range of 10-300  $\mu\text{M}$  for reactions with *SmAA10A* variants. The standard was also run as triplicates for each round on the ICS. Figures S.1 and S.2 display examples of standard curves of Chitobionic acid ( $A2^{OX}$ ). S1 from our experiment with *SmAA10A* under in-situ peroxygenase conditions and HRP, and S.2 under added  $\text{H}_2\text{O}_2$  conditions.

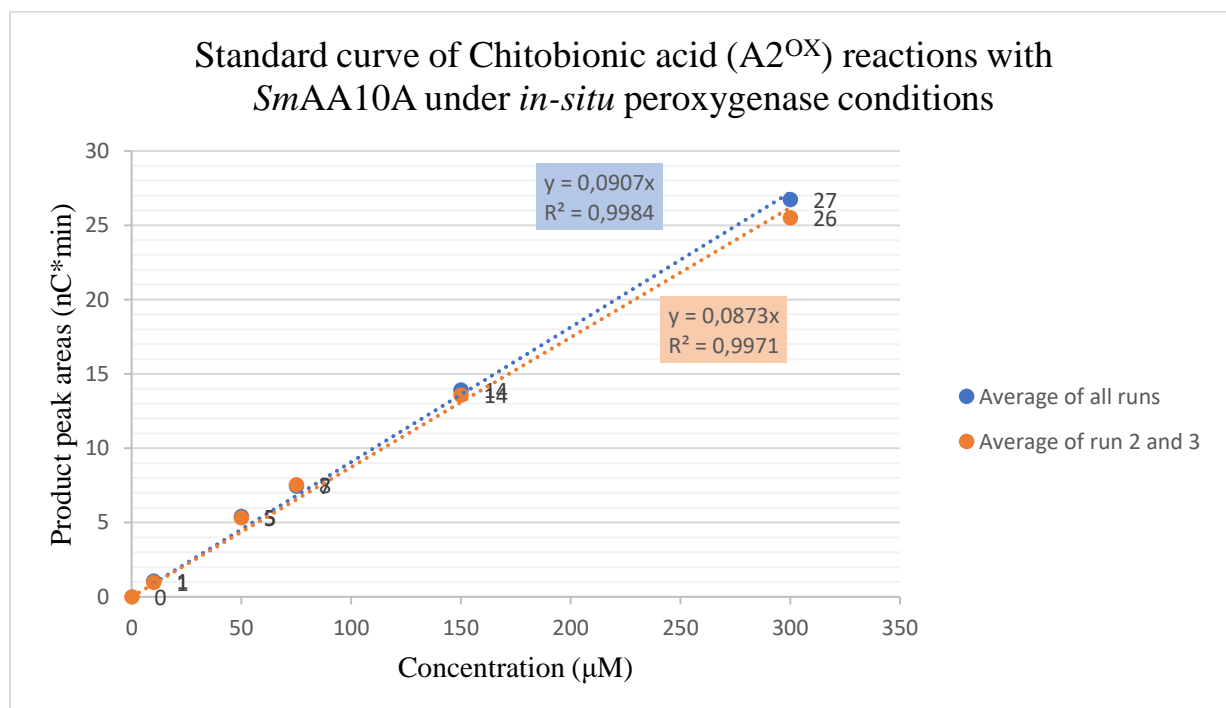


Figure S.1 Standard curve for chitobionic acid ( $A2^{OX}$ ) reactions with *SmAA10A* under *in-situ* peroxygenase conditions. The X axis represents concentration of  $A2^{OX}$  in  $\mu\text{M}$  and the y-axis represents the volumes of peaks in a chromatogram. We had three runs of five standards of known concentration: 10 $\mu\text{M}$ , 50 $\mu\text{M}$ , 75 $\mu\text{M}$ , 150 $\mu\text{M}$ , and 300 $\mu\text{M}$  in between the measurements of our samples. The average of all standard runs (blue) and the last two standard runs (orange) is visualized in this figure, with a linear equation and  $R^2$ .

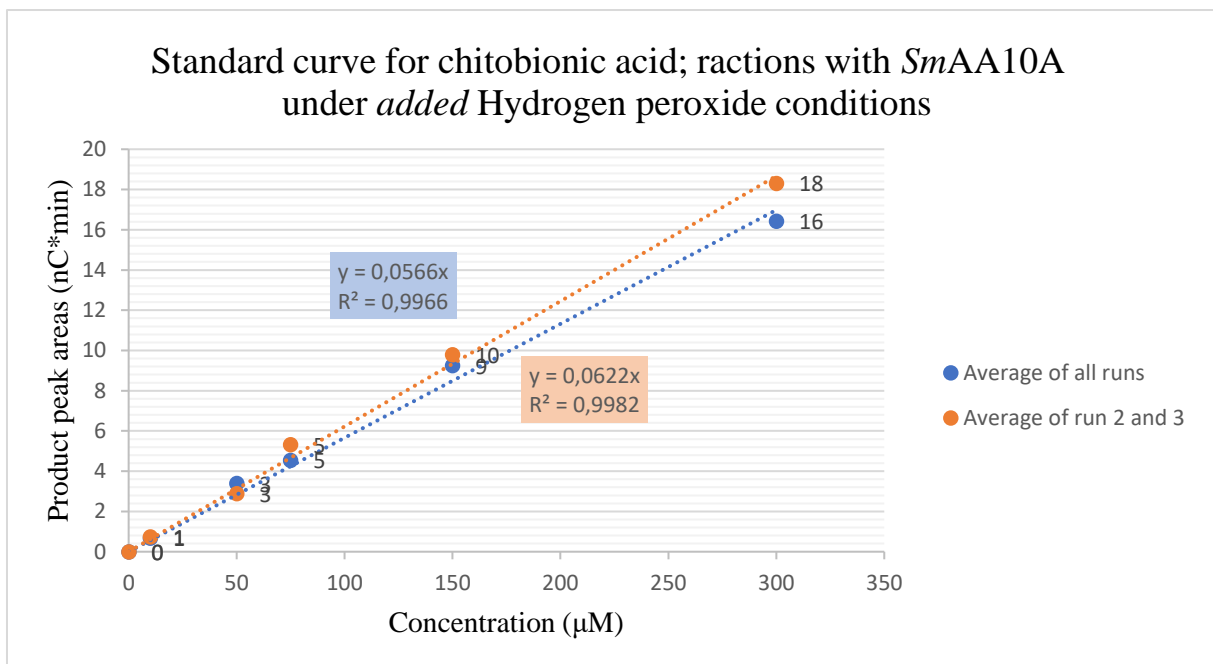
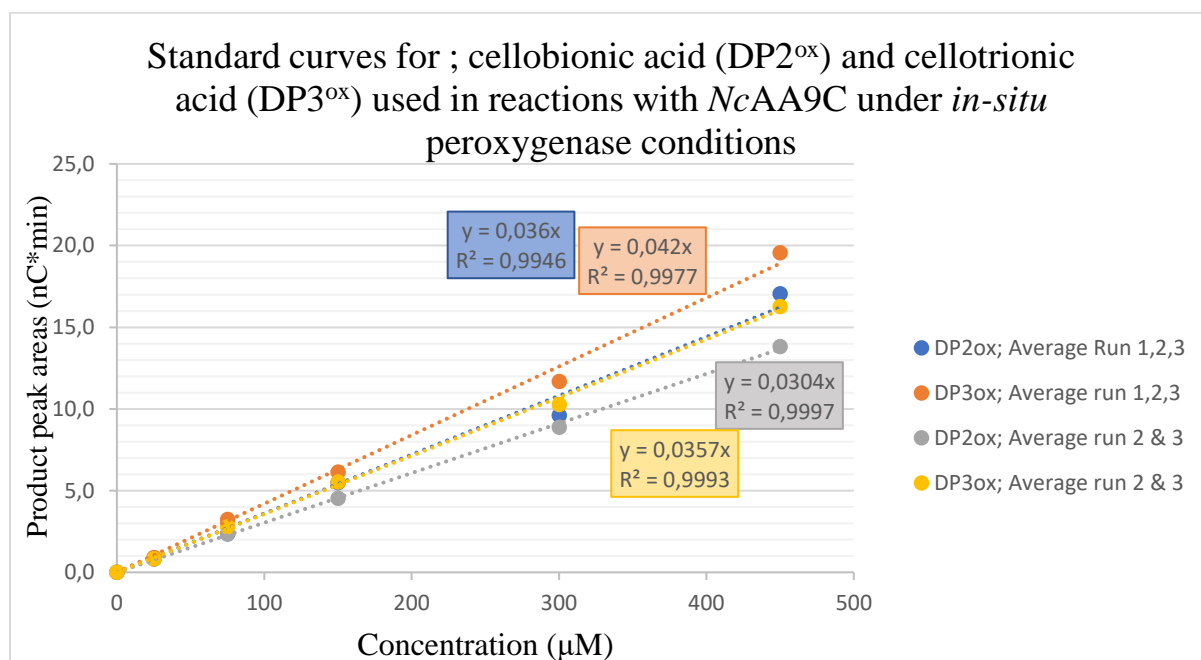


Figure S.2 Standard curve for chitobionic acid ( $A2^{ox}$ ); reactions with *SmAA10A* under added Hydrogen peroxide conditions. The Y axis represents concentration of  $A2^{ox}$  in  $\mu M$  and the y-axis represents the volumes of peaks in a chromatogram. We had three runs of five standards of known concentration:  $10\mu M$ ,  $50\mu M$ ,  $75\mu M$ ,  $150\mu M$ , and  $300\mu M$  in between the measurements of our samples. The average of all standard runs (blue) and the last two standard runs (orange) is visualized in this figure, with a linear equation and  $R^2$ .

In our experiments with *NcAA9C* wild-type and mutants cellopentaose was used as substrate. Cellopentaose yield two soluble oxidized products when degraded by *NcAA9C*; cellobionic acid (DP2<sup>ox</sup>) and cellotrionic acid (DP3<sup>ox</sup>). Therefore, we made standard curves for both DP2<sup>ox</sup> and DP3<sup>ox</sup> for reactions with *NcAA9C*. Standards was prepared in the concentration range 25  $\mu$ M-450  $\mu$ M. Figure S.3, shows an example standard curve.



**Figure S.3 Standard curves for cellobionic acid (DP2<sup>ox</sup>) and cellotrionic acid (DP3<sup>ox</sup>) from reactions with *NcAA9C* under *in-situ* peroxygenase conditions.** The X axis represents the concentration cellobionic acid (DP2<sup>ox</sup>) and cellotrionic acid (DP3<sup>ox</sup>) in  $\mu$ M and the y-axis represents the volumes of peaks in a chromatogram. We had three runs of five standards of known concentration: 25 $\mu$ M, 75 $\mu$ M, 150 $\mu$ M, 300 $\mu$ M, and 450 $\mu$ M in between the measurements of our samples. The average of all standard runs of DP2<sup>ox</sup> (blue), the average of all standard runs of DP3<sup>ox</sup> (orange), the average of the last two standard runs of DP2<sup>ox</sup> (gray) and the average of the last two standard runs DP3<sup>ox</sup> (yellow) is visualized in this figure, with a linear equation and R<sup>2</sup>.

## Time course activity assays with *SmAA10A* under *in-situ* peroxygenase conditions.

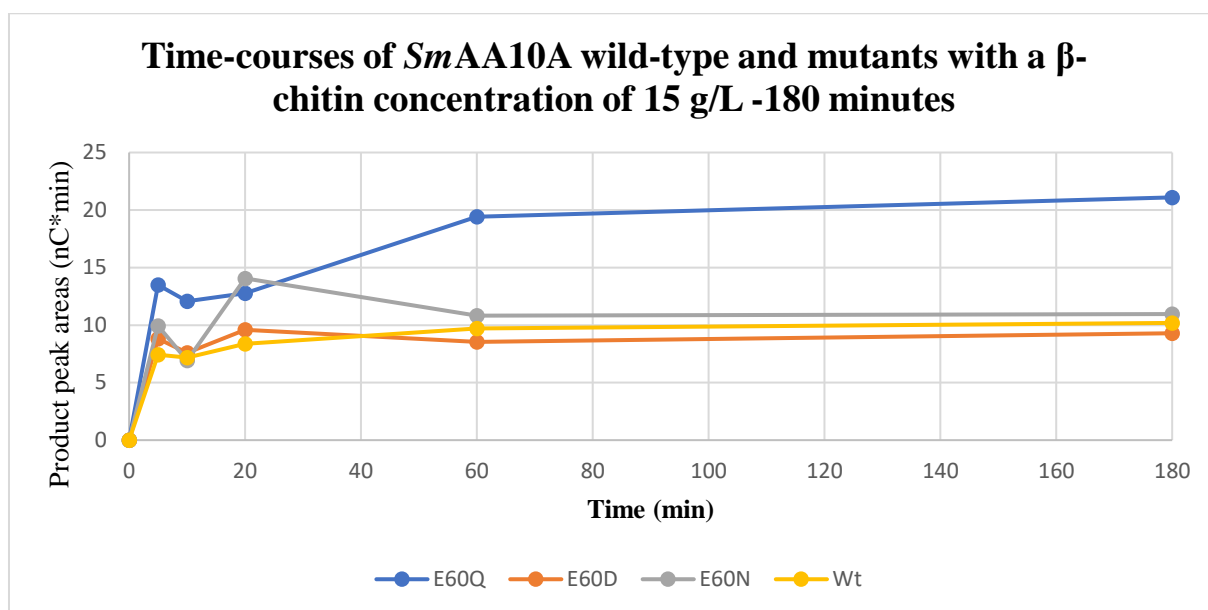


Figure S4 Time course activity assays of *SmAA10A* wild-type and mutants with a  $\beta$ -chitin concentration of 15 g/L under *in-situ* peroxygenase condition, 180 minutes. For each experiment, a suspension of *b*-chitin (15 g/L) and ascorbic acid (1mM) in Bis-tris buffer (50 mM, pH 6.5) was incubated with *SmAA10A* variant (1  $\mu$ M) at 37  $^{\circ}$ C in a thermomixer (1000 rpm), for varying amounts of time (5 min, 10 min, 20 min, 60 min and 180 min). The graph visualizes the concentration of oxidized products (y-axis) detected in the final reaction mixture (expressed as Area of chromatogram peak), at the time of enzyme heat inactivation (x-axis). There are four unique reactions with the *SmAA10A* variants: E60Q (blue), E60D (orange), E60N (gray) and wild type (yellow).

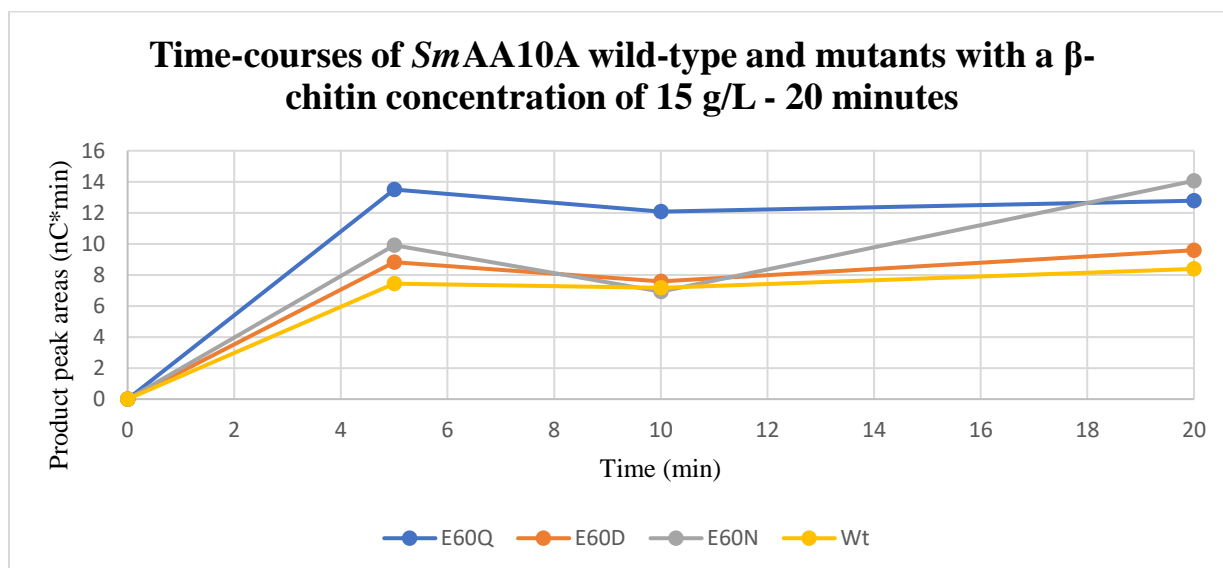


Figure S5 Time course activity assays of *SmAA10A* wild-type and mutants with a  $\beta$ -chitin concentration of 15 g/L under *in-situ* peroxygenase condition, 20 minutes. For each experiment, a suspension of *b*-chitin (15 g/L) and ascorbic acid (1mM) in Bis-tris buffer (50 mM, pH 6.5) was incubated with *SmAA10A* variant (1  $\mu$ M) at 37  $^{\circ}$ C in a thermomixer (1000 rpm), for varying amounts of time (5 min, 10 min and 20 min). The graph visualizes the concentration of oxidized products (y-axis) detected in the final reaction mixture (expressed as Area of chromatogram peak), at the time of enzyme heat inactivation (x-axis). There are four unique reactions with the *SmAA10A* variants: E60Q (blue), E60D (orange), E60N (gray) and wild type (yellow).

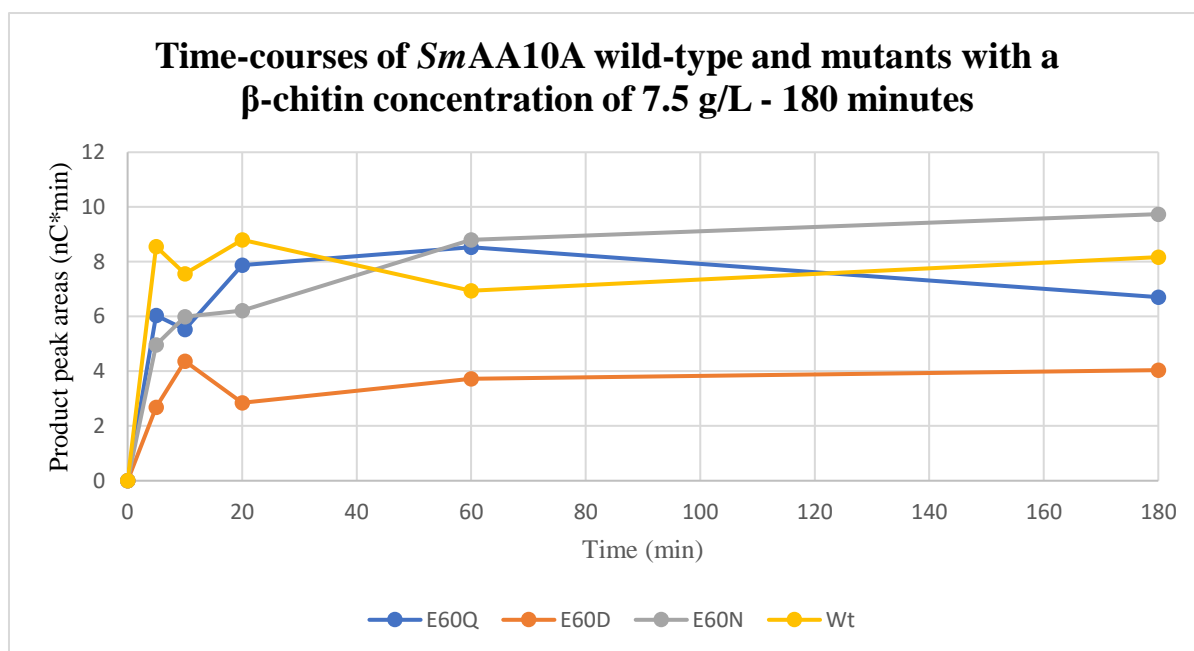


Figure S6 Time course activity assays of *SmAA10A* wild-type and mutants with a  $\beta$ -chitin concentration of 7.5 g/L under *in-situ* peroxygenase condition, 180 minutes. For each experiment, a suspension of *b*-chitin (7.5 g/L) and ascorbic acid (1mM) in Bis-tris buffer (50 mM, pH 6.5) was incubated with *SmAA10A* variant (1  $\mu$ M) at 37  $^{\circ}$ C in a thermomixer (1000 rpm), for varying amounts of time (5 min, 10 min, 20 min, 60 min and 180 min). The graph visualizes the concentration of oxidized products (y-axis) detected in the final reaction mixture (expressed as Area of chromatogram peak), at the time of enzyme heat inactivation (x-axis). There are four unique reactions with the *SmAA10A* variants: E60Q (blue), E60D (orange), E60N (gray) and wild type (yellow).

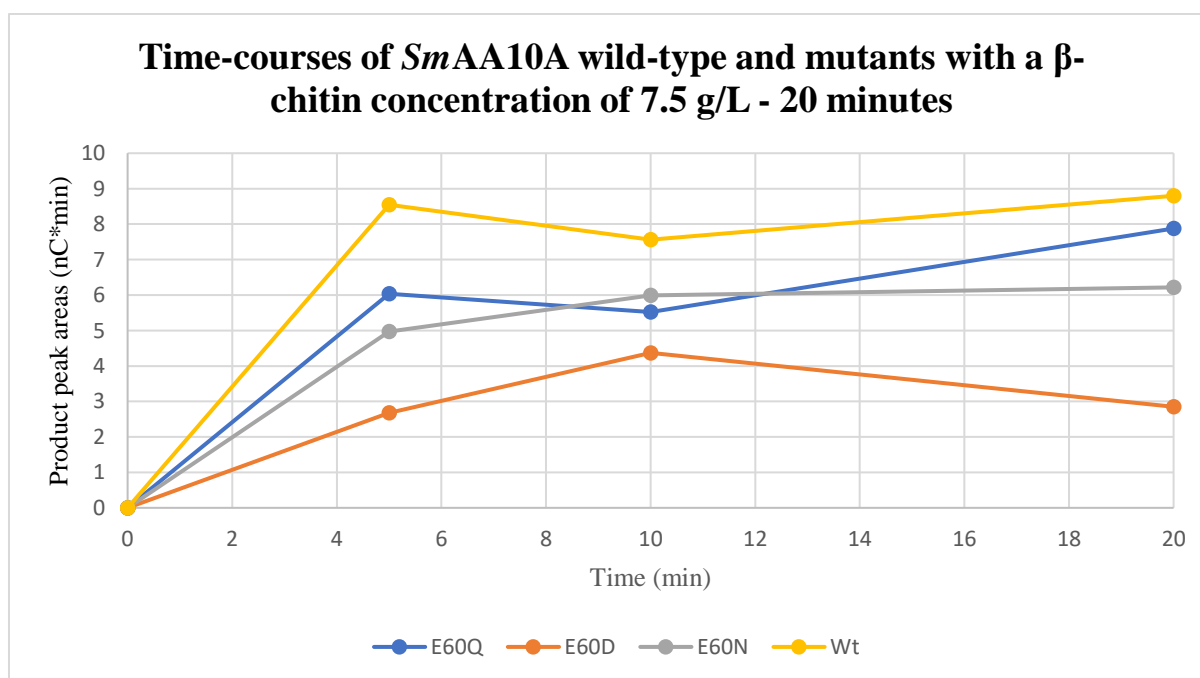


Figure S7 Time course activity assays of *SmAA10A* wild-type and mutants with a  $\beta$ -chitin concentration of 7.5 g/L under *in-situ* peroxygenase condition, 20 minutes. For each experiment, a suspension of *b*-chitin (7.5 g/L) and ascorbic acid (1mM) in Bis-tris buffer (50 mM, pH 6.5) was incubated with *SmAA10A* variant (1  $\mu$ M) at 37  $^{\circ}$ C in a thermomixer (1000 rpm), for varying amounts of time (5 min, 10 min and 20 min). The graph visualizes the concentration of oxidized products (y-axis) detected in the final reaction mixture (expressed as Area of chromatogram peak), at the time of enzyme heat inactivation (x-axis). There are four unique reactions with the *SmAA10A* variants: E60Q (blue), E60D (orange), E60N (gray) and wild type (yellow).

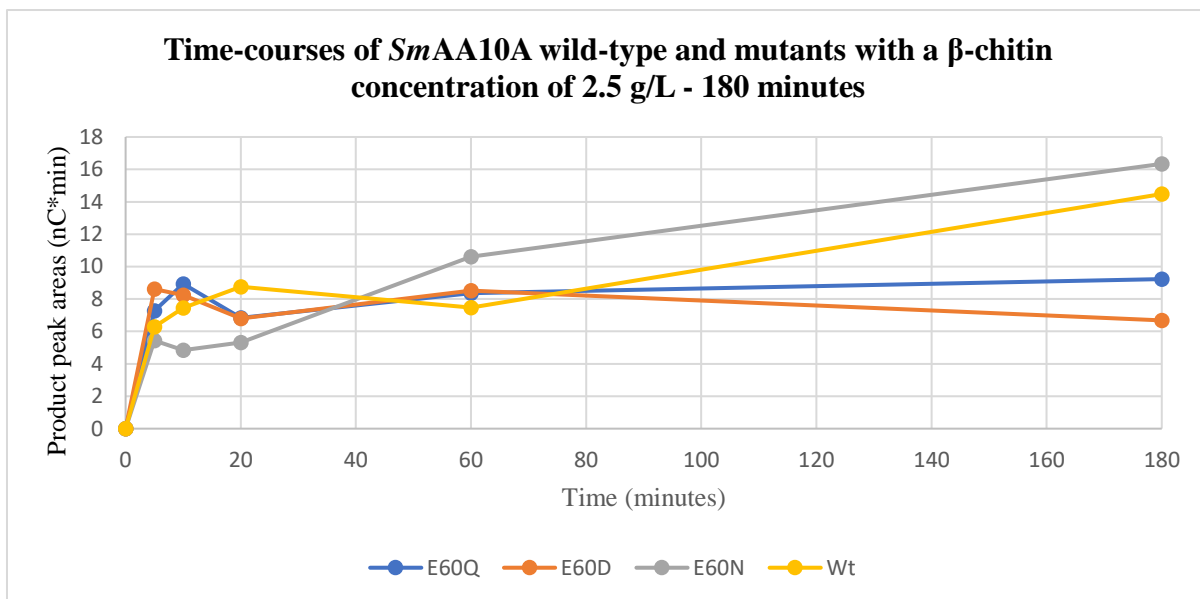


Figure S8 Time course activity assays of *SmAA10A* wild-type and mutants with a  $\beta$ -chitin concentration of 2.5 g/L under *in-situ* peroxygenase condition, 180 minutes. For each experiment, a suspension of *b*-chitin (2.5 g/L) and ascorbic acid (1mM) in Bis-tris buffer (50 mM, pH 6.5) was incubated with *SmAA10A* variant (1 $\mu$ M) at 37 °C in a thermomixer (1000 rpm), for varying amounts of time (5 min, 10 min, 20 min, 60 min and 180 min). The graph visualizes the concentration of oxidized products (y-axis) detected in the final reaction mixture (expressed as Area of chromatogram peak), at the time of enzyme heat inactivation (x-axis). There are four unique reactions with the *SmAA10A* variants: E60Q (blue), E60D (orange), E60N (gray) and wild type (yellow).

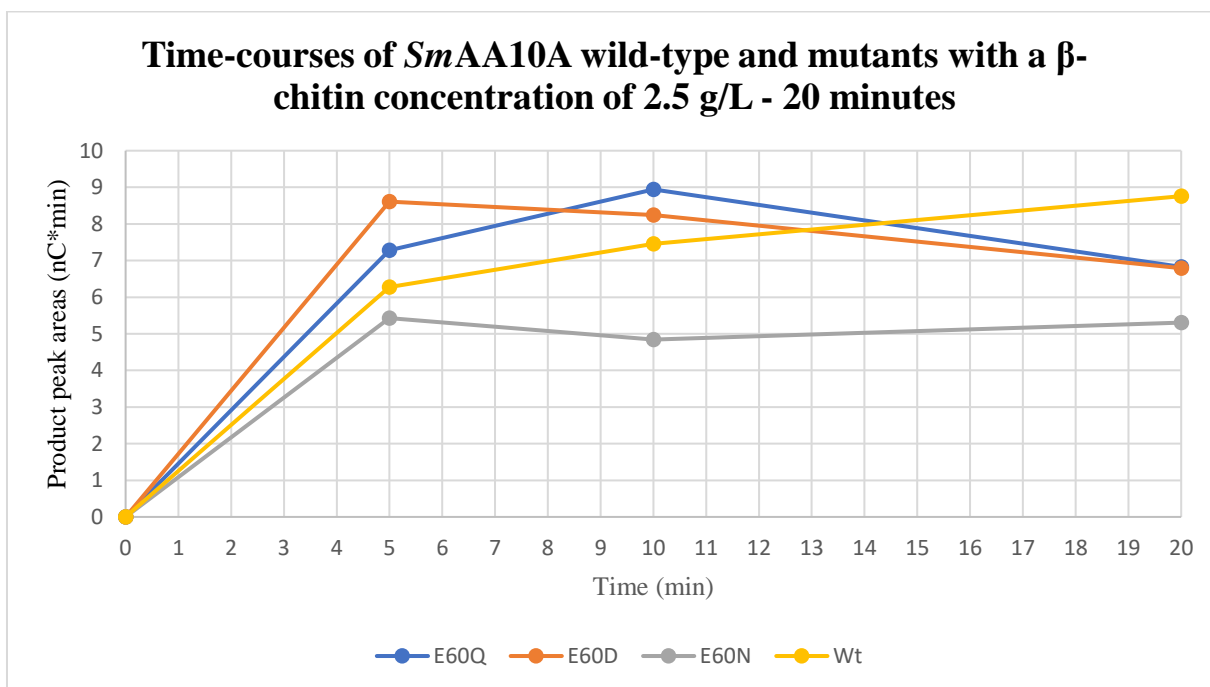


Figure S9 Time course activity assays of *SmAA10A* wild-type and mutants with a  $\beta$ -chitin concentration of 2.5 g/L under *in-situ* peroxygenase condition, 20 minutes. For each experiment, a suspension of *b*-chitin (2.5 g/L) and ascorbic acid (1mM) in Bis-tris buffer (50 mM, pH 6.5) was incubated with *SmAA10A* variant (1 $\mu$ M) at 37 °C in a thermomixer (1000 rpm), for varying amounts of time (5 min, 10 min, 20 min). The graph visualizes the concentration of oxidized products (y-axis) detected in the final reaction mixture (expressed as Area of chromatogram peak), at the time of enzyme heat inactivation (x-axis). There are four unique reactions with the *SmAA10A* variants: E60Q (blue), E60D (orange), E60N (gray) and wild type (yellow).

## **SmAA10A – No added electron donor - Parallel 1**

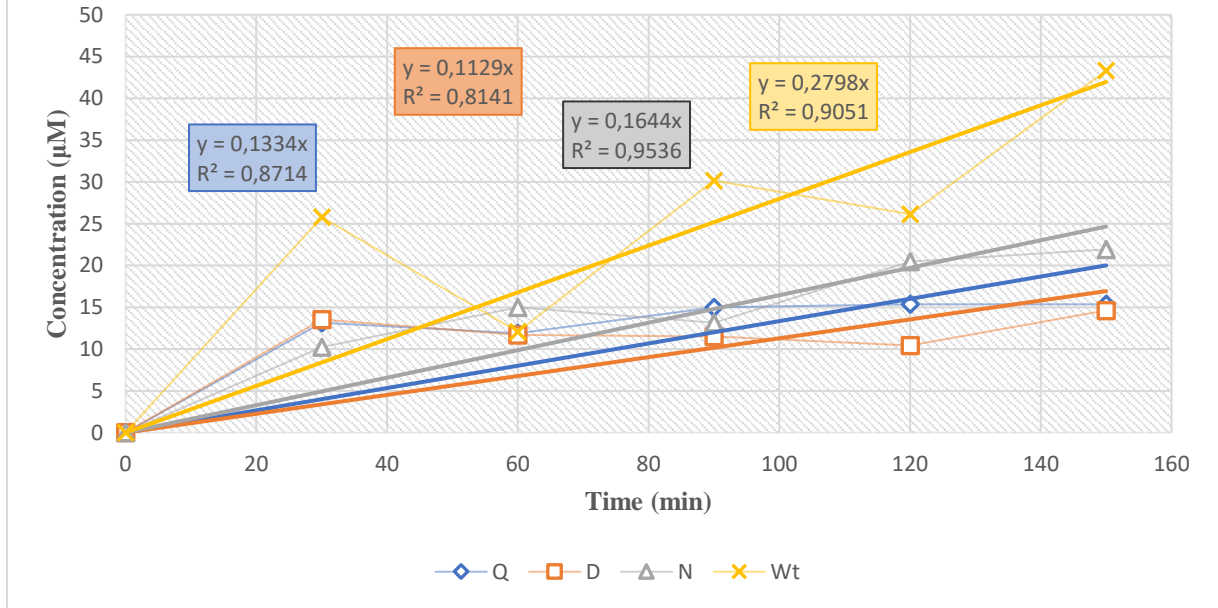


Figure S10 Time course activity assays of SmAA10A wild-type and mutants without electron donor – parallel 1. For each experiment, a suspension of  $\beta$ -chitin (10 g/L) in Bis-tris buffer (50 mM, pH 6.5) was incubated with SmAA10A variant (1 $\mu$ M) at 37 °C in a thermomixer (1000 rpm), for varying amounts of time (30 min, 60 min, 90 min, 120 and 150 min). The graph visualizes the concentration of oxidized products (y-axis) detected in the final reaction mixture (expressed as A2<sup>ox</sup>), at the time of enzyme heat inactivation (x-axis). There are four unique reactions with the SmAA10A variants: E60Q (blue), E60D (orange), E60N (gray) and wild type (yellow). Trendline and R-squared is also supplied for each of the runs with the different SmAA10A variant.

## **SmAA10A – No added electron donor - Parallel 2**

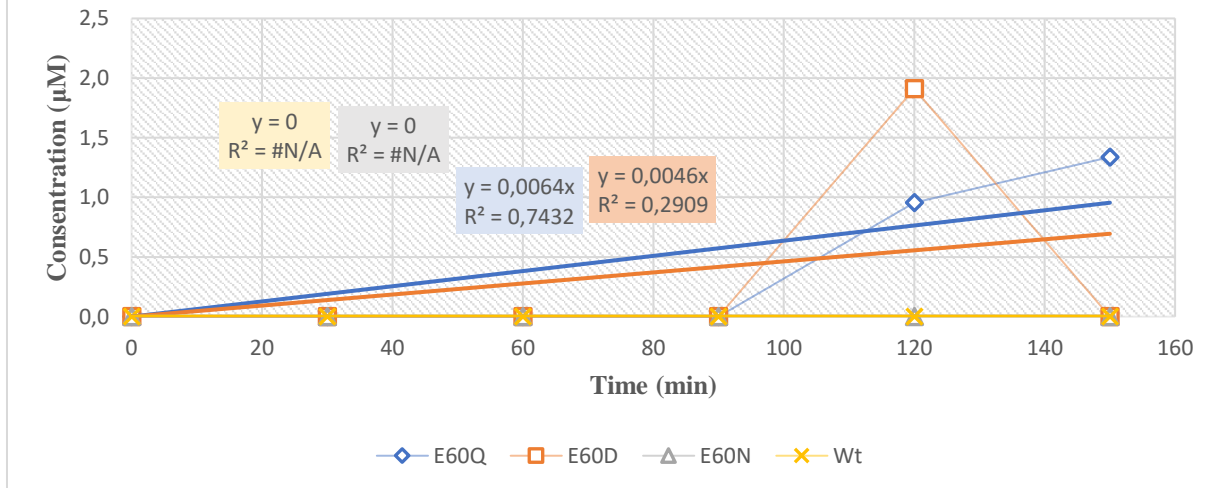


Figure S11 Time course activity assays of SmAA10A wild-type and mutants without electron donor – parallel 2. For each experiment, a suspension of  $\beta$ -chitin (10 g/L) in Bis-tris buffer (50 mM, pH 6.5) was incubated with SmAA10A variant (1 $\mu$ M) at 37 °C in a thermomixer (1000 rpm), for varying amounts of time (30 min, 60 min, 90 min, 120 and 150 min). The graph visualizes the concentration of oxidized products (y-axis) detected in the final reaction mixture (expressed as A2<sup>ox</sup>), at the time of enzyme heat inactivation (x-axis). There are four unique reactions with the SmAA10A variants: E60Q (blue), E60D (orange), E60N (gray) and wild type (yellow). Trendline and R-squared is also supplied for each of the runs with the different SmAA10A variant.